Characterization of incoming tsunamis for the design of coastal structures

A numerical study using the SWASH model

T. Glasbergen

TU Delft

Characterization of incoming tsunamis for the design of coastal structures

A numerical study using the SWASH model

By

Toni Glasbergen

In partial fulfilment of the requirements for the degree of

Master of Science

At the Delft University of Technology,

to be defended publicly on Tuesday January 23, 2018 at 11:00 AM.

Supervisor:	Dr. ir. B. Hofland	TU Delft
Thesis committee:	Prof. dr. ir. A.J.H.M. Reniers,	TU Delft
	Dr. M. Esteban,	University of Tokyo
	Dr. ir. J.D. Bricker,	TU Delft
	Dr .ir. M. Zijlema	TU Delft

TUDelft

Abstract

The Tohoku Tsunami of 2011 in Japan flooded a large part of the coastal area of Japan. The tsunami was caused by an earthquake with a magnitude of 9.0 just of the coast of Tohoku. The inundation height of the tsunami exceeded the design height of the tsunami barriers. This event led to thousands of fatalities.

To prevent this damage from a tsunami event to happen again, the coast should have a good defence system. The government of Japan has built or raised hundreds of meters of seawall in areas that where hit the most. The effectiveness of the barrier is questioned and also the design standards of the barriers are unclear. The tsunami events are categorized in two protection levels after the 2011 tsunami. An 1 in about 100 year return period is level 1 and an 1 in about 1000 year return period is level 2. This does not give a clear view on what the tsunami wave, where the coastal defence structure should be designed on, looks like.

The aim of this study is to find the characteristics of the incoming tsunami waves for the design of coastal defence structures. This incoming tsunami wave close to the shore or on the shore is influenced by a lot of offshore factors that will change the wave and its behaviour. The tsunami wave will either develop into a bore or just run up the coast. This has large influence on the forces on the barrier. Potential influencing factors are examined on if and how they influence the tsunami wave when it travels to the coast.

A numerical one-dimensional SWASH model is used throughout this study to simulate the tsunami wave. The tsunami factors and the factors that influence the wave were studied in several steps.

The first step is to validate and calibrate the model by using reference studies. The town of Yuriage near Sendai, Japan, that was ruined by the 2011 Tohoku tsunami is used to validate and calibrate the SWASH model. Another validation is done with the Solitary wave simulations of Grilli et al. (1997). This shows that waves in the SWASH model break a little earlier than the reference case.

The second step is the offshore generation of the tsunami wave. The elevation of a tsunami is simulated by locally raising the water level in the SWASH model at the location where the wave is generated. This occurs offshore where two tectonic plates meet. This elevation slits in two equal waves travelling in opposite direction with half the height of the initial elevation.

The third step is to model the wave from offshore to the nearshore area and the forth step is to model the wave behaviour at the coast. The wave undergoes changes due to shoaling. This is important for the development of a bore. The factors that could influence this shoaling are simulated. These factors are changes in the bathymetry or in the offshore wave parameters. The bathymetry factors are the slope of the continental slope, the slope of the continental shelf and the offshore depth at which the wave is generated. The offshore wave parameters are the wave length, the wave height and the skewness of the

wave. This resulted that the offshore bathymetry is less of influence compared to the nearshore bathymetry. The continental slope has very little influence on the wave. Although, the offshore depth has a bigger influence on the shoaling. The continental shelf is the most important factor of the bathymetry. The wave length and wave height are also very important. The skewness has no large influence on the wave.

The factors that have the most influence on the wave are used to simulate bores. From all these bores the important characteristics for the design of a barrier are investigated. These are the bore height, the bore velocity and the corresponding Froude number. With the simulations a new definition of the bore height is introduced. This is the height at the maximum velocity of the bore. The bore characteristics are also tested with an existing formula for the impact forces on a structure.

The behaviour of the breaking wave is studied and a breaker parameter [$\xi_{tsunami}$] for tsunami waves is made. This breaker parameter defines if the tsunami wave develops into a bore before it reaches the coastline or that the wave runs up the coast without breaking. This is important for the location of the coastal structure.

This breaker parameter and the Froude number of the bore give a relationship between the important parameters that influence the development of a bore and the characteristics of the incoming tsunami bore.

Finally, physical tests were performed at the Waseda University in Tokyo, Japan, to simulate the bore attack on a coastal defence structure with a dam-break. The bore of the tests is compared to the bore from the SWASH simulations. This resulted that the velocities of the tests seem too high. However, with a new method to find the bore front characteristics is a Froude number constructed. This Froude number matches very well for the tests and SWASH simulations. The Froude numbers of the test represent a bore at the coastline.

Preface

This thesis is the final step in fulfilment of the requirements for the Master's program Hydraulic engineering at the Delft University of Technology. The aim of this thesis is to predict design tsunami parameters and to gain deeper insight into the tsunami wave behaviour.

I would like to express my sincere gratitude to the members of my graduation committee, consisting of dr. ir. B. Hofland, prof. dr. ir . A.J.H.M. Reniers, dr. ir. J.D. Bricker, dr M. Esteban and dr. ir. M. Zijlema, for their guidance, feedback and assistance during the period writing this thesis. Furthermore, I would like to thank prof T. Shibayama and his students from the Waseda University in Tokyo for their help and assistance during the experiments. I would also like to thank the Delta Infrastructure and Mobility Initiative (DIMI) of TU Delft for the funding for the trip to Japan. Finally, I would like to thank my family and friends for supporting me during this research.

Toni Glasbergen
January, 2018

Contents

1.

Introduction

1.1   Research Motivation

At the Japanese coast, there is a large probability of the occurrence of a tsunami wave. In 2011, there was an earthquake with a magnitude of 9.0, which resulted in a tsunami wave on the coast of Japan. Large areas were inundated and there was a high amount of fatalities. The wave exceeded the design level of the coastal barriers and overtopped the barrier. This destroyed a large amount of buildings, Figure 1.1.

Figure 1.1: Left: Damaged building that survived the 2011 tsunami. Right: Location of houses that were destroyed by the 2011 tsunami in Yuriage, Japan.

To prevent this damage from a tsunami event to happen again, the coast should have a good defence system. The government of Japan has built hundreds of meters of seawall in areas that where hit the most. These walls are designed to withstand a Level 1 tsunami event. However, it is unclear what the parameters of typical tsunami event are.

It is therefore interesting to know what kind of wave the barrier will have to withstand. The wave can have many different periods and wave heights. The bottom profile of the coast influences the wave. The velocities on a barrier might be very different for a wave that breaks and a wave that does not break. A better understanding of the processes near shore of a tsunami is necessary to predict the tsunami waves.

In this thesis, a numerical model will be made to predict a tsunami wave that reaches the coast. This model will be made with SWASH (simulating waves till shore) and many different scenarios will be tested to see what the influences are on tsunami waves. Horsten [2016] and Okumura [2016] made a 1D SWASH model to predict the run-up of tsunami waves. Their model will be used to validate the model in this thesis. Factors like the bathymetry and the wave height or the sensitivity of these factors will be tested. From the model results a method is defined to describe the characteristics of the tsunami bore is defined. With this method a new design of the seawall can be made.

This thesis is part of an interdisciplinary project of the Delft Deltas, Infrastructures & Mobility Initiative (DIMI). This is a group of student from multiple disciplines working on a project and a group of students working on their thesis. The overall subject is the town of Yuriage, Japan. This town was ruined during the 2011 Tohoku tsunami. The town is being rebuild. The interdisciplinary group is interested in what to rebuild in this town with high tsunami risk. Yuriage is a recurring topic in this thesis.

1.2   Objective and research question

The objective of this thesis is to predict design tsunami characteristics and to gain deeper insight into the tsunami wave behaviour.

Question:
What are the characteristics of an incoming tsunami bore needed for the design of coastal defence structures?
Sub-questions:
- What parameters of an incoming tsunami bore are needed for the design of a tsunami barrier?
- What are the deep water properties of the wave to model a tsunami, what wave parameters have influence on the tsunami bore?
- What is the effect of the coastal geometry on the incoming wave, does the tsunami wave develop a bore?
- What are the relevant parameters of a tsunami wave at the location of the coastal defense structure and how do we determine their values?

1.3   Approach

To find the properties of a tsunami bore for the design of a coastal structure with the numerical model SWASH, several steps are taken. Firstly, the dimensions of tsunami waves and bathymetries of the coastal areas that are subject to tsunamis are investigated. These are the boundary conditions for the model.

The SWASH model is calibrated and validated for two different cases. The first case is the 2011 Tohoku tsunami in Yuriage, Japan. This is a town close to Sendai, Japan. Yuriage is part of a DIMI interdisciplinary project and the case is also used by Okumura [2016] and Horsten [2016]. The second case covers the testing of the breaking of solitary waves on different slopes [Grilli et al.1997]. These small scale tests are looking at breaking of soliton waves near the shore. This is the same area as this thesis is looking at.

The tsunami is simulated from the source to simulate a real tsunami as truthfully as possible. Simulating the cause of an earthquake in SWASH would be the best way to simulate a tsunami wave in the model. However, this is not possible. The wave is simulated by elevating the water level above the fracture zone of the earthquake. The tsunami is simulated with two one-dimensional models. First, the offshore wave is simulated with a coarse grid size and the time series of this model is used as input for a nearshore simulation. [Chapter 3]

The next step is the simulation of different tsunami waves with SWASH. This is done by changing different parameters that influence the tsunami wave and the development of a bore. The sensitivity on these parameters is investigated. [Chapter 4]

The SWASH model is used to develop multiple bores under different conditions. The results of these simulations are analysed to find the largest parameters of the tsunami bore. The differences between the bores are analysed for changes in bathymetry. This is done in order to find a breaker parameter, which is then related to the characteristics of the bore. The characteristics of the bore are expressed with the Froude number. [Chapter 5]

The tsunami wave is tested with physical tests and compared to the wave from the SWASH model. [Chapter 6]

1.4   Definition of parameters and sketch

In Figure 1.2 a sketch is given of a tsunami wave generated at the fracture zone of an earthquake. The wave has a wave elevation [η] with maximum wave height [H_0] and the water depth is given by [d]. The continental slope is[α_1]. The slope on the continental shelf is given by [α_2] and the slope above water level by [α_3]. The horizontal distance is given by [x] with the location [x_0] at the tsunami generation area.
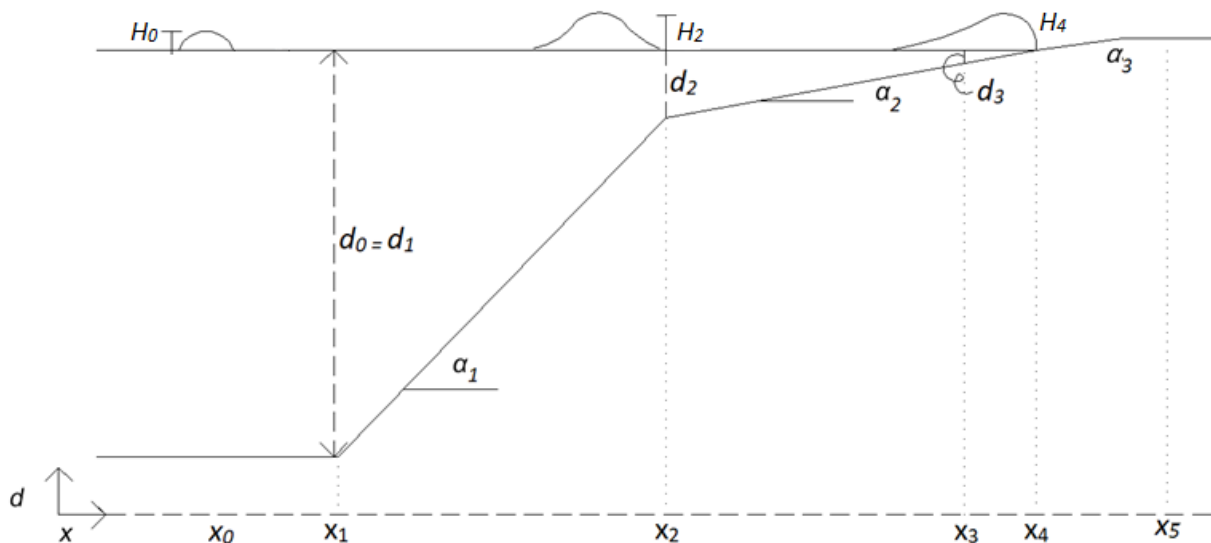
Figure 1.2: Sketch of parameters

In a sketch of the shoreline (Figure 1.3), some extra parameters are shown. The bore following from a tsunami approaches a seawall with height [h_{wall}]. The height of the bore is given with [H_{bore}]. The velocity of the bore at bore height is [u_{bore}]. The velocity of the bore front is shown with [v_{front}].
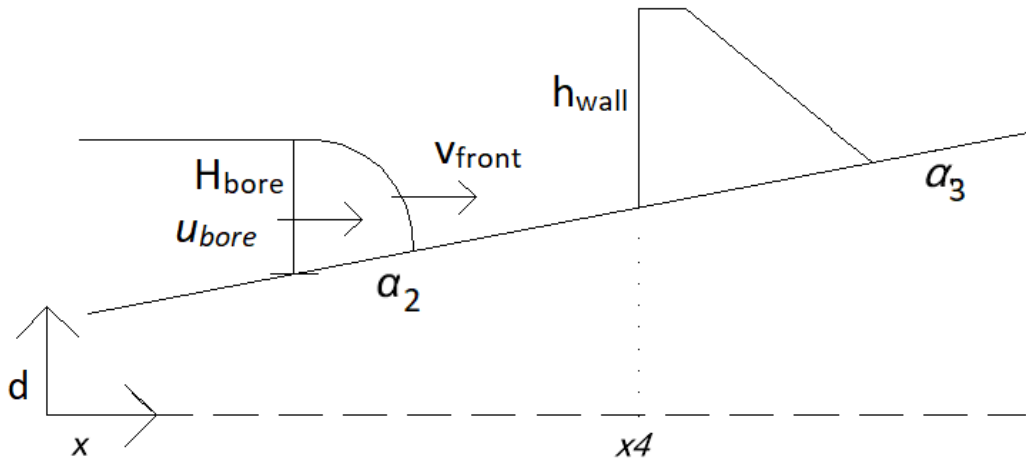
Figure 1.3: Sketch of bore approaching wall

1.5 Bathymetry of past tsunami events.

The bathymetry of five locations that had a tsunami event in the past are shown in the Figure 1.4. These are the Sendai Bay in Japan (2011), Kesennuma in Japan (2011), Valdivia in Chile (1960), Panganderan on Java (2006) and the coast of Sri Lanka (2004). In Chile and Sri Lanka the offshore depth reaches 4 km and in Japan and in Java, Indonesia, it becomes 6 km. These bathymetries look all very different, however, there are some similarities. They show a fast decrease in depth, with slope α_1, from offshore up to 500 to 200 m depth. This slope is in reality not as straight as shown in the sketch in Figure 1.4. Slope α_1 is averaged 1:20 for these locations. A 1:10 to 1:20 slope is the most common slope. At the shore the bottom slope α_2 becomes shallower.

In Figure 1.5 the bathymetries show large varieties in angle [α_2]. The depth H_2, at the transition between α_1 and α_2, is different for all five locations, however, H_2 is set constant at 500 meter in the SWASH computations. The third slope α_3 is the slope on land above mean water level. In most studies on tsunamis, only slope α_2 is investigated. In this thesis also α_1 is taken into the model to investigate if this has an influence on the tsunami wave.
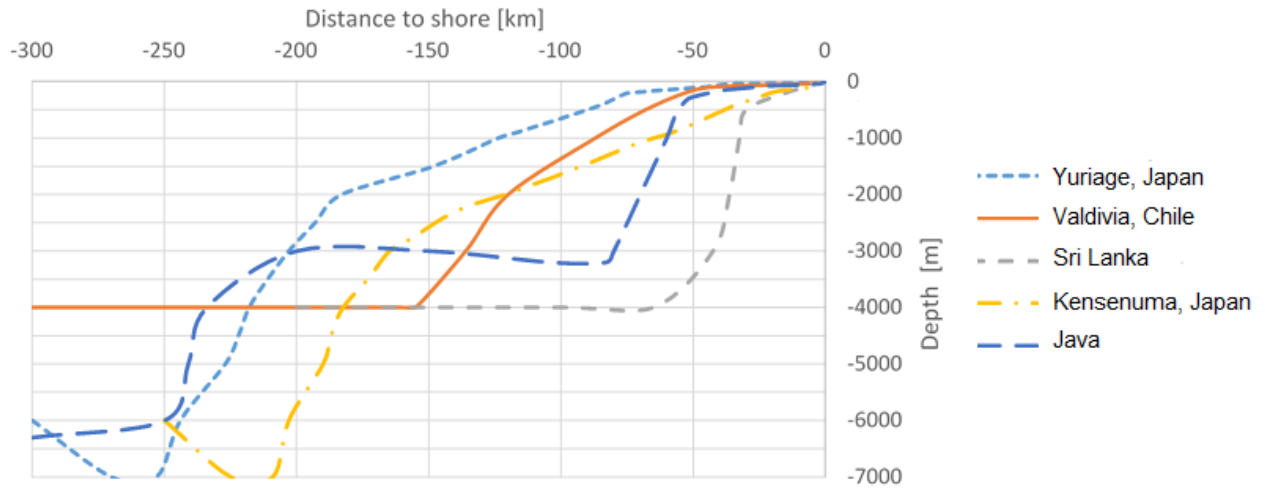
Figure 1.4: Cross-sectional bathymetry of Yuriage Japan, Kesennuma Japan, Valdivia Chile, Java and Sri Lanka [Navionics].
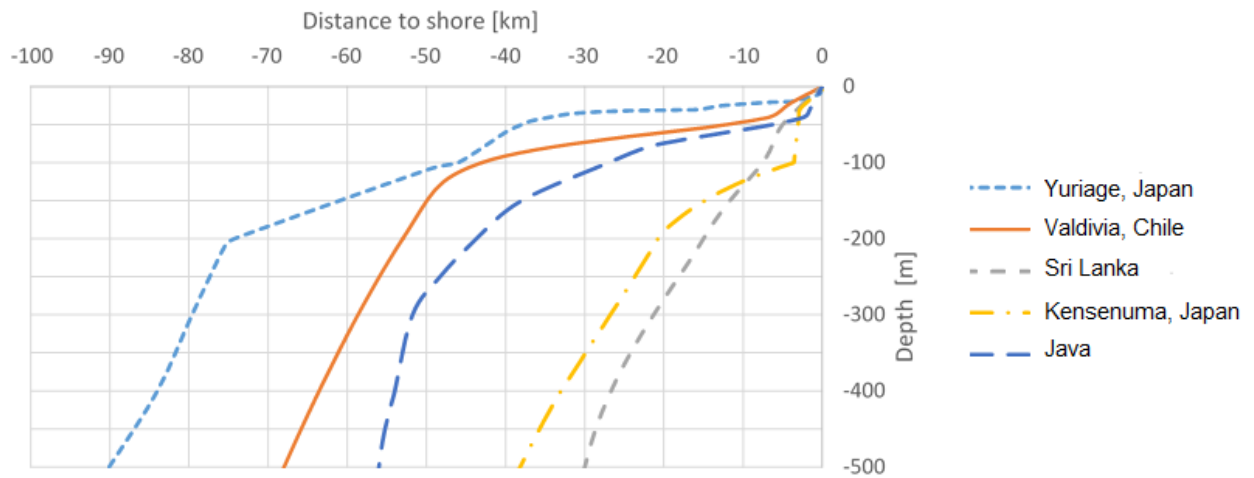
Figure 1.5: Near-shore cross-sectional bathymetry of Yuriage Japan, Kesennuma Japan, Valdivia Chile, Java and Sri Lanka [Navionics].

2.

Theoretical Background Information

2.1   Introduction to Tsunamis

A tsunami is a wave, or series of waves, generated by the sudden vertical displacement of a column of water. This water can be displaced due to seismic activity, explosive volcanism, a landslide above or below water, an asteroid impact, or certain meteorological phenomena. The term tsunami is Japanese for harbour wave [Bryant, 2008].

A tsunami is created by the displacement of a large body of water. An earthquake is in most cases the cause of this displacement. The earthquake that induces the largest tsunami is caused by a tectonic plate that slides beneath the adjacent plate. This is called a "subduction zone". These subduction zones usually have either land or shallow ocean on one side and deep ocean on the other side. This is for instance the case in Japan, where the Pacific Ocean lies on one side and the islands of Japan on the other side of the fracture line.
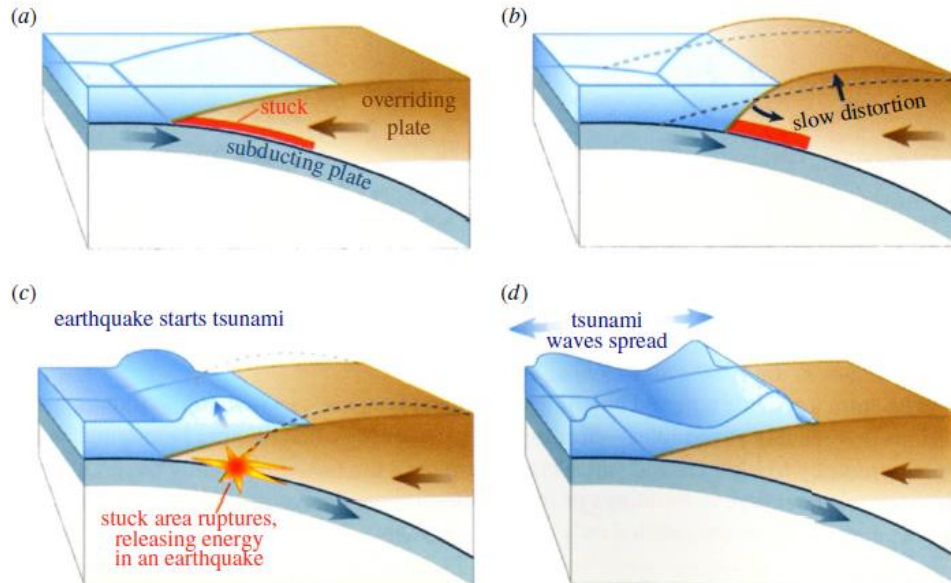
Figure 2.1: Tsunami caused by an earthquake in the subduction zone [Arcas and Segur., 2012].

Figure 2.1 shows the mechanism of a tsunami caused by a subducting plate. Figure 2.1.a: The plate slides beneath the adjacent plate until the two plates get stuck. Figure 2.1.b: The motion of the two plates continues but the subducting plate tends to drag the overriding plate down with it. The overriding plate bends and results in a stress that can build up for decades. Figure 2.1.c: The stress is too large for the stuck

area and releases all the energy and the edge of the plate jumps up causing a displacement of water. At the same time the lifted part of the plate drops down. Figure 2.1.d: The displacement of water generated a tsunami [*Arcas and Segur,* 2012]. The sea bed motion generates a depression travelling landward and an elevation travelling seaward. This is why the leading wave is mostly a depression in a tsunami event [Labeur et al., 2014].

2.2   Tsunami Characteristics

Tsunami waves differ a lot from storm waves or swell waves. Storm or swell waves dissipate their energy mostly in the surf zone while tsunamis lose little energy as they approach the shore and can run up much higher than storm waves. This behaviour is mainly due to the wave length that is several km for tsunamis. The wave length is of the same order as the length of the displaced area of the earthquake and can be 10 to 500 km long. Another important parameter of a tsunami is the wave period and is typically ranging from several minutes to hours. Waves with this period travel at speeds of 166 to 250 ms^{-1} offshore, 28 to 83 ms^{-1} on the continental shelf and 10 ms^{-1} at shore. [Bryant, 2008]

The shape of the wave is undergoing a transformation from offshore deep water to the shallow shore. In deep water the wave has a sinusoidal shape. The peaks and troughs are of the same height. When the wave crosses the continental shelf the wave peak sharpens and the trough flattens. This more peaked wave is mathematically described by stokes wave theory. The water particles in a stokes wave do not follow closed orbits, and mass movement of water due to the wave occurs. As the wave reaches the shore it becomes so peaked that the through disappears. The tsunami wave then becomes a solitary wave. Here all the water mass moves in the direction of the wave. In many tsunami waves there is a through proceeding the tsunami wave crest. Such waves are better described by N-waves [Bryant, 2008]. N-waves are not based on any theory, they are mathematically based to describe a wave that looks like a tsunami with a trough. The N-wave is created by multiplying a solitary wave with an inclined straight line.
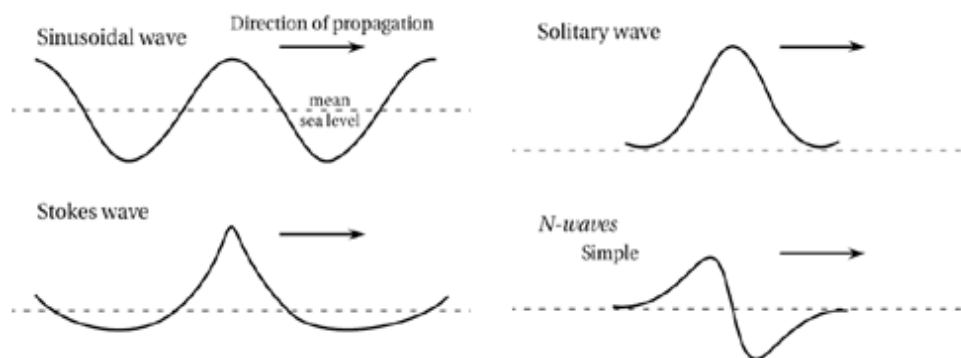
Figure 2.2: Schematization of different wave shapes [Bryant, 2008].

2.2.1 Solitary wave equation

The solitary wave was described by Boussinesq in 1972. Munk [1947], Dean and Dalrymple [1984], Madsen et al. [2008] and Horsten [2016] used the Boussinesq solitary wave in their study. The time series for the SWASH model to describe a solitary wave will be derived from the following formula [Schimmels et al., 2016]:

$$\eta(t) = H * sech^2(k * c(t - t_0))$$
[2.1]

Where η is the surface elevation, H is the amplitude of the wave, d is the initial water depth and k is the wave number. In the entire wave profile there is no η less than zero. The H therefore represents the height of the wave. To get a time series from equation 2.1, the propagation speed and wave number of the wave are required and are given in equation 2.2.

$$k = \sqrt{\frac{3}{4}\frac{H}{d^2}}, \qquad c = \sqrt{g(d + H)}$$
[2.2]

2.2.2 N-wave equation

A tsunami wave is generally preceded by a water depression. This is not represented in the solitary wave. A N-wave would be a better wave if the water depression will be included in the model. The N-wave however, has no mathematical connection to a real tsunami wave. The N-wave is a transformed solitary wave to make it look like a tsunami wave. The solitary wave is manipulated, by multiplying it with a linear line, until it has the desired shape. The wave can either have a leading depression or a leading crest followed by a water depression, depending on the slope of the linear line (Tadepali, 1994). An equation of the N-wave can be found in the report of Tadepali and Synolakis [1994] and is stated as follows:

$$\eta(x, 0) = (\epsilon * H)(x - X_2) * sech^2(\gamma_s(x - X_1))$$
[2.3]

Where $\varepsilon*H$ is a scaled N-wave amplitude, the distance $L = X_2\text{-}X_1$. A L of zero leads to a wave with equal trough and crest. For [γ_s] holds:

$$\gamma_s = \sqrt{\frac{3}{4}\cot H}$$
[2.4]

2.3   Propagation

Because of the long wave length, the ratio of water depth over wave length is very small (d/L < 0,05). This means a tsunami wave is a shallow water wave, even in deep water. The wave propagation can be expressed as $c \approx \sqrt{gd}$ and is therefore influenced by the water depth [Battjes and Labeur, 2014]. This influence of the water depth has effect on four processes: The increase of the wave amplitude due to the decrease in water depth near the coast (Shoaling), the change in wave direction due to the bathymetry (Refraction), the change in wave direction and attenuation due to islands and structures (Diffraction), and the wave reflection due to interaction with the coast or structures (Reflection) [Jager et al., 2015]. To model these effects a 2D model should be used.

2.3.1 Wave transformation

A tsunami has four different stages: the generation (see introduction to tsunamis), the propagation in relatively deep water to the coastal region, deformation in shoaling water up to breaking and run-up onto land.

The propagation from the generation area to the coastal region can take several minutes to several hours, depending on the distance. In deep water, the individual waves in a tsunami wave train have a large wave length of approximately a hundred km. Combined with the moderate wave heights in deep ocean, less than a meter, gives the waves a very low steepness. This causes that the waves can pass unnoticed by ships in deep ocean [Battjes and Labeur, 2014].
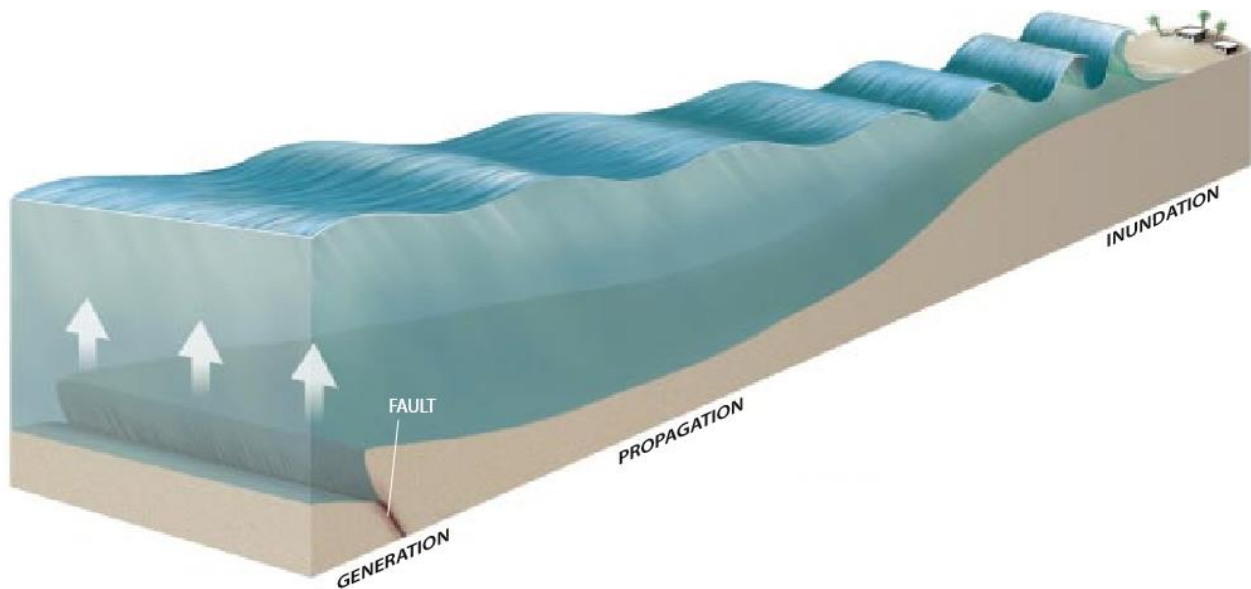
Figure 2.3: Wave transformation from generation area until shore [González, 1999].

2.3.2 Shoaling

When a tsunami enters water of decreasing depth the wave speed decreases, the wave lengths shorten and waves start to overtake one another, decreasing the distance between them. Wave energy will be concentrated in a smaller volume. This increased energy density steepens the wave and increases the wave height and currents, possibly up to the point of breaking [González, 1999]. This process is clearly illustrated in Figure 2.3 [González, 1999]. This process gives the tsunami wave most of its destructive power. The relation between the wave height and the water depth is known as Green's law [Camfield, 1980].

$$\frac{H_2}{H_1} = \left(\frac{h_1}{h_2}\right)^{0.25}$$
[2.5]

2.3.3 Breaking

Most tsunamis do not result in a giant breaking wave. They rather come in like very strong and fast-moving tides, i.e., strong surges and rapid changes in sea level. Then much damage is inflicted by floating debris and strong currents. When the wave reaches a point during shoaling where the steepness becomes too large, the wave will break. The wave then often forms a vertical wall of turbulent water called a bore.

2.3.3.1 Breaking characteristic solitary waves

Grilli et al. [1997] give breaking characteristics for solitary wave. This can be described with a dimensionless number. The slope parameter [S_0] is used where [H_0] is the initial wave height, [α] is the slope, [d_0] the initial water depth and [L_0] is the initial length scale of the wave.

$$S_0 = \frac{\tan \alpha * L_0}{d_0} = 1.521 \frac{\tan \alpha}{\sqrt{H_0}} \qquad [2.6]$$

This parameter determines what type of breaker will occur [Grilli et al., 1997]. The parameter is described in Figure 2.4.

- Surging breaker: $0.30 < S_0 < 0.37$
- Plunging breaker: $0.025 < S_0 < 0.30$
- Spilling breaker: $S_0 < 0.025$

Also the breaking depth can be calculated with this parameter with the following relationship (Grilli, 1997):

$$\frac{H_b}{h_b} = 0.841 \, exp \, 6.421 S_0 \qquad [2.7]$$

Where H_b is the wave height at breaking and h_b is the water depth at breaking.
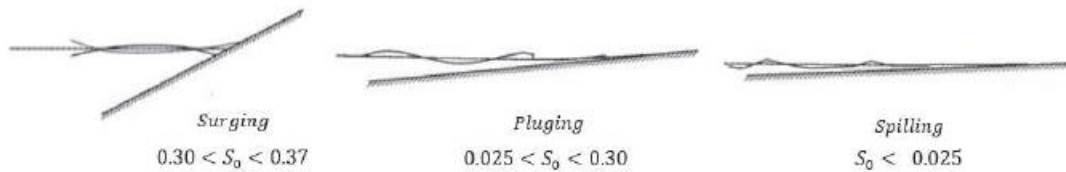
Figure 2.4: Breaker types [Bosboom and Steve, 2015].

The slope parameter S_0 is related to the Iribarren number [ξ] or the breaker parameter [Iribarren and Nogales, 1949]. Both dimensionless numbers determine what type of breaker will occur. By using equation [2.6] and $\xi = \tan \alpha / \sqrt{\dfrac{H}{L_0}}$ from Battjes [1974] the relationship between the slope parameter and the Iribarren number is derived.

$$\xi = \sqrt{\frac{H}{h_0 \tan \alpha}} \sqrt{S_0} \qquad or \qquad \xi = \sqrt{\frac{HL_0}{h_0}} S_0 \qquad [2.8]$$

2.3.3.2 Bore formation and soliton fission

Long tsunami waves can break into multiple short solitons, called soliton fission. Short waves split from the tsunami due to non-linearity and dispersion. In deep ocean and on the continental shelf the non-linearity is low and no solitons are formed.

During shoaling asymmetry increases and close to the beach the front face may become too steep and disintegrates into an undular bore [Madsen et al., 2008]. If the undular bore advances in decreasing depth, the interaction with the bottom results in the formation of a sequence of isolated solitons. This soliton wave train is attached to and propagating ahead of the bore [Ei et al., 2012]. Transitions from a bore to a leading soliton take time and therefore rarely happen due to geophysical constraints [Madsen et al., 2008]. Larger period waves are more likely to decompose than waves with smaller periods and equal wave heights [Matsuyama et al., 2007].

According to Madsen et al. [2008], these short waves on the tsunami break are usually not the tsunami itself. Most likely the run-up is not really influenced by breaking. This questions the relevance of breaking.

2.3.4 Run-up

Synolakis [1987] found a run-up law that gives an estimate of the run-up of non-breaking solitary waves, equation [2.9.a]. There is no run-up law for breaking solitary waves. There is a relationship given for the run-up of breaking solitary waves by Synolakis [1987], equation [2.9.b].

$$\frac{R}{d_0} = 2.831(cot\,\alpha_3)^{\frac{1}{2}}\left(\frac{H}{d_0}\right)^{\frac{5}{4}} \tag{2.9.a}$$

$$\frac{R}{d_0} = 0.918\left(\frac{H}{d_0}\right)^{0.606} \tag{2.9.b}$$

[R] is the vertical run-up, [d_0] is the offshore water depth, [α_3] is the linear onshore bottom slope and [H] is the tsunami wave height [Synolakis, 1987]. Tadepalli and Synolakis [1994] found a run-up law for n-waves. It is unclear which wave is the most accurate [Okumura, 2016].

2.3.5 Energy dissipation

While wind waves lose most energy in the surf-zone, the energy in tsunamis remains rather constant. This leads to large inundation depths and high run-up [Horsten, 2016].

Battjes [1986] derived an dissipation formula [2.10] for solitary waves and gentle slopes (α< 1:30), which is a spilling breaker according to [2.6]. Instead of a spilling breaker, he used a bore of the same height to estimate the dissipation. The formula is derived from the energy balance and is written as a function of the breaker condition [Battjes, 1986].

$$\tilde{H}^{-9/2} = \left(1 - \frac{1}{3}K'\right)\tilde{h}^{9/2} + \frac{1}{3}K'\tilde{h}^{-9/2} \tag{2.10}$$

Where [K'] is a dissipation factor, [$\tilde{H}$] and [$\tilde{h}$] are non-dimensional parameters for the wave height and depth depending on the breaking wave height and the corresponding depth.

$$\tilde{H} = H/H_b \qquad \text{and} \qquad \tilde{h} = d/d_b$$

With K'=32.4 the formula is empirically a good fit, in large part of the dissipation region, with data for solitary waves breaking on a 1:100 slope [Battjes, 1986]. The Battjes model shows the energy is completely

dissipated at the shoreline, however, due to run-up there is still energy at the shoreline. The Battjes model does not give a good prediction at the shoreline, which is the study area of this thesis.

2.4   Current design methods

Flood defences in Japan were always designed based on worst case scenarios. In this approach the return period is not taken into account. After the 2011 tsunami, there has been an improvement in the design tsunamsi. Two levels based on political decisions, with insight from coastal engineers, were identified for tsunami events [Shibayama et al., 2013]. A level 1 event has a return period of 100+ years and a level 2 event has a return period of a few 100 to a few 1000 years.

The coastal structures have to protect human lives and property against level 1 events. The wall can provide more time for evacuation. For level 2 events measures like evacuation buildings and shelters are most important. Also during a level 2 event no structural damage may occur on the coastal structure, however, overtopping can occur. Evacuation is still required during a tsunami event of any level and information on tsunami heights is therefore not provided.

Okumura [2016] used a risk based approach based on the data extrapolated from historical events, and designs according to chosen failure probability [Okumura, 2016]. This approach can be used if sufficient historical data is available. The categorization of 2 levels is mainly used because of the low frequency of occurrence.

2.4.1   ASCE - Tsunami loads and effects

A new coastal defence structures design method is introduced by the American Society of Civil Engineers [ASCE, 2016]. The ASCE 7-16 Tsunami loads and effects chapter provides loads and other requirements for tsunami and its effects. The ASCE standard defines results of a Probabilistic Tsunami Hazard Analysis (PTHA) embodied in offshore tsunami amplitude maps. PTHA generates large probabilistic catalogues of tsunami waveforms from the source to the offshore regime of the coastline. These maps are defined at a standardized depth of 100m and give the offshore tsunami period and amplitude above sea level of a probabilistic maximum tsunami. These maps are applicable in five states of the United States . [Chock, 2016].

The ASCE [2016] also gives a method to calculate the tsunami loads on a structure and the velocities at the location of a structure.

The velocities of the tsunami waves that run-up the coast are calculated based on the run-up. This run-up can be calculated with a Surf Similarity parameter [ξ_{100}] calculated from the predominant tsunami wave period [T_{TSU}] and the offshore tsunami amplitude [H_T] at 100 meters depth. The surf similarity parameter is calculated with equation [2.11].

$$\xi_{ASCE} = \frac{T_{TSU}}{\cot\phi} \sqrt{\frac{g}{2\pi H_T}} \qquad\qquad [2.11]$$

[Φ] is the mean slope from 100 meter depth to mean water level at the coast. With Figure 2.5 the run-up height [R] can be found.
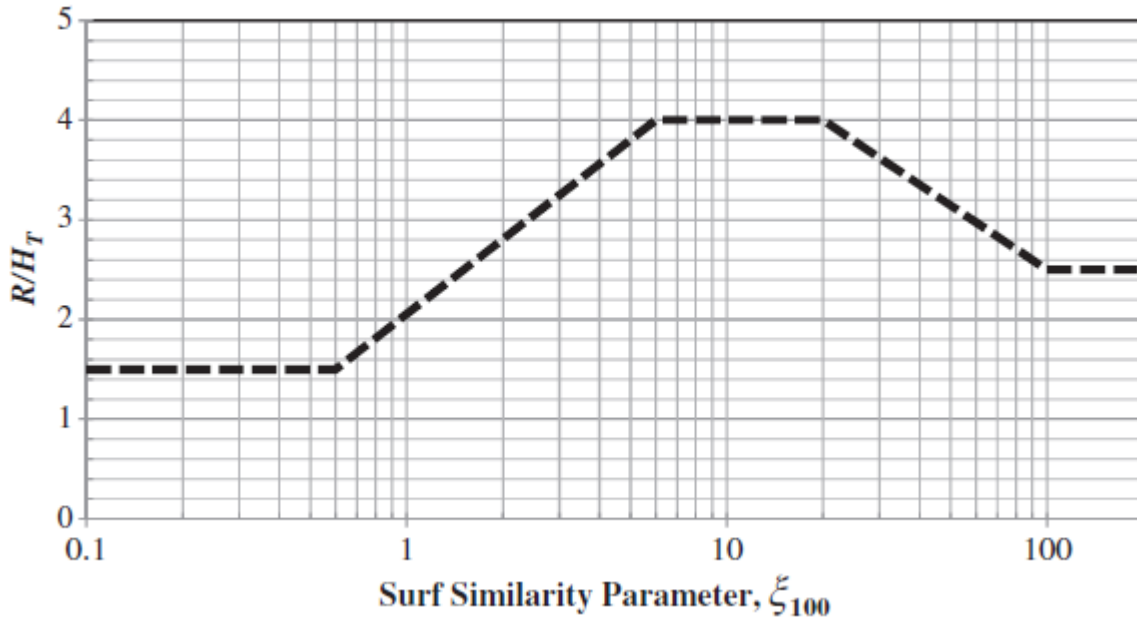
Figure 2.5: Run-up ratio R⁄H_T , as a function of the mean slope of the Surf Similarity parameter ξ_{100} [ASCE, 2016].

In the ASCE [2016] norm the maximum velocity is calculated based on the maximum run-up and the inundation depth. Calculated flow velocity cannot be taken less than 3.0 m/s and not be taken as greater than the lesser of $1.5 * \sqrt{gd}$ or 15.2 m/s.

The maximum flow velocity [u_i] and the maximum inundation depth [$H_{max,inun}$] along the ground elevation profile up to maximum run-up are determined using the Energy Grade Line Analysis. In this analysis the ground transect from the maximum run-up point to the coast line is divided in segments with horizontal distance [Δx_i] and a Manning's coefficient [n] corresponding to the terrain segment. The velocity at every segment is calculated with equation [2.12] starting at point of maximum run-up.

$$E_{g,i} = E_{g,i-1} + (\varphi_i + s_i)\Delta x_i = H_{max.inun} + \frac{u_i^2}{2g} = H_{max.inun}(1 + 0.5Fr_i^2) \qquad [2.12]$$

Where [$E_{g.i}$] is the hydraulic head at point *i*, [$H_{max.inun}$] the inundation depth at point *i*, [ϕ_i] is the average ground slope between points *i* and *i-1*. [Fr_i] is the Froude number at point *i* and [s_i] is the Friction slope of the energy grade line between points *i* and *i-1* and depends on the manning's coefficient and the Froude number. At the point of maximum run-up the hydraulic head is zero. The Froude number is calculated according to $Fr_i = \alpha(1 - \frac{x}{x_R})^{0.5}$. A Froude number coefficient [α_{Fr}] of 1.0 shall be used and for tsunami bores a value of 1.3 shall be used. According to ASCE [2016], tsunami bores shall be considered where the prevailing nearshore bathymetry slope is 1:100 or milder or where this is historically documented.

For structures with a high risk category a site-specific Probabilistic Tsunami Hazard Analysis (PTHA) needs to be performed [ASCE, 2016].
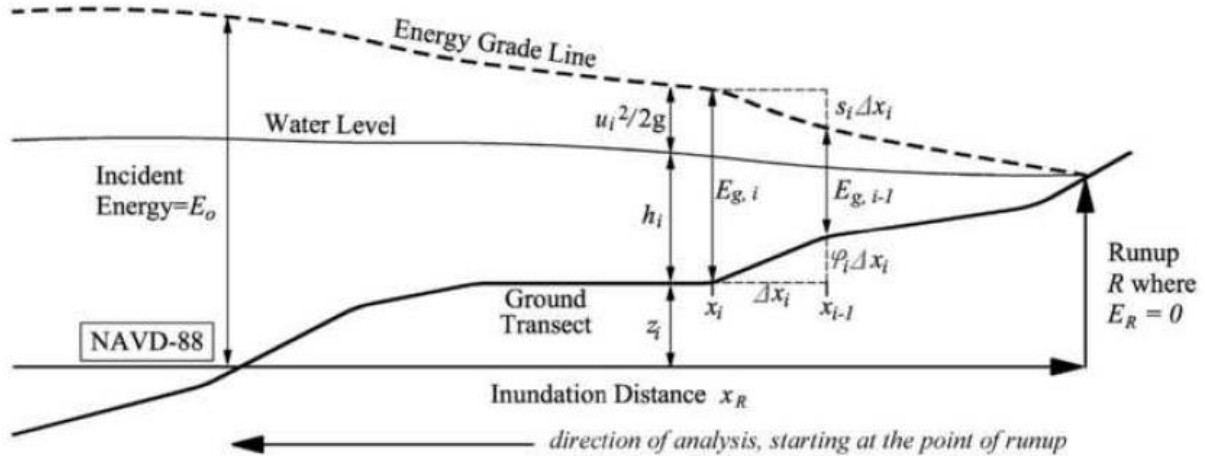
Figure 2.6: Energy method for overland tsunami inundation depth and velocity [ASCE, 2016].

2.5 Forces of incoming bore on a seawall

2.5.1 Hydrodynamic force

Three theories to calculate the force, per meter width, of the incoming bore on the wall are shown here. The first theory by Ramsden and Raichlen [1990] depends on the height [H_{bore}] of the bore and can be estimate by 7.5 times the hydrostatic force of the incoming bore height [Ramsden and Raichlen, 1990].

$$F_{Ramsden} = 7.5 * \frac{1}{2} \rho_w g H_{bore}^2$$ [2.13]

In the experiments of Ramsden and Raichlen a soliton wave is generated by a wave paddle and the forces of the bore that follow are measured. This bore is not followed by a large wave as in an actual tsunami. The height of the bore [H_{bore}] is defined as height at the instant its tip strikes the wall. This is still not a clear height and leads to confusion. The height of the bore is difficult to define for a tsunami with this theory. The bore height for which the theory of Ramsden is valid is unclear. It is only stated that it is valid for large bores.

The more recent second theory of FEMA [2012] depends on the maximum momentum flux per unit mass per meter width [$(Hu^2)_{max}$] of the incoming bore. Here not only the bore height but also the velocity is part of the equation [FEMA, 2012]. Note that $(Hu^2)_{max}$ is not equal to $H_{max}u_{max}^2$. The value for $(Hu^2)_{max}$ comes from the largest combination of h and u that occur at the same time during the tsunami.

$$F_{FEMA} = 1.5 * \frac{1}{2} C_d \rho_w (Hu^2)_{max}$$ [2.14]

C_d is the drag coefficient and is advised to be equal to 2. There is a significant difference in magnitude for the two theories. This is because the Ramsden theory depends on the bore height only while the theory of FEMA also depends on the velocity.

The ASCE [2016] also gives a tsunami force based on the inundation depth and the velocity calculated with the Energy Grade Line Analysis in section 2.4.1. The theory looks like the theory of FEMA although it is not

the same. This theory calculates the momentum flux at maximum inundation and the maximum velocity at the specific location and not the maximum combination of $(Hu^2)_{max}$. The tsunami loads are calculated with equation [2.15].

$$F_{ASCE} = \frac{3}{4}\rho_s I_{tsu} C_d (H_{imax.inun} u_i^2)_{bore}$$ [2.15]

Factor [I_{tsu}] is the importance factor and is 1.25 for a high risk category [ASCE,2016]. From these three theories it is clear that the height and the velocity are the important parameters to find the forces on a seawall.

2.5.2 Hydrostatic force

Another large force on the wall is the hydrostatic force when the water level is high. The highest water level is at maximum inundation [$H_{max.inun}$], although the flow velocity is low at this time. The horizontal hydrostatic force per meter width on the wall can be computed with [2.16]. In the condition where the flow overtops the wall, [$H_{max.inun}$] is replaced with the height of the wall [h_{wall}] [ASCE,2016].

$$F_h = \frac{1}{2}\rho_s g H_{max.inun}^2$$ [2.16]

2.5.3 Wall height

Esteban et al. [2017] did laboratory experiments to find the design height of the seawall. He found that the energy head, equation [2.17], of the incoming bore is very important for the overtopping. It should be mentioned that this equation only holds for stationary flow which is not the case for a bore. The relationship that is found is still interesting. To know if inundation occurs behind the structure, also the energy should be considered and not only the bore height.

$$E_{g.i} = \frac{v_{front}^2}{2g} + H_i$$ [2.17]

According to the experiments of Estebal et al. [2017] can the relationship between the incoming bore height [H_i] and the inundation height behind the seawall [H_{behind_wall}] be expressed with the following empirical relationship:

$$H_{behind\_wall}/H_i = \tanh\left(0.51\frac{E_i}{h_{wall}} - 0.36\right)$$ [2.18]

[h_{wall}] is the height of the seawall. This equation should be considered valid between 0.2< H_i/h_{wall} <1.3.

3.

SWASH Simulations

The model tool that will be used in this thesis is SWASH. This is short for Simulating WAves till SHore. Many other tools are possible for this kind of research. However, SWASH seems the most appropriate tool because it is possible to do tests on a large variety in scales. The model can be used from the tsunami generation area until the shore or close to the shore. SWASH is developed at the Technical University of Delft.

SWASH is a numerical tool for simulating unsteady, non-hydrostatic flow phenomena in coastal waters driven by waves. SWASH is a phase resolving wave model and is capable of simulating a large number of phenomena in the nearshore. SWASH is based on the nonlinear shallow water equations including non-hydrostatic pressure correction, and it thus not a Boussinesq-type wave model. The vertical structure is included either by depth averaged mode or by a multi-layered mode. The accuracy of the frequency dispersion in the SWASH model increases with an increasing number of layers. This model has good lineair frequency dispersion up to $kd < 7$ (k and d are the wave number and the water depth, respectively). The input file of the SWASH model is shown in appendix E [The SWASH team, 2017].

3.1   Series of simulations with SWASH

In this thesis several simulations will be conducted to find answers on the research questions stated in section 1.2. Different tests with SWASH will be performed. The simulations are divided in different test series. A description of the simulations is listed below, including what parameters will be altered and what the goal of the simulations is:

Model validation and calibration:

1. The model will be validated with the Yuriage, Japan case study. The type of wave used is a raise of the water level obtained from measurements during the 2011 Tohoku tsunami. This will also done to calibrate the model.
2. Tests of soliton waves breaking on slopes [Grilli et al. 1997] will be reproduced to validate the SWASH model for wave breaking and to see if the model can produce stable soliton waves with dispersion effects.

Influence of bathymetry and wave on the tsunami:

3. The influence of the seabed characteristics on the development of the waves is tested. The geometric parameters that were tested are the foreshore slope [α_1], the offshore depth [d_0] and the offshore wave length [L_0]. The results of these simulations is used in simulation series 4.

4. The slope α_2 of the shore will be varied. This test should tell if the wave breaks and develops a bore or that the wave just runs up and down the slope. It is important to know whether or not a bore forms because it has influence on the forces on the seawall. Different lengths of the tsunami generation area, or wave lengths, and different slopes α_2 will be simulated to see if this has influence on the formation of a bore. This will be analysed in chapter 4.

The Results of the bore simulations are analysed in chapter 5. From this the velocities and wave heights, at possible locations of the wall, are studied.

3.2   Yuriage case: Validation and calibration of SWASH model

The SWASH model will be validated with a reference case study at the city of Yuriage, Japan. In this area a lot of data is available from the 2011 Tohoku tsunami. The Yuriage/Sendai case study is also investigated by Okumura [2016] and Horsten [2016]. Their findings are also used for validation of SWASH. In section 3.2.1 to 3.2.4 is the SWASH simulation compared to measurements from the 2011 tsunami for validation. This case will also be used to calibrate the roughness parameter used in the model in section 3.2.4. This is done by comparing the run-up in the model with observed run-up during the 2011 Tohoku tsunami.

To validate the SWASH model, various steps in the wave transformation will be compared with measurements of the 2011 Tohoku tsunami, or with analytical theories from chapter 2.

The bathymetry profile of Yuriage, obtained from Navionics in chapter 1 and the profile used by Okumura [2016] and Horsten [2016], is used in the SWASH model, figure 3.1.a. This profile is chosen because it runs close to a GPS and a coastal wave gauge, Figure 3.2. The data of these gauges is obtained from NOWPHAS and the buoys are deployed by the Port Airport Research institute (PARI).
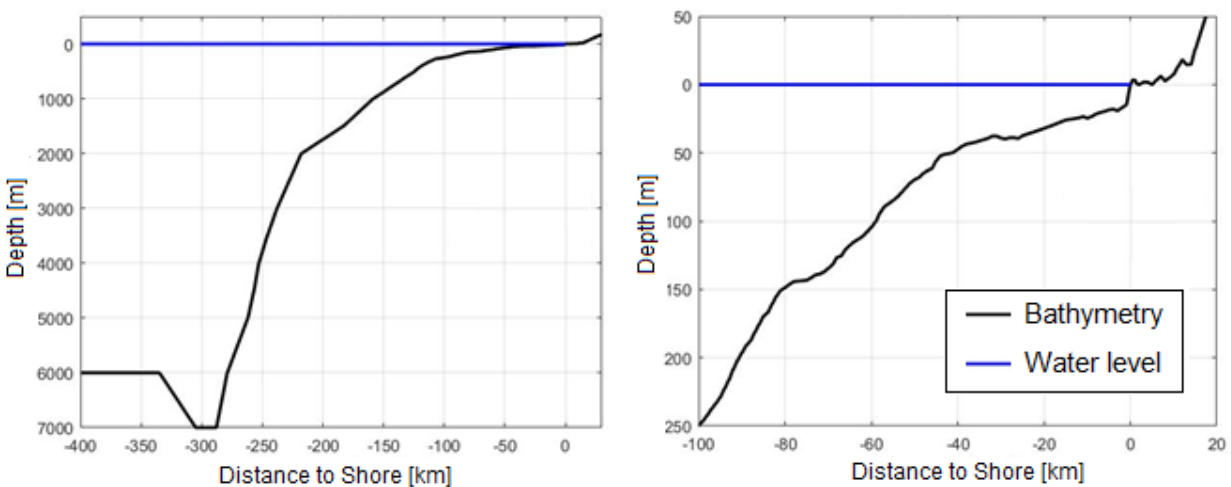
Figure 3.1: Left: Bathymetry of the Yuriage case. Right: Bathymetry of the Yuriage case nearshore.
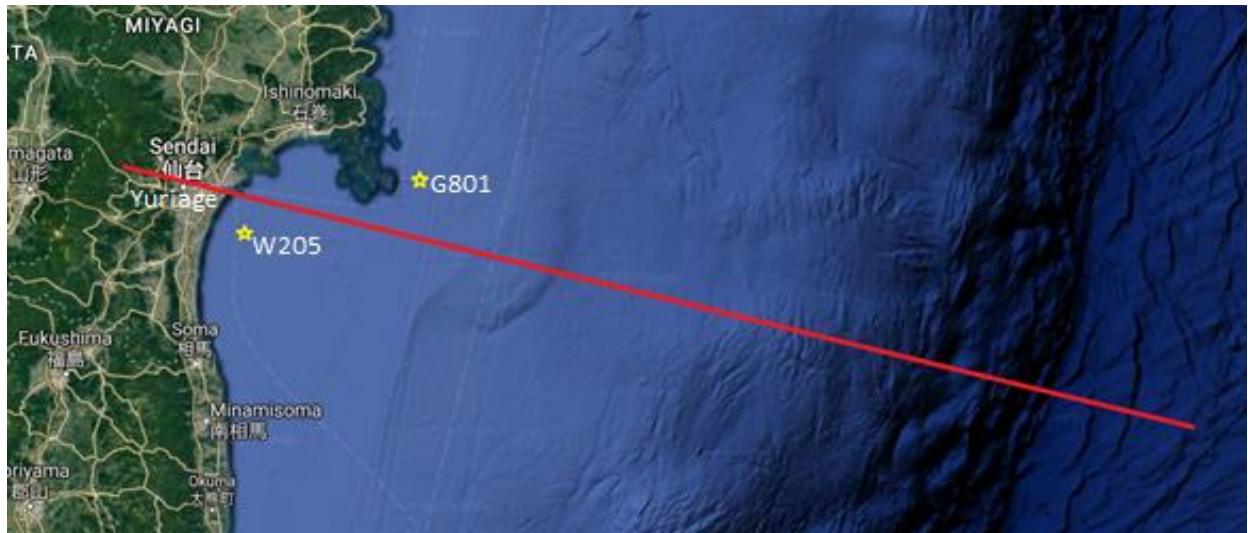
Figure 3.2: Top view of Yuriage coast. Red line: model trajectory, yellow: wave gauges.

The validation of the model is done with an elevation of the water level that simulates the effects of the earthquake. An initial water elevation is used to simulate the 2011 Tohoku tsunami. The elevation of figure 3.3 is obtained from Saito et al. [2011]. This elevation is a reconstruction of the water elevation of the 2011 Tohoku tsunami using available gauge data. The water level elevation that is used for the SWASH simulations is constructed from this wave reconstruction and shown in Figure 3.3.

Figure 3.3: Elevation input of SWASH, of the Tohoku Tsunami 2011 after interpolation.

Figure 3.4: Initial wave height distribution. Epicenter plotted by star [Saito et al., 2011].

3.2.1   Time series at wave gauges

The results from the SWASH simulation is shown in Figure 3.5 at two locations. The time series of the wave is plotted next to the gauge measurements of wave gauge G801 and W205 at 58.6 and 4.2 km from the shore, Figure 3.5. Wave gauge G801 and w205 give a maximum wave height lower compared to the model. However, the maximum wave heights are of the same order. There are a lot of uncertainties about the initial wave and the bottom profile that could give this height difference.

The wave gauge w205 stopped measuring when the tsunami passed. It is unclear if this is the maximum value at this location or if the actual wave was higher. The SWASH model is breaking at the location of the wave gauge w205. This could explain why the wave gauge broke and stopped measuring.
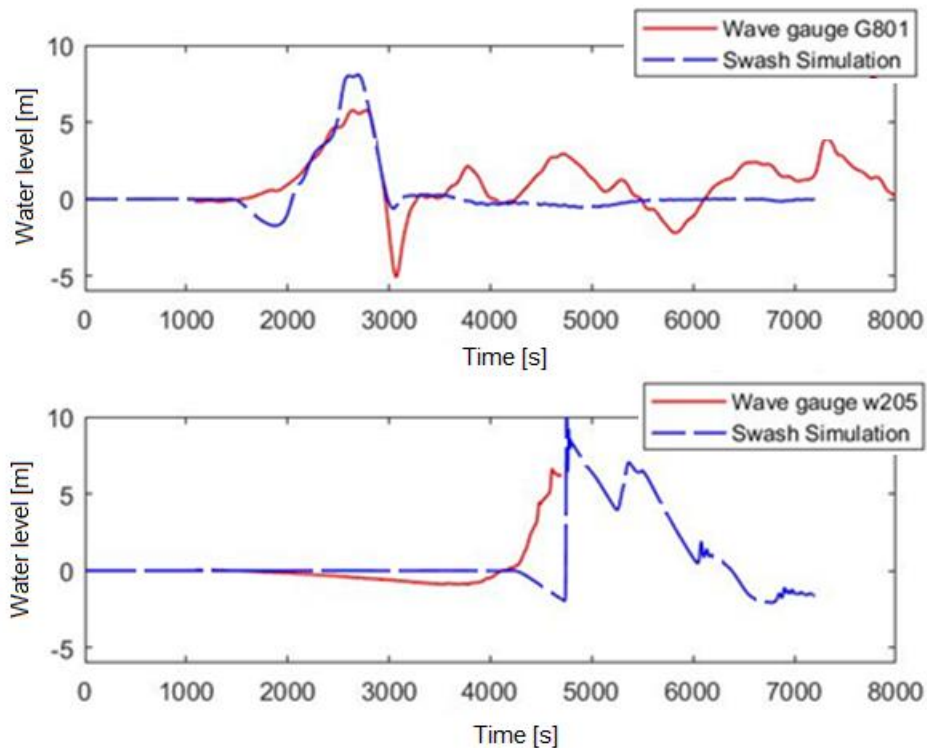
Figure 3.5: Comparison of SWASH model with wave gauges. Wave gauge w205 stopped measuring during the tsunami. Top: Time series at 60 km offshore. Bottom: Time series 4 km offshore.

3.2.2   Shoaling

The shoaling of the SWASH model is compared with the Green's Law [section 2.3.2.] and with the measurements of the GPS wave gauges GB801 and WG205 (Figure 3.6). The maximum water level of the tsunami wave (black line) at every location is used as the wave height of the wave. The green line shows the analytical Green's law. The SWASH simulation with the water elevation is, according to Figure 3.6, a rather good match with Green's Law and also with the G801 wave gauge. At approximately 20 km from the shore the wave starts breaking.
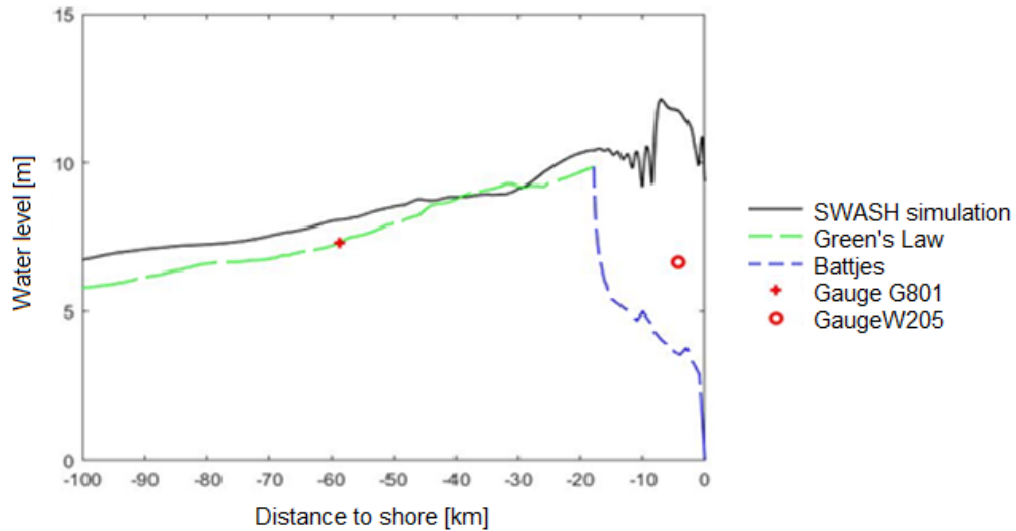
Figure 3.6: Shoaling of the SWASH model compared to the Green's Law, the Battjes [1986] Dissipation and the wave gauges.

3.2.3   Dissipation

The energy dissipation of the wave is compared with the dissipation formula of Battjes [1986] [equation 6.10] and with the wave gauge (w205) at 4 km from the shore, Figure 3.6.

The amount of dissipation does not coincide with the Battjes model [1986]. According to the Battjes model [1986] the energy should dissipate starting at the breaking point. The tsunami wave in the model, initially does not dissipate much energy. The wave height in the model is better when compared to the wave gauge. This measured data is from an actual tsunami wave and therefore a better indicator if the model works. Due to the long wave lengths the waves do not dissipate as much energy as in the Battjes model [1986].

Although the simulated water elevation wave is still higher than the measured gauge value at 4 km from the coast, it seems to be realistic. Note that the gauge stopped measuring and is thus at least this height or probably even higher. Not all the energy in the wave is dissipated when the wave reaches the shore line. The energy that is not dissipated then remains in the transported water onshore.

3.2.4   Run-up

The inundation height of the 2011 Tohoku tsunami was between 5 and 15 meters and the run-up distance [x_R] was between 6 and 7 km, according to Horsten [2016]. This is the inland distance that was reached by the wave. At the shore the inundation depth was about 13.7 meters, as can be seen in Figure 3.7. Figure 3.8 shows the run-up distance and inundation depth for SWASH models with different Manning roughness coefficients for the onshore locations. Kaiser et al. [2011] give the Manning friction coefficient for multiple types of land covers to use for tsunami modelling. Their Manning roughness coefficient ranges from 0.4 $m^{-1/3}$s for buildings to 0.03 $m^{-1/3}$s for barren land. This calibration is done to find the roughness that can be used in further simulations. Both roughness coefficient 0.04 $m^{-1/3}$s and 0.06 $m^{-1/3}$s have a run-up distance between 6 and 7 km. However, a coefficient of 0.06 will be used in further simulations because the inundation depth at the shore is about 13.7 meters. A coefficient of 0.06 $m^{-1/3}$s is stated by Kaiser et al. [2011] as a middle density urban area. The town of Yuriage, can be described as a low density urban area.

Then a factor of 0.04 m$^{-1/3}$s would be appropriate. However, a middle density urban area is more common to be protected with a coastal defence structure.
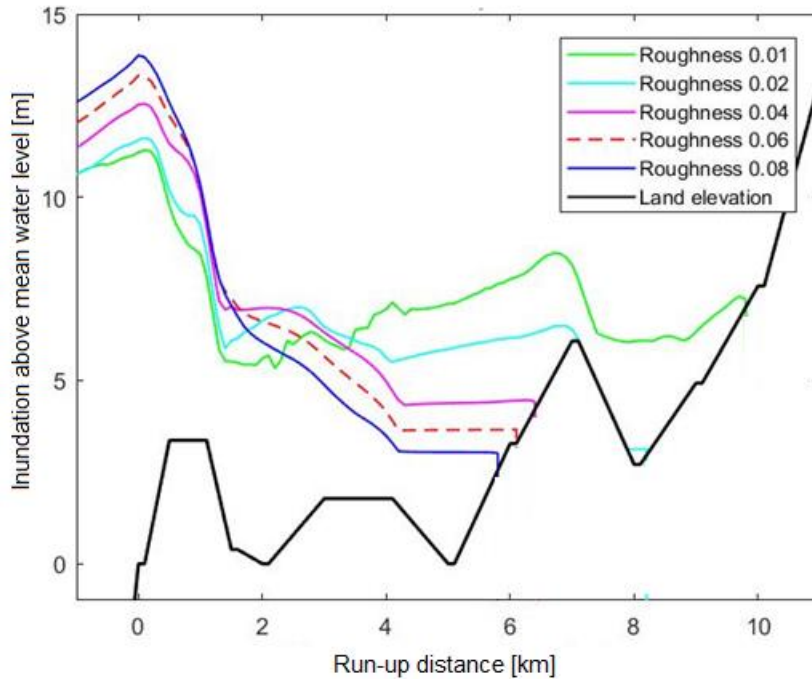
Figure 3.8: Inundation depth of SWASH model with different roughness's. Bottom slope obtained from Okumura [2016].

Figure 3.7: Monument at Natori coast, inundation depth is shown on the monument.

3.3   Soliton breaking criterion small scale simulations

In this series of simulations the goal is to reproduce the research on the breaking criterion of solitary wave by Grilli et al. [1997]. This is done to validate the SWASH model for breaking. The tests of Grilli et al. [1997] are chosen because the area of interest in this research is breaking close to the shore line. This is also the area of interest in this thesis. In this section the results are shown of the SWASH model and are compared to the results from Grilli et al. [1997]. The SWASH simulation should have a stable soliton with a horizontal bed. This simulation series will show that the soliton wave is stable in SWASH. More results are shown in appendix A.

Grilli et al. [1997] tested the breaking of solitary waves on different slopes [s]. With slopes ranging from 1:100 to 1:8 and wave heights 0.2m 0.4m and 0.6m. The solitary waves were formed at a water depth of 1 meter. A sketch with definitions of different parameters is given in Figure 3.9.
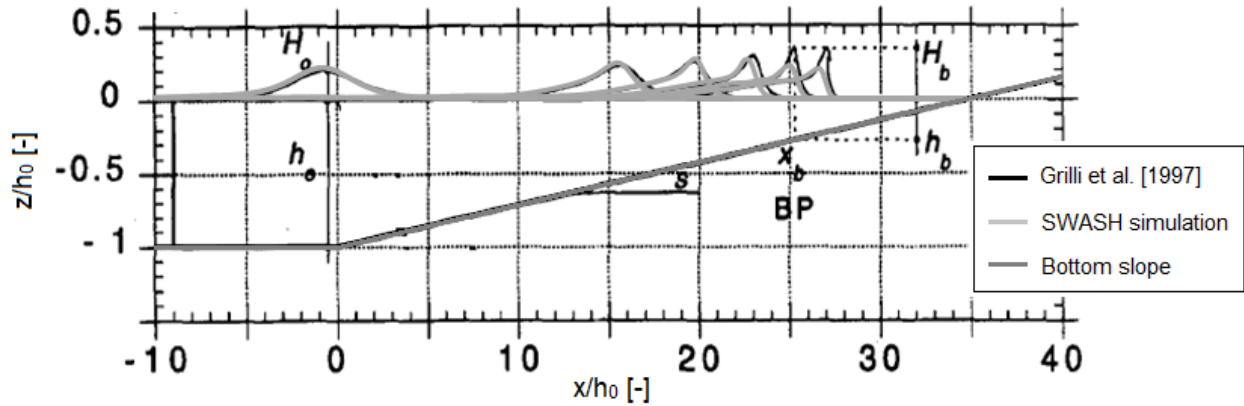
Figure 3.9: Definitions of calculation of solitary wave of height H_0 with shoaling and breaking over slope s [Grilli et al. 1997].

3.3.1 SWASH simulations

Nine simulations are done to validate the SWASH model. A solitary wave height [H_0] of 0.2, 0.4 and 0.6 are used on an 1:100, 1:35 and 1:8 slope [s]. The simulation is done with a time step of 0.01s and a grid cell of 0.1m. The time series of the soliton is calculated with equation [2.1] and used as input for the simulations.

The breaking point is of interest in this test. At this point the breaking height [H_b], the breaking depth [h_b] and the breaking location [x_b] can be found. For all simulations these three parameters are calculated and shown in Table 3.1. The parameters found by Grilli et al. [1997] are also given in Table 3.1.

slope	Ho [m]	Grilli et al. [1997]			SWASH		
		H_b [m]	h_b [m]	x_b [m]	H_b [m]	h_b [m]	x_b [m]
1:100	0.2	0.36	0.34	66	0.32	0.45	55.4
	0.4	0.63	0.60	39	0.48	0.66	33.8
	0.6	0.78	0.76	24	0.60	0.81	18.9
1:35	0.2	0.36	0.25	26	0.28	0.36	22.4
	0.4	0.59	0.43	20	0.46	0.58	14.6
	0.6	0.75	0.57	15	0.58	0.74	9
1:8	0.2	-	-	-	0.23	0.18	6.6
	0.4	0.41	0.08	7.4	0.41	0.41	4.7
	0.6	0.59	0.13	7	0.55	0.56	3.5

Table 3.1: Breaker height, Breaker depth and breaker location for the test by Grilli et al. [1997] and the SWASH simulations.

For all three slopes and a H_0 of 0.2 and 0.4 meters the result of the simulation is shown in Figure 3.11 and 3.12. The wave at which breaking starts is shown and is plotted with the results of Grilli et al. [1997]. The thick lines are given by the output of SWASH and show that breaking occurs. This parameter from SWASH is used to find the breaking waves in the simulations. In Figure 3.10, the results of the SWASH simulation are shown, for the 1:35 slope and H_0 is 0.2m, plotted over the results from Grilli et al. [1997].
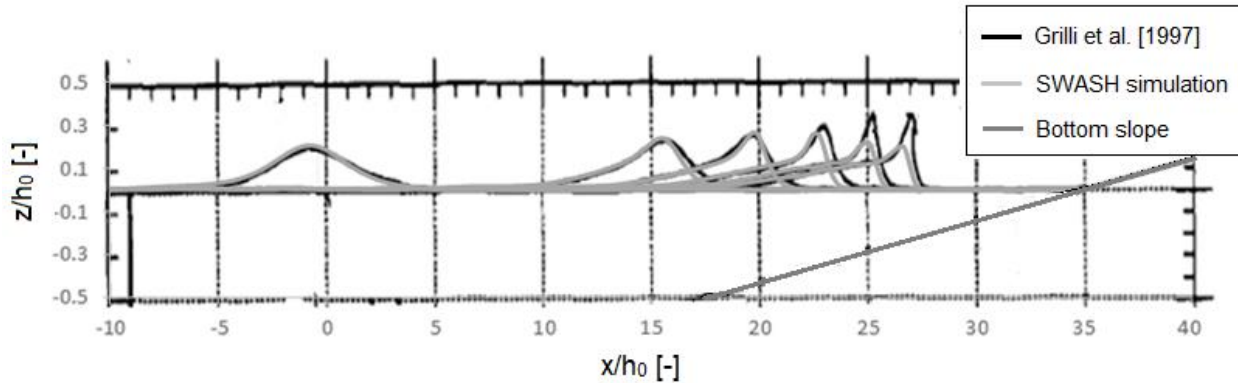
Figure 3.10: Wave from SWASH simulation plotted over results from Grilli et al. [1997]. Grey: Simulations. Black: Grilli et al. [1997].

The results of the simulations give a rather good result when compared to the test from Grilli et al. [1997] in Figure 3.10. This is the same test as in figure 3.12.b. The simulated wave has the same shape at $x/h_0 = 0$ as Grilli's tests. Up to $x/h_0 = 22.5$ is the result the same. At this point the wave in the SWASH simulation starts to dissipate energy and drops in height while the Grilli et al. [1997] tests continue shoaling.

The breaking height has on average a difference of 20% as shown in Table 3.1. The differences are around 20% for waves with a mild slope, while the simulations with a steep slope only differ 3%. This is mainly due to the breaking location. In the SWASH simulations, the wave starts breaking in deeper water compared to the Grilli et al. [1997] test. This difference is larger for a steeper slope. For the 1:100 slope simulations the wave breaks approximately at 0.06m deeper water compared to the Grilli et al. [1997] tests, while this is 0.15 for the 1:35 slope. This is even 0.35 m deeper for the 1:8 slope. In the 1:8 slope simulations the breaking location is quite far off. The results are still rather good for the mild slopes and SWASH simulates the soliton waves in this small scale test close to the results of Grilli et al. [1997]. The results are best for simulations with a mild slope while the accuracy gets less for higher waves.

The soliton before breaking is equal to the Grilli et al. [1997] tests. This solitons are stable and the simulation shows that the dispersion in model is good. Also the speed of the wave is in the simulations is good because the front of the wave is at the same location as the tests. However, the wave height at the breaking point is not good in the SWASH model. There is possibly a vertical acceleration that is not modelled.

3.3.2   Breaking in SWASH

The waves of the SWASH simulations in Figure 3.11 break earlier compared to Grilli's test. This is due to how the breaking is calculated by SWASH. By using a hydrostatic pressure distribution around the location of breaking, the model will correct dissipation for models with low vertical resolution. The location of breaking is when the slope or steepness of the free surface is larger than a factor $\alpha = 0.6$. The factor of 0.6 is advised by Smit et al. [2013]. This corresponds with a local front slope of 25%. SWASH calculates the steepness criterion in terms of surface rise, when the vertical speed of the free surface exceeds equation [3.1]. Then the wave is considered breaking.

$$\frac{\partial \eta}{\partial t} > \alpha \sqrt{gd} \qquad\qquad [3.1]$$

The non-hydrostatic pressure in the corresponding grid points is then neglected. A point becomes non-hydrostatic again if the crest of the wave has passed. For neighbouring grid points of a breaking grid point the criterion of breaking is reduced to equation [3.2] with β = 0.3.

$$\frac{\partial \eta}{\partial t} > \beta \sqrt{gd}$$ [3.2]

The first wave that is breaking according to equation 3.1 and 3.2 is shown in Figure 3.11 with a thick line where breaking occurs. The breaking by Grilli et al. [1997] starts when a vertical tangent is reached. This is never the case in SWASH. Several simulations with values of α up to 0.8 have been performed. The wave starts breaking at the same location for all simulations and changing this value does not change the results [Smit et al, 2013].

The breaking at larger depth could also be due to friction. The Manning roughness coefficient is reduced, in one simulation from the default value of 0.019 $m^{-1/3}$s to 0.001 $m^{-1/3}$s. This is done to see if this has effect on the breaking. However, the SWASH results show very small differences and for the breaking location there is no significant effect.

3.3.3 Run-up

Another validation of the model with the run-up law by Synolakis was not possible. This validation was to see if the SWASH model gives the correct run-up. The run-up law is given in equation [2.9]. This law is for non-breaking waves. The relationship for breaking waves, equation [2.9.b], is also not good for validation because this equation is not dependent on the slope. The SWASH results show large dependency on the slope. The steep 1:8 slope reaches a run-up of 0.54 m while the mild slope 1:100 reaches a run-up of 0.085 m for a 0.2 m high soliton. This difference is quite significant and the equation of 2.9 can therefore not be used to analyse the run-up.
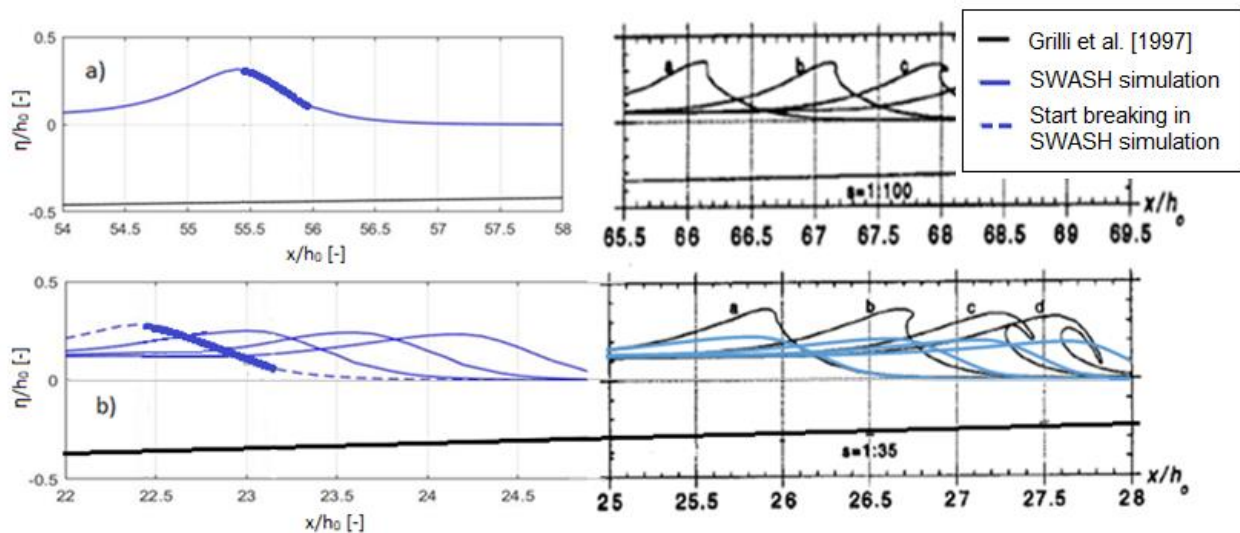
Figure 3.11: Simulation of solitary wave with H_0 = 0.2m and a) s = 1:100, b) s = 1:35 and Grey area and between green vertical lines show the first moment wave breaking starts to take place. Blue line on the left is the SWASH simulation. Black lines on the right show the Grilli et al. [1997] results. Line a is the first breaking wave of Grilli et al. [1997]. Dotted line in figure b shows where breaking starts in the SWASH simulation. Thick line shows breaking by SWASH.
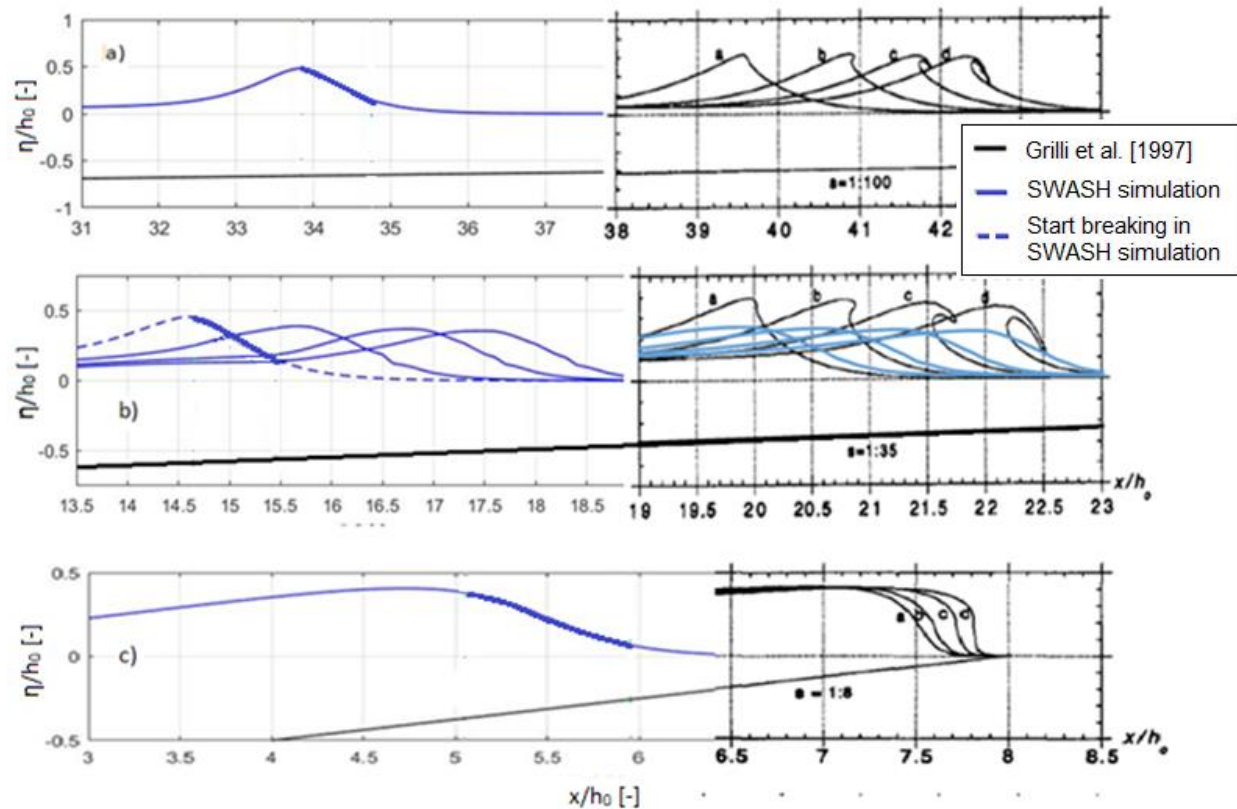
Figure 3.12: Simulation of solitary wave with H_0 = 0.4m and a) s = 1:100, b) s = 1:35 and c) 1:8. Blue line on the left is the SWASH simulation. Thick blue line shows where the wave breaks for the first moment of breaking. Black lines on the right show the Grilli et al. [1997] results. Line a is the first breaking wave of Grilli et al. [1997]. Dotted line in figure b shows the wave when first breaking starts.

3.4   Conclusion

The SWASH model is validated for two cases. The Yuriage, Japan case validates the SWASH model on large scale with data from the 2011 Tohoku tsunami. The SWASH results are in good agreement with the tsunami data and analytical theories. The second case is the soliton breaking criterion by Grilli et al. [1997]. These SWASH simulations show a stable soliton, except for the details of the breaking wave crest, and the same shape as the wave from Grilli et al. [1997]. However, the wave of the SWASH simulations breaks earlier or in deeper water. The run-up of these tests could not be validated because there is no clear run-up law for breaking solitary waves. However, the run-up has been calibrated for the Yuriage case.

4.

Sensitivity of wave and bathymetry parameters

4.1   Offshore parameters

In this thesis all the simulations are performed with an initial elevation that represents the elevation due to an earthquake offshore. The model will have a length of a few hundred km. The first part of the model is the simulation of the wave from the offshore wave generation to close to the coast. In this part the wave is undergoing some changes due to shoaling. The influence of a wave parameters and bathymetry parameters are investigated in this thesis. The offshore elevation [H_0], offshore wave length [L_0], offshore depth [d_0] and continental slope [α_1], are investigated in these tests. To see the influence of these parameters, several simulations are performed with changes in these three parameters. The tsunami wave sof these simulations are compared at a depth of 500m (x_2) and 100m (x_3). Two locations are chosen to see if a small difference at location x_2 grows to a big difference at location x_3.

The wave used for this test is a sine-wave that looks like the 2011 Tohoku tsunami wave. It has a high crest of 8m and is proceeded by a small trough of 2m. The length of the trough wave is 50 km and the crest wave is 100 km giving the wave a combined length of 150 km. The slopes α_2 and α_3 are set constant at 1:200 and 1:100 and the offshore depth [h_0] is set at 4000m. The water elevation is just in front of the slope α_1, between 350 and 200 km from the shore depending on the [d_0].

The water level obtained from SWASH is the total water level. The total water level is the incoming wave and the reflection wave.

4.1.1   Continental slope α_1
The influence of the slope α_1 is investigated by using various slopes. Because 1:10 or 1:20 is the usual value for α_1, the slope is ranged from vertical to 1:50. See also Figure 1.2 for all the parameters.

The time series of the simulations are plotted in Figure 4.1. At location x_2 the waves show a small difference in height. The simulation with a vertical slope is 5.94 m at location x_2 and 8.47m at location x_3. The simulations with slope 1:50 have had a higher wave of 6.688m at x_2 and 9.53m at x_3. The wave height decreases slight for a steeper slope. The longer distance of the 1:50 slope resulted that the wave has more time shoal before reaching location x_1 compared to steeper slopes. At location x_2 there is an 11.1%

difference between the smallest and highest wave elevation. This is considered as a very small difference and the influence is thus also small. At location x_3 the difference is 11.2%. The difference has thus not grown between the two locations. The wave length calculated with $L = \sqrt{gd} * Period\ [T]$ gives a 6.4% longer wave length for the steepest slope compared to the 1:50 slope. This is also a very small increase.

The most common slopes are the 1:10 to 1:20 slopes. The difference between these two slopes is only 4% for the wave height and 1.2% difference in wave length. The changes in the slope are thus very small and the continental slope will be kept constant for following simulations. A 1:20 slope is taken as this is the most common slope.
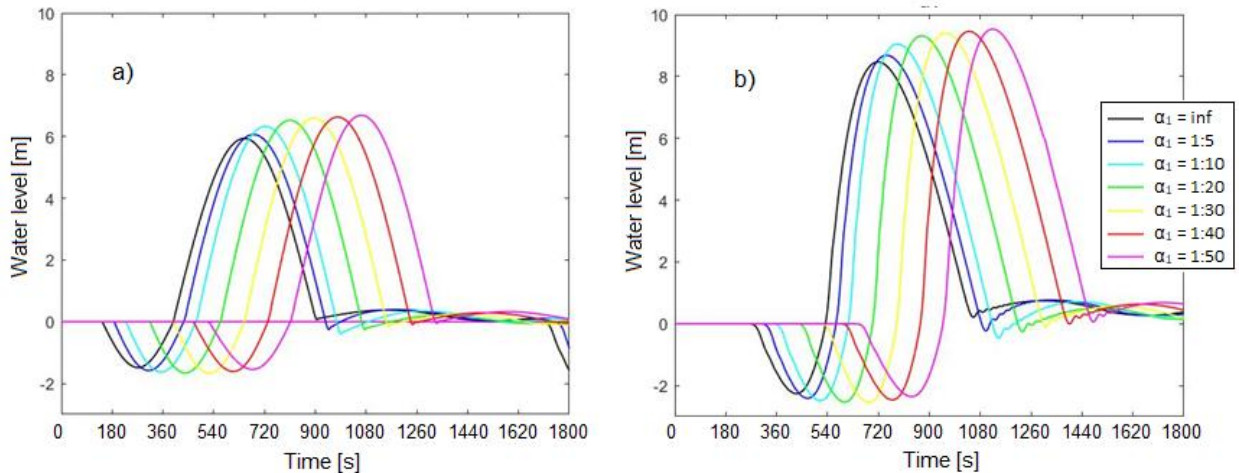
Figure 4.1: Time series of wave for different slopes a_1, a) at location x_2 and b) at location x_3.

4.1.2   Offshore depth d_0

The same analysis is done for simulations with different offshore depth. This is investigated by ranging the depth from 3000m to 6000m. The time series of the simulation at the two locations are shown in Figure 4.2. The elevation height differences between the highest and smallest wave is a 14% difference. This also does not change between the two locations. However, the wave length has a quite larger difference. The wave length of the simulation is 30% larger for the simulation with d_0 = 3km compared to the d_0 = 6km simulation. In the next test series in section 3.5 is shown what the influence of this wave length is on the bore. The larger d_0 with a shorter wave and the increased wave height has a steeper wave. This could be important for the breaking of the wave to develop into a bore.
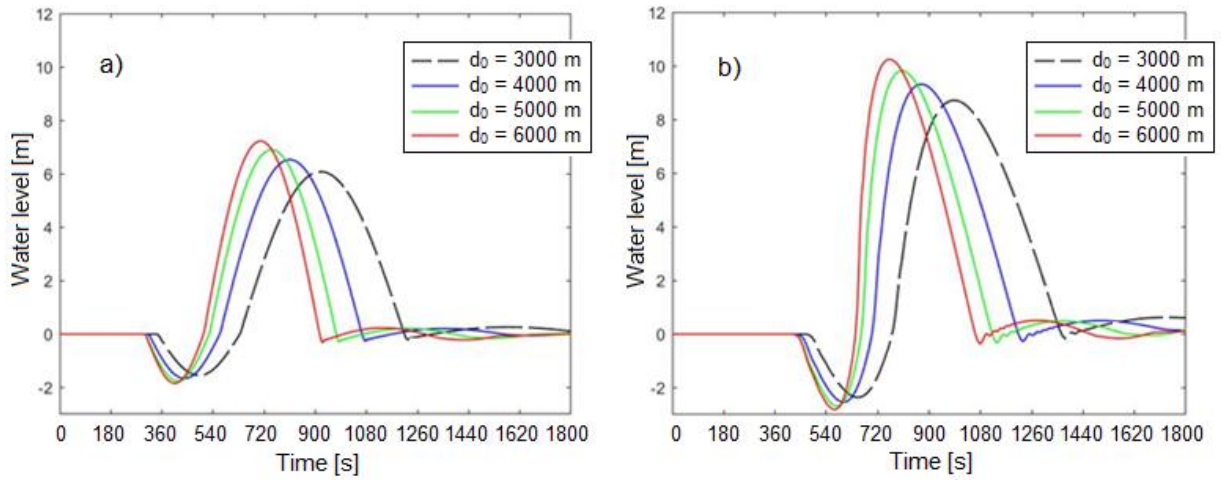
Figure 4.2: Time series of tsunami wave for different d_0. Left at location x_2, right at location x_3

4.1.3 Initial wave Length L_0

The influence of an initial difference in wave length is investigated by using three different wave lengths. Figure 4.3 shows the simulations. Although the differences are very small, the shortest wave of 100 km has the highest water elevation. This difference is only 1.3% and is very small. The initial wave length does not influence the shoaling as much while the initial depth has a larger influence.
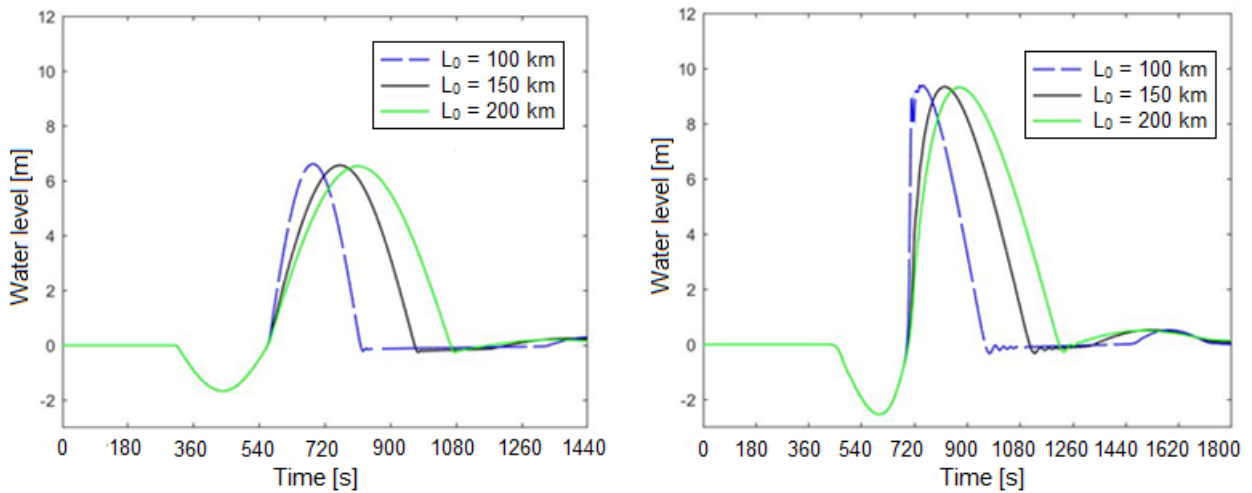
Figure 4.3: Time series of wave for different L_0. Left at location x_2, right at location x_3.

4.2   Simulation of tsunami bore

In this section the wave model is used to simulate several bores. These simulations all have a little difference. With multiple simulations the effect of these differences can be analysed. These simulations show how a bore looks in SWASH. From this a clear description of the bore characteristics is opted.

The SWASH model is used to simulate a bore. This is first done by using a water elevation of a cos-wave at the generation area in deep-water. With large grid steps of 100 m the wave transformation to the nearshore area is modelled. The time series of the wave at the location where the depth is 100m is taken as the input for a SWASH simulation of the bore with a grid size of 1 m.

This simulation is done for multiple different situations. First, a reference simulation or standard simulation is done. This standard wave is a 6 meter high wave where L_{front} and L_{tail} of the cos-wave are both 75 km. This gives the wave an offshore wave length of 150 km. The slope α_2 is 1:200. Onshore the bed is flat with a Manning roughness coefficient of 0.06 m$^{-1/3}$s.

A total of 10 simulations are performed, all with a slightly different situation. Table 4.1 gives an overview of the parameters of all the tests.

Test nr	Water elevation [H_0] (m)	Initial Wave length [L_0] (km)	L_{tail} /L_{front} (-)	Slope α_2 (-)	Offshore depth [d_0] (m)
1	6	150	1	1:200	5000
2	6	150	1	1:100	5000
3	4	150	1	1:200	5000
4	8	150	1	1:200	5000
5	10	150	1	1:200	5000
6	6	150	1	1:400	5000
7	6	100	1	1:200	5000
8	6	200	1	1:200	5000
9	6	150	2	1:200	5000
10	6	150	0.5	1:200	5000
11	6	150	1	1:200	4000
12	6	150	1	1:200	6000

Table 4.1: List of SWASH Simulations with Parameters. Values that are changed from test nr. 1 are shown in grey.

There are two types of parameters that can be changed. Firstly, the bathymetry. Test 2 and 6 show the influence of the slope [α_2]. Test 11 and 12 show the influence of the offshore depth [d_0]. Secondly, the wave shape. Parameters that can be changed in the cos-wave are shown in a sketch in Figure 4.4. Test 3 to 5 show the influence of the tsunami elevation height. Test 7 and 8 show the influence of the wave length and test 9 and 10 show the influence of the skewness of the wave. The wave is skewed backwards when $L_{tail}/L_{front} > 1$, and the wave is skewed forward when $L_{tail}/L_{front} < 1$.
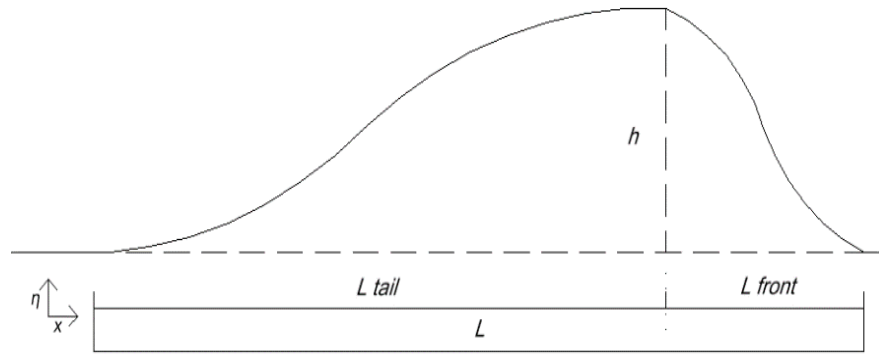
Figure 4.4: Sketch of cos-wave and parameters of the wave.

4.2.1   Grid cell size of offshore simulation

The simulations are performed in two steps. From offshore with a grid step of 100 m and a second simulation with a grid step of 1m nearshore. The time series of the first simulation is the input for the second simulation. It is tested first if the simulations with the 100 m grid cells are correct. To see if this time series are correct is this simulation done with much smaller grid cell size. This test is also performed with a grid cell of 20 m. In Figure 4.5.a the time series are at different depths near the shore given for a simulation with grid cells of 100 m. In Figure 4.5.b the exact same simulation is given with grid cells of 20m. There is no large difference between these time series. The error in water elevation are below 1% for all the time series at different depths. Also the period of the waves are equal. The only difference between the simulations are the fluctuations of the time series behind the tail of the wave. However, this is no problem because the breaking of the tsunami wave front is of interest in this study. The simulations with the larger grid cells of 100 m can therefore be used to create time series for the smaller scale simulations near the shore and it is not necessary to use smaller grid cells in the offshore simulation.
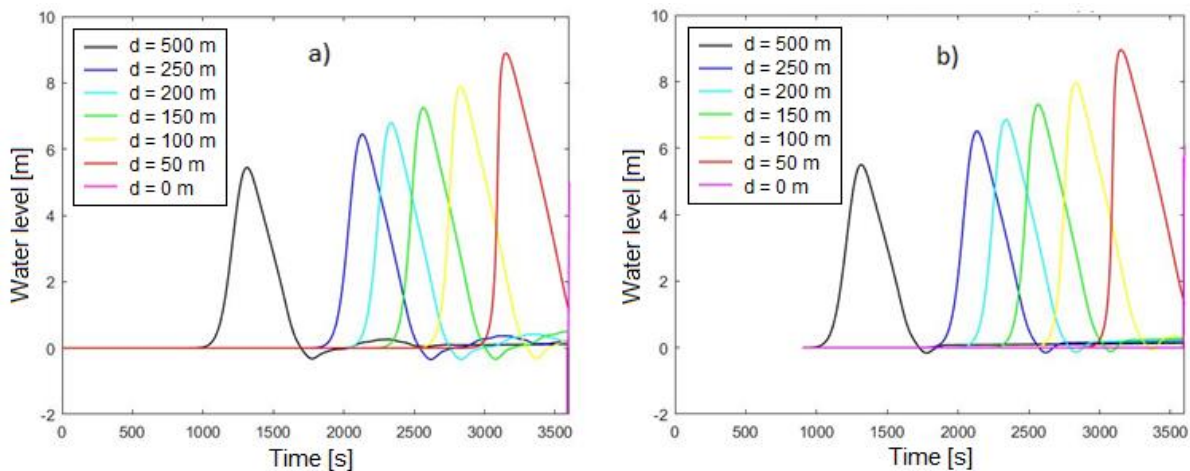
Figure 4.5: Time Series at locations near shore. (a) dx = 100m (b) dx = 20 m.

4.2.2 Model from Generation area until nearshore

At first, a model is made that simulates the tsunami wave from the generation area until the nearshore. The tsunami is simulated by elevating the water level with the wave as sketched in Figure 4.4. The first results of the simulations show the water elevation from the simulation with water elevation H_0 is 6m and a wave length L_0 of 150 km.

This water elevation creates two waves in opposite direction, both with a wave height half the original elevation, Figure 4.6. The wave is travelling to the shore with a velocity of $\sqrt{gh}$ since the tsunami wave is in shallow water with such a long wave length. The wave starts to shoal as the water depth gets less near the shore. As long as there are no dispersion or non-linear effects can the time series at the start of the continental shelf be predicted. With the green's law can the time series in shallower, but still deep, water be approached.
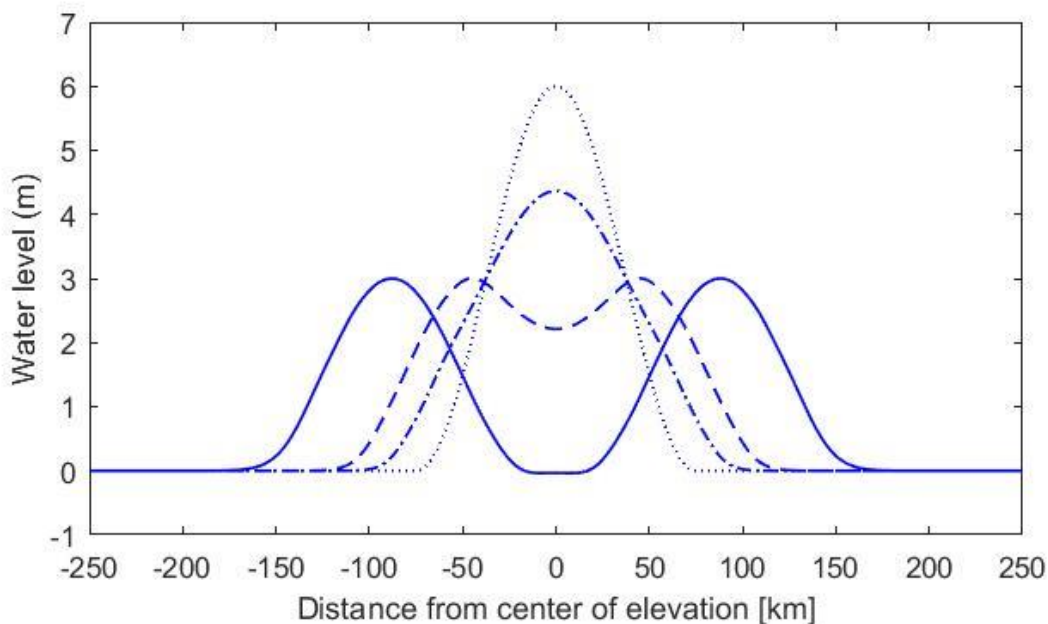
Figure 4.6: Tsunami elevation split in two waves in opposite direction.

4.2.3 Offshore simulation

The time series of the waves at location x_2 are shown in Figure 4.7. In this figure multiple time series of simulations 1,2 and 6 to 10 are shown. The striped lines are waves that are skewed forward and the dotted lines are skewed backwards, the solid line is not skewed. The skewness has big influence on the time series of different waves at location x_2. The difference in steepness can clearly be seen between these waves. In the next section will be discussed if this has effect on the bore. The difference in water level between the forward skewed waves and the non-skewed waves is average 5.4%. The difference between the backward skewed wave and the non-skewed wave is on average 3.6%. These differences are very small.

The slope α_2 has very little influence on the wave at location x_2. The times series at x_2 is nearly the same for every α_2. The difference in water level is at maximum only 1.8% between the simulations. The time series have therefore almost no changes at location x_2. The offshore simulation can thus be done once and

used for multiple simulations with the same wave height, wave length and skewness but different slope. However, the offshore simulations are still performed for every simulation.
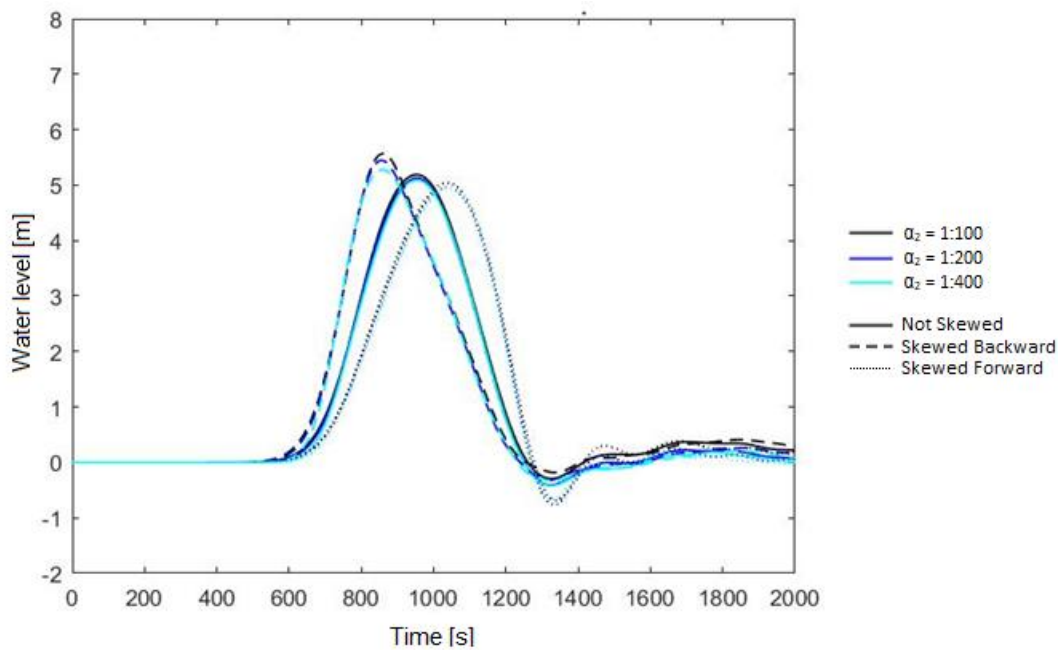
Figure 4.7: Time series at x_2 for different a_2. Dotted line: Skewed backwards, Dashed line: Skewed forward and solid line not Skewed

4.3   Nearshore simulation

The nearshore simulations are the next step in order to simulate the tsunami bore. This simulation is done with smaller grid cell size than the offshore simulation. The simulation is started at 100 m depth with a time series of the wave elevation obtained from the offshore simulation. In these simulations, bores are formed in different situations as shown in Table 4.1.

The onshore slope shown in Figure 1.2 as α_3 is a flat slope at an 1 m elevation above zero water level. The first part of the coast is a 1:200 m slope of 200 m long. The slope becomes flat when it reaches 1 m elevation at x = 200. This topography is used in the nearshore simulations in chapter 4 and 5. The flat slope is used to match the circumstances of the physical tests in chapter 6.

4.3.1   Definition of bore front parameters
Definitions like the bore height and bore velocity have to be clear to analyse the bore. Two pairs of bore height velocities are used in this analysis. The maximum inundation with its corresponding velocity [$h_{max.inun}$ and $u_{max.inun}$] is the first pair. The other pair is the local depth averaged bore velocity and the local bore height at the bore front [h_{bore} and u_{bore}]. A third velocity is the actual velocity at the bore front called the bore front velocity [v_{front}]. The difference between [u_{bore}] and [v_{bore}] is illustrated in Figure 4.8. The bore front velocity [v_{front}] is not used in this section.
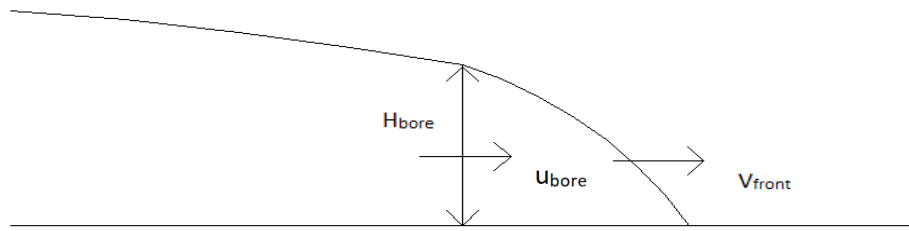
Figure 4.8: Sketch of Bore with V_{front} at the front of the bore and H_{bore} and u_{bore} behind the front.

There is no clear definition of the bore front height since there is no maximum height at the bore front. The bore height only keeps increasing until it reaches maximum inundation. The bore is plotted for simulation 1 when the bore is at the coastline In Figure 4.9.a. It is hard to define what the height of the wave front from the bore is in Figure 4.9.a. There is however, a maximum velocity at the bore front. This is the maximum local depth averaged velocity [u_{bore}] of the bore just behind the bore front. This is used as the location of the bore front height [H_{bore}].
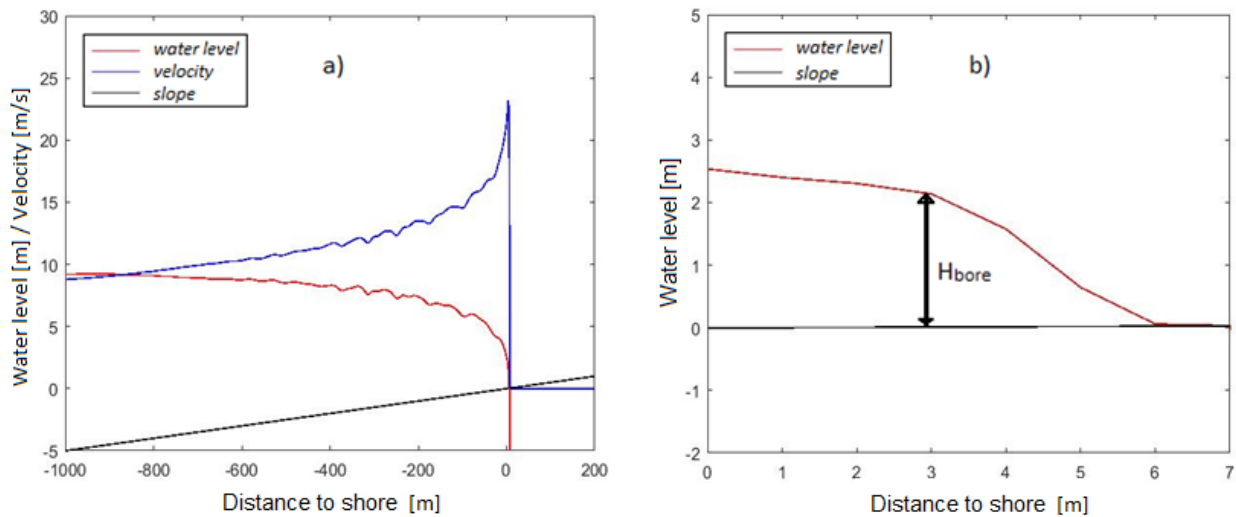
Figure 4.9: a) Water level [η_4] and Velocity at the moment the bore reaches the coastline. b) Bore front with location of bore height at maximum velocity. Simulation 1.

The location of the wave height can be seen with a closer look at the bore front in Figure 4.9.b. The wave shows a sloped wave front with a change in slope at the location of the wave front height. The slope is steeper in front of this point and flattens behind this point. This definition of the bore front parameters is used throughout the thesis. The bore height is 2.14 m and the corresponding velocity is 23.1 m/s in the case of Figure 4.9.

This front is followed by the remaining wave with much higher inundation height and a lower velocity. The maximum inundation [$H_{max.inun}$] is the maximum height of the wave at that location.

To analyse these parameters for the different bores, a dimensionless parameter is needed. The local Froude number [Fr_{bore}] in equation [4.1] includes both the parameters velocity and height. The Froude number is 5.04 in the case in Figure 4.10. This Froude number is used to express the characteristics of the bore.

$$Fr_{bore} = \frac{u_{bore}}{\sqrt{g*h_{bore}}}$$

[4.1]

This definition of [H_{bore}] and [u_{bore}] holds when there is a bore before the coast or on the coast. In case there is no bore before the coast line is reached the maximum velocity is not at the front. In the case of simulation number 2, where the slope [α_2] is 1:100, the wave is not breaking when the wave reaches the coast and the bore only develops on land. The wave is shown five seconds apart at multiple times in figure 4.11. The solid lines show no bore and the wave is not breaking. The stripped lines show the moments where the wave is breaking and the bore is formed.

Li et al. [2017] describes a tidal bore progressing on a small slope in an estuary or a river. There was tried to use the description of the tidal bore to describe the tsunami bore. The Froude number in this article is described with the water level in front of the bore which is non zero in a river or estuary. The water level in front of the bore in this study is zero because the bore runs-up the shore. This definition of the Froude number is thus not be used.
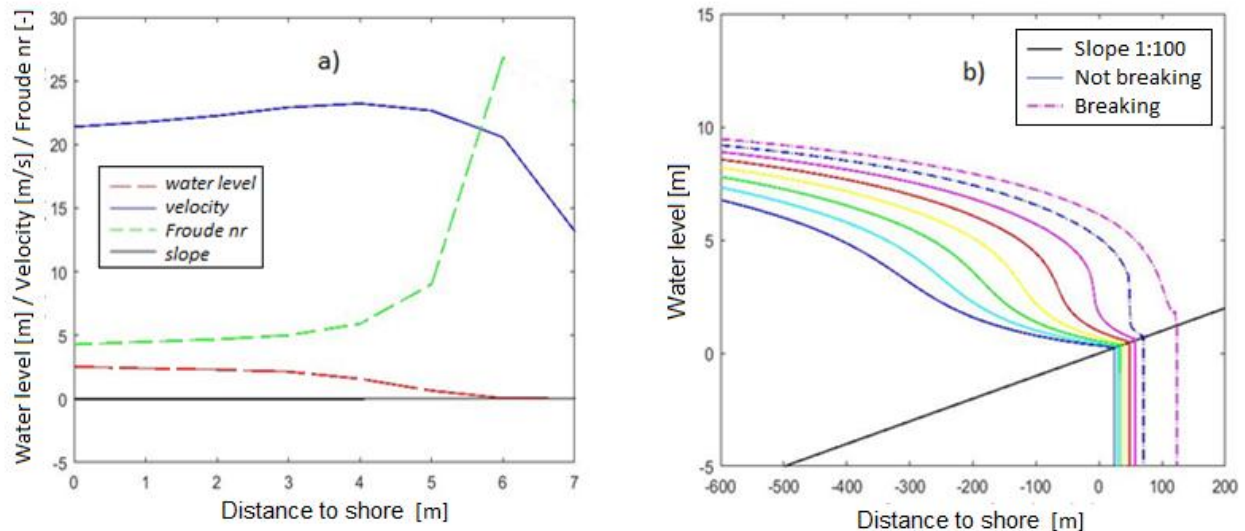
Figure 4.10: a) local Water level [η_4] , local Velocity and local Froude number with bore just onshore. Simulation 1: Slope 1:200. b) Development of a Bore onshore for the 1:100 Slope. Simulation 2. Dashed line is breaking waves..

4.3.2   Bore simulation

The results of the bore simulation are shown and discussed extensively in appendix B. The conclusion of these test is given here. The influence of the bathymetry and wave parameters on the velocity and height of the bore should be investigated in order to analyse different bores with different height and velocities. The influence of four parameters are tested in this section. These parameters are the slope [α_2], the offshore wave elevation [H_0], the offshore wave length [L_0] and the wave skewness [L_{tail} / L_{front}].

The wave length and the wave skewness do not influence the Froude number of the bore, they only influence the steepness of the bore. Where the wave breaks and forms a bore or if the wave breaks is dependent on the steepness of the wave. However, the influences on the characteristics of the bore can be considered very small for the wave length and the skewness.

The slope [α_2] does influence the Froude number of the bore. The slope of 1:200 hast the highest Froude numbers while the 1:400 slope which is milder and the 1:100 slope which is steeper have a lower Froude number. The slope has thus large influence on the bore characteristics.

The Froude number of the bore [Fr_{bore}] is higher due to an increase in velocity of the bore for larger wave heights [H_0]. A larger water elevation leads to a higher inundation height and higher velocity. However, the increase of the Froude number is very mild. The bore velocity has a large increase and the bore height has a small increase for a higher elevation. This leads to a slightly larger Froude number for an increased elevation. The peak of the Froude number and the velocity is at the shoreline for these simulations with a 1:200 slope.

The offshore depth [d_0] has very little influence on the characteristics of the bore. In section 4.1.2 is shown that the wave is much steeper for a simulation with a deeper offshore depth due to shoaling. This steeper wave does not lead to differences in the bore.

A more extensive analysis is shown in appendix B.

5.

Bore Analysis

In chapter 4 the factors that influence the bore are investigated. In this chapter the bore characteristics are analysed. In section 5.1 is the bore formation and where the bore forms discussed. In section 5.2 the bore characteristics are analysed for the parameters as defined in chapter 4. In section 5.3 the applicability of the model on the existing force theory by FEMA [2012]. The theory of FEMA [2012] for the impact forces on walls is mentioned in section 2.5.1. This theory uses the maximum momentum flux of the bore to calculate the maximum force on the wall. In section 5.4 are the simulations divided into groups of breaker type and a theory for a breaker parameter is constructed. The relationship between the breaker parameter of section 5.4 and the bore characteristics of section 5.2 is analysed in section 5.5.

Until now the parameters that influence the bore were investigated. In this chapter these parameters are used to simulate many different bores with different heights and velocities. The results of the simulations are used to see what the important parameters for the forces on the wall, bore height and velocity, are for the different simulations and are studied quantitatively.

Three parameters are variable in all the simulations. These are the wave height $[H_0]$, the near shore slope $[\alpha_2]$ and the wave length $[L_0]$. The skewness is not varied because the influence is very small, as seen in chapter 4.
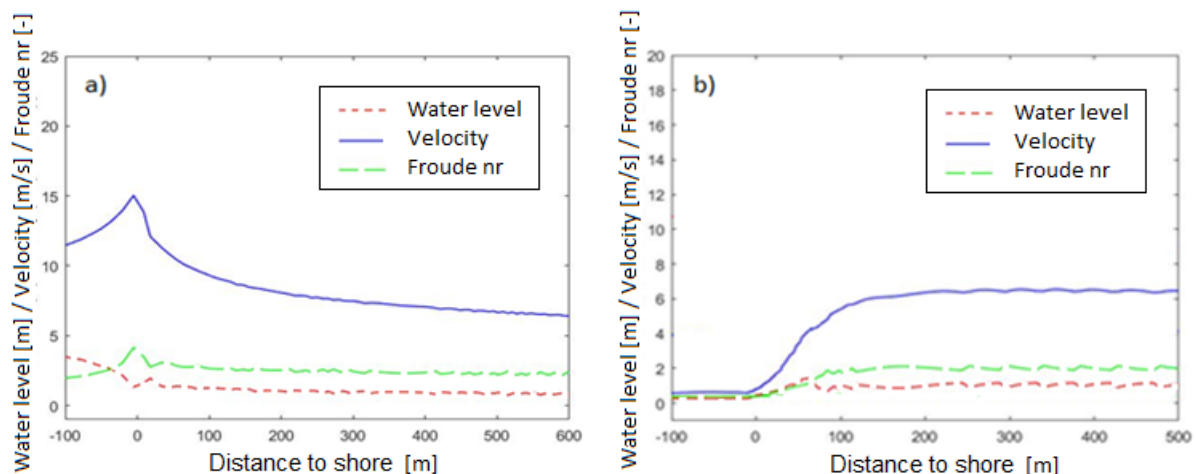
Figure 5.1: Water level (red small dash), Velocity (blue solid line) and Froude number (green long dash) for the wave front, local depth averaged. for a) $H_0 = 4m$, $L_0 = 150km$ and $\alpha_2 = 1:200$. and b) $H_0 = 4m$, $L0 = 150km$ and $\alpha_2 = 1:100$.

Table C.1 and C.2 in appendix C show the simulations that have been carried out. Simulations with a wave length of 150km are done with a wave height between 2 and 15 meters with a 1 meter interval between the wave heights. Simulations with wave lengths of 100 and 200 km are done with a 2 meter interval. Thus for 2, 4, 6, 8 and 10 meters wave height.

Figure 5.2: Picture taken on top of the Seawall at Yuriage, Tohoku Japan. This was built after the 2011 tsunami. [picture: T. Glasbergen]

5.1 Breaker type

From every simulation a profile of the bore can be made that gives the local depth averaged bore front velocity [u_{bore}], bore front height [H_{bore}] and the corresponding Froude number [Fr_{bore}], as defined in section 4.3.1. The profile in Figure 5.1.a is given for the simulation with H_0=4m, L_0=150km and the slope of 1:200. This profile has a peak in velocity of 15m/s, at the coastline. This is the location with the highest velocities and also the highest Froude number. At this location the seawall is usually built. However, from Figure 5.1.a, it seems better to build the wall a few 100 meters inland, where the velocity is much lower. At x = 100 m the velocity is reduced to 9 m/s. The sea wall in Tohoku, Japan is at most locations around 100 m inland. In Figure 5.2 below, a photo taken from on top of the wall in Yuriage is shown. On the left side of the wall is a stretch of beach between the wall and the ocean.

Figure 5.1.b shows the profile for the simulation with H_0=4m, L_0=150km and the slope of 1:100. The profile in this simulation looks completely different. The velocity and height is close to zero just of the coast and it builds up velocity on land until a maximum is reached at 350 m inland. In this case the optimal location of the coastal tsunami barrier seems to be at the coastline where the velocities are low.

This difference in profile can be explained by the breaking of the wave. In the simulation of Figure 5.1.a the wave is breaking before the wave reaches the coast while the wave in figure 5.1.b is not yet breaking at the coast. Figure 5.3 shows the waves of figure 5.1 at two times, first when the wave has not yet reached the coast and second when the wave is on the coast.

The second wave in Figure 5.3 a and b clearly shows a reflective wave going in offshore direction. The water level shown is thus the incoming bore height and the reflection of the wave on the coast. This reflective wave shows soliton fission while this is not seen on incoming waves close to the shore.

Wave 1 in figure 5.3.a is breaking while wave 1 is not breaking in figure 5.3.b. The velocity of the front is very low because the wave is not breaking with a 1:100 slope and an initial water elevation of 4m. Its velocity builds up until it becomes a developed bore when the wave starts breaking on the coast. The profile of Figure 5.1.b is found for waves with an 1:100 slope and a H_0 below 6m and for a wave length of 200km smaller than 8m. The same holds for simulations with an 1:150 slope and H_0 smaller than 4 m. For higher initial wave elevations the wave starts breaking before the coastline and the velocity is thus much higher.

The breaker type in these cases is different. Situations where the wave breaks before it reaches the coast are for convenience called plunging breaker while situations where the wave is not breaking are called surging breakers. The case as in Figure 5.1.a is a plunging breaker type while in the case of Figure 5.1.b is a surging breaker type. This breaker type has influence on the design of a coastal tsunami barrier. The best location of the coastal tsunami barrier in the plunging breaker type is further inland as in Figure 5.1.b while the best location for the surging type is at the coast line where the velocities are low.
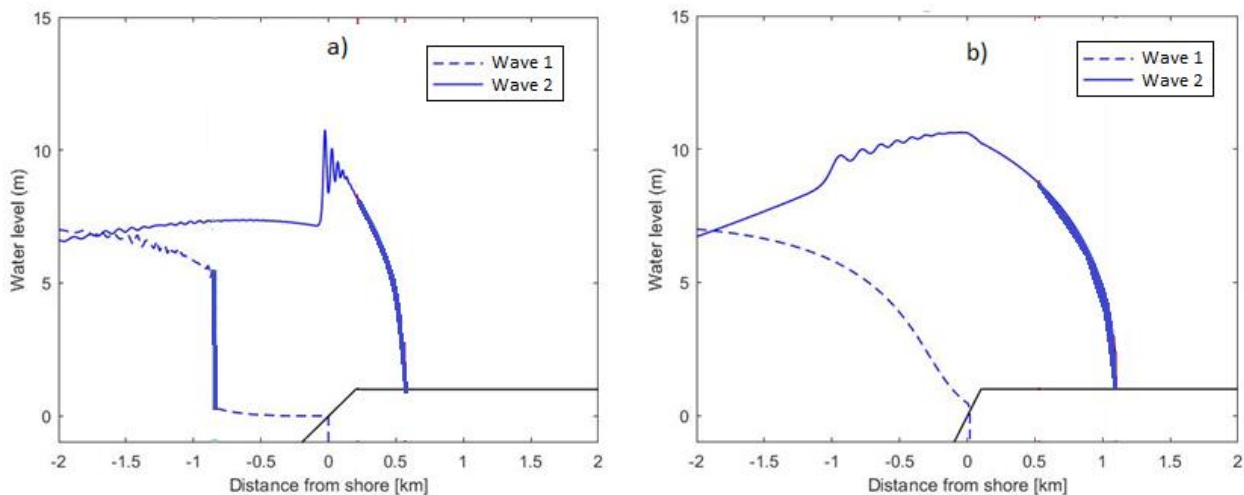
Figure 5.3: Wave at two times during simulation. 1. just in front of the coast, 2. on the coast. a) α_2 = 1:200, H_0 = 4m. b) α_2 = 1:100, H_0 = 4m. Thick line shows breaking. In figure b is wave 1 not breaking.

5.2   Bore Parameters

From every simulation the maximum local front Velocity [$u_{bore.max}$], the bore height [$h_{bore.max}$] and the local Froude number [$Fr_{bore.max}$] at maximum velocity is taken. This is the maximum velocity in Figure 5.1. The values for every simulation at this maximum velocity are given in tables D.1 and D.2. This maximum velocity is located close to the coast line for most simulations. The simulations that are not breaking at the coastline, like Figure 5.1.b, have a maximum at an inland location.

5.2.1 Bore height

The Froude number at maximum velocity [$Fr_{bore.max}$] is plotted against the bore height divided by the initial elevation height [$H_{bore.max}/H_0$] in Figure 5.1. This factor is given the name bore height ratio. This factor is a dimensionless term for the bore height and it describes how high the bore front height is compared to the initial elevation. The red markers have a high initial wave height and the blue dots have a small initial wave height. The figure shows two groups. The first group has low Froude numbers of 1.5 unto 2 for low initial elevations of slope 1:100 and 1:150 while the bore height ratio is constant around 0.25-0.35. From Figure 5.5.c, can be seen that these are the simulations with the 1:100 slope and the plunging breaker type simulations. The second group has Froude numbers of 2.75 for low initial elevations with a bore height ration of 0.7 and for high waves the Froude number is 4.5 with a bore height ratio of 0.3. The elevation in between show a trend as illustrated in figure 5.4. The simulations with a 1:100 slope that do have a breaking wave at the coastline match the plunging trend while the simulations that do not break deviate from the trend. There are however, some simulations that deviate from this trend that are categorized as plunging.

From the first group of surging breakers follows that the bore height at maximum velocity is around 25% of the initial elevation and the Froude numbers are low. When the wave starts breaking sooner is the Froude number higher. The Froude number and the bore height is much higher for plunging breakers. The bore height ratio decreases for higher initial elevations with a minimum of 25%.

In Figure 5.5 and Figure 5.6 the same data as Figure 5.4 is plotted but now the dots of simulations with equal slope and wave length are connected. The difference in the simulations along these lines is the initial wave height.

The Froude numbers of the simulations with a 1:200 and 1:400 slope, are around 2.5 to 3 for the waves with an initial height of 2m. The bore height ratio of these simulations is between 0.55 and 0.75. The Froude numbers of the simulations with an initial height of 8 and 10 m are around 3.5 unto 4.5, see Figure 5.5 a and b. For these simulations the bore height ratio is between 0.25 and 0.35. Even larger waves of initially 15m have a bore height ratio also around 0.25. These lines clearly follow the trend of a plunging breaker.

The results are different for the simulations with a 1:100 slope with small wave heights in Figure 5.5.c. In these simulations the wave is not breaking at the coastline and a bore can therefore not be present. The bore starts to develop when it passed the coastline. The 1:100 slope simulations with low wave height have their maximum velocity more inland where the bore is more developed. The Froude numbers of the 1:100 slope simulations is much smaller than for the 1:200 and 1:400 slope simulations. Since the maximum velocity is located further inland this maximum velocity will be much smaller. At this point, the wave will be slowed down considerably due to friction. The bore height ratio is rather constant for the 1:100 simulations. Although the bore height ratio increases for longer waves. This can be seen in Figure 5.5.c where the waves with an initial length of 100km have a bore height ratio around 0.25 and waves with a length of 200km have a bore height ratio around 0.35. Although, for a high initial wave height of 15 m, the ratio drops to 0.25.
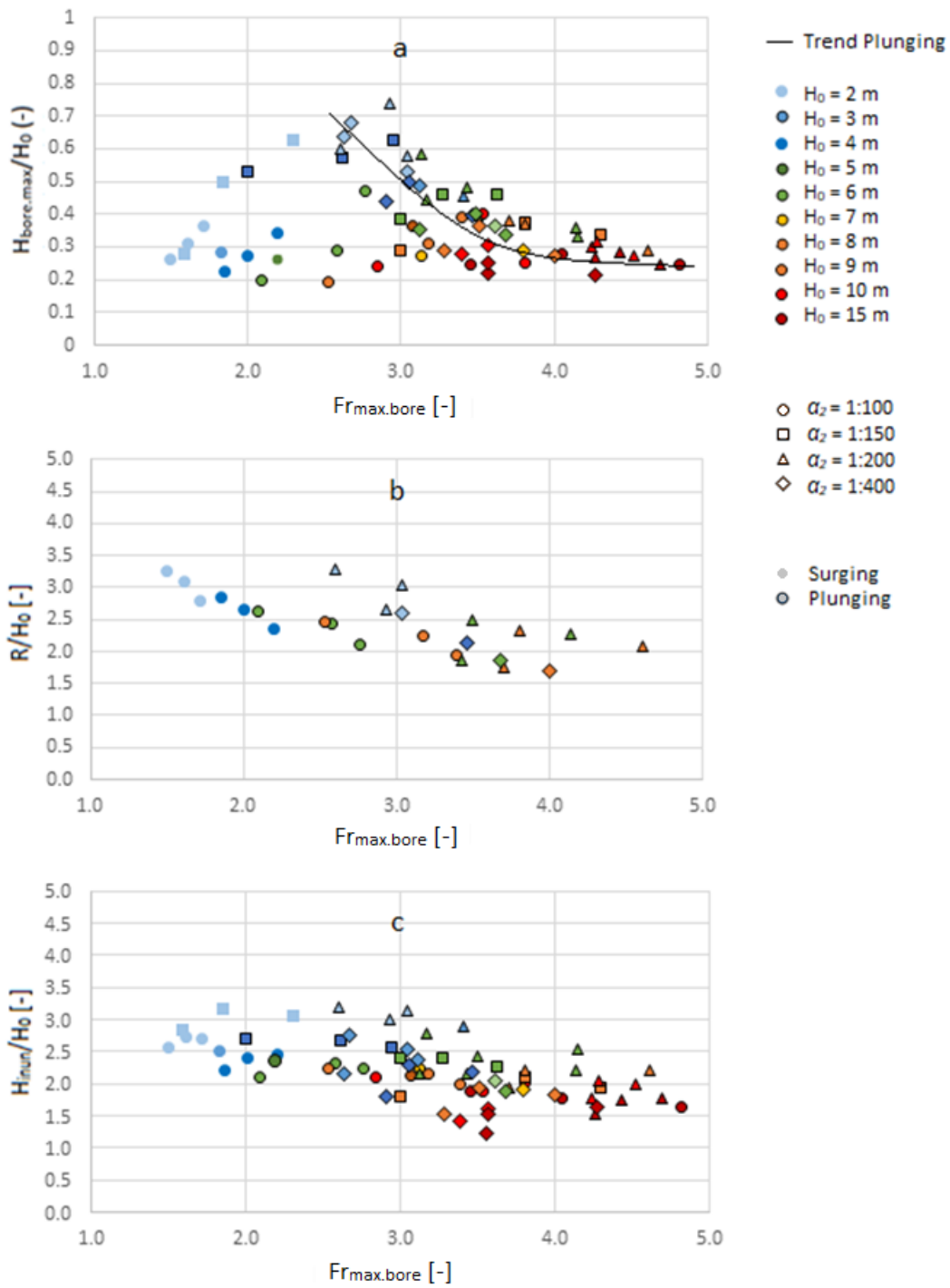
Figure 5.4: Froude number at the maximum velocity for simulations with slope 1:100, 1:150, 1:200 and 1:400 plotted against the bore height ratio. The trend of the plunging type is drawn with a line. Different colors display initial wave height. Marker shapes display the slope and the line around the marker shows the plunging waves.

The simulations of the 1:100 slope are difficult to compare to the 1:200 and 1:400 slope tests because the maximum velocity is situated at a different location. However, the difference between the 1:200 and the 1:400 slope simulations can be compared. In Figure 5.6 the initial wave length is constant and the slope is different. The simulations with the 1:200 and 1:400 slopes follow the trend of the plunging breaker. This is logical because all the simulations are categorized as plunging. However, the 1:400 slope simulations have smaller Froude numbers. This difference becomes smaller for longer wave lengths.

The Froude number does not seem to get bigger than approximately 4.5 for the case with a slope of 1:200 and a wave length of 150km in Figure 5.5.b. The green line has a cluster of simulations around a Froude number of 4.4. The same is visible for the 1:400 slope simulations in the same figure. However, this cluster is around 3.7. The maximum Froude number is thus different for an 1:200 and a 1:400 slope case. The largest initial wave height used in these simulations is 15m, which is a very high wave since the 2011 Tohoku tsunami had an elevation of 8m in Figure 3.3. Larger waves are therefore considered not likely. This maximum shows a dependency on the wave length. The 100 km initial wave length simulations show a smaller maximum Froude number of 3.5 for 1:400 slope and 4.2 for an 1:200 slope. The simulations with 200 km initial wave length do not show this maximum, Figure 5.6.c. This maximum is probably not reached. However, higher waves are possible but not likely.

The Froude number [$Fr_{bore.max}$] and bore height ratio can be estimated for different tsunami elevations when the wave length derived from the fault length and the slope α_2 from the bathymetry are known. The bore front height [$H_{bore.max}$] can then be calculated from the bore height ratio and the bore velocity [$u_{bore.max}$] then follows from the Froude number.

5.2.2   Run-up
Figure 5.4.a can also be made for the run-up instead of the bore height ratio. In figure 5.4.b the run-up divided by the initial elevation is plotted against the Froude number at maximum velocity. This is given the name run-up ratio. This run-up is obtained with SWASH simulations with an onshore slope of 1:200. These tests are done for tests with an initial elevation height of 2, 4, 6 and 8 m and for slopes [α_2] of 1:100, 1:200 and 1:400. In figure 5.4.b can be seen that the run-up ratio decreases linear for increasing Froude number. The run-up is approximately 3 times the initial elevation for Froude numbers around 1.5 and approximately 2 times the initial elevation for Froude numbers around 4. This result is found with a roughness coefficient of 0.06 m$^{-1/3}$s.

5.2.3   Inundation depth
The inundation depth at the location of maximum velocity is shown in figure 5.4.c. The vertical axis shows the inundation depth divided by the initial elevation. This factor is given the name inundation depth ration. The same decrease in inundation depth ratio is found as for the Run-up. With approximately 3 times the initial elevation for Froude numbers around 1.5 and approximately 2 times the initial elevation for Froude numbers around 4. The maximum inundation is thus the same as the run-up. It is recommended that this is examined further in the future.
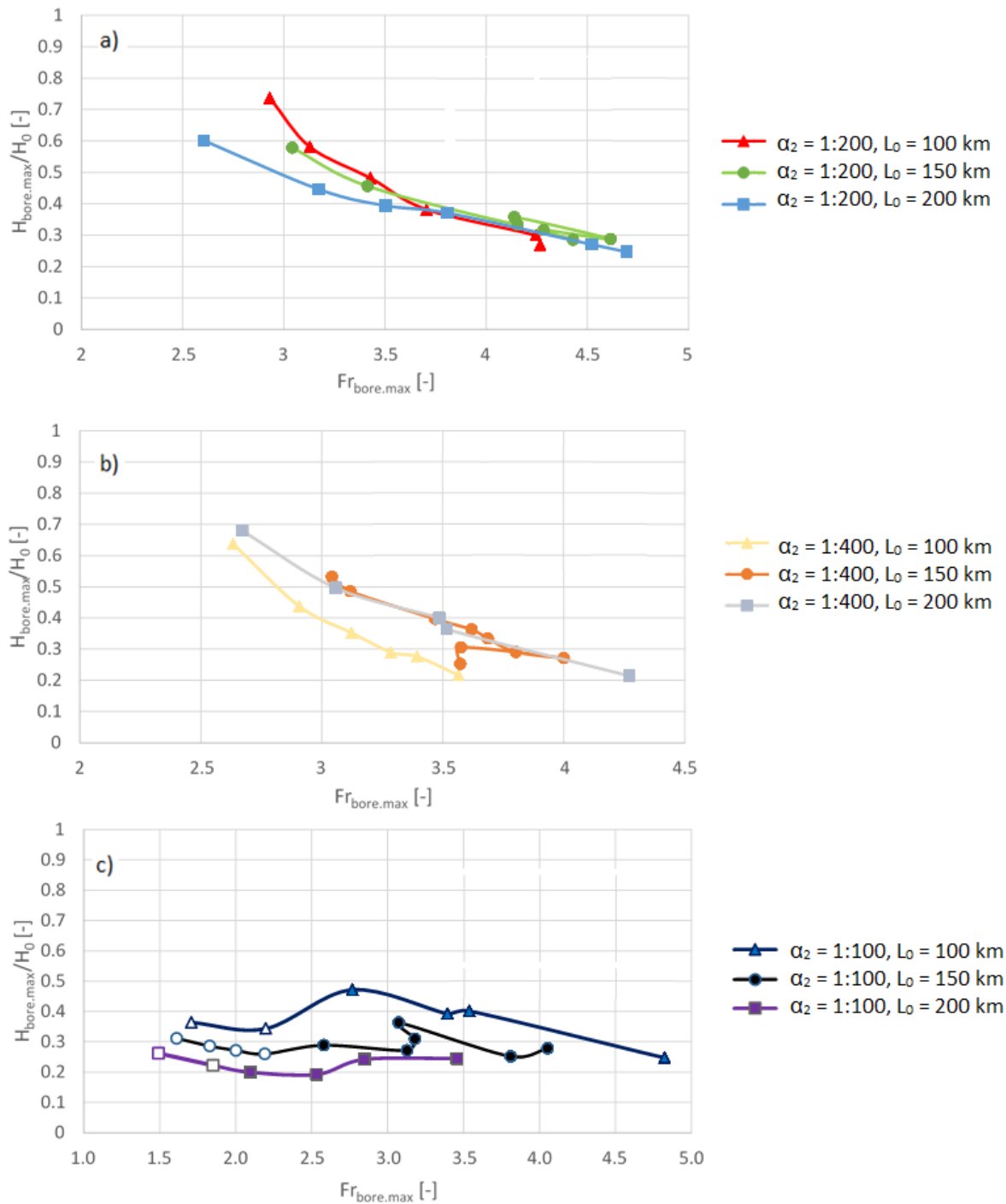
Figure 5.5: Froude number for simulations with equal slope and different wave length plotted against the bore height ratio. with a) $\alpha_2 = 1:200$, b) $\alpha_2 = 1:400$ and c) $\alpha_2 = 1:100$. White markers are plunging type.
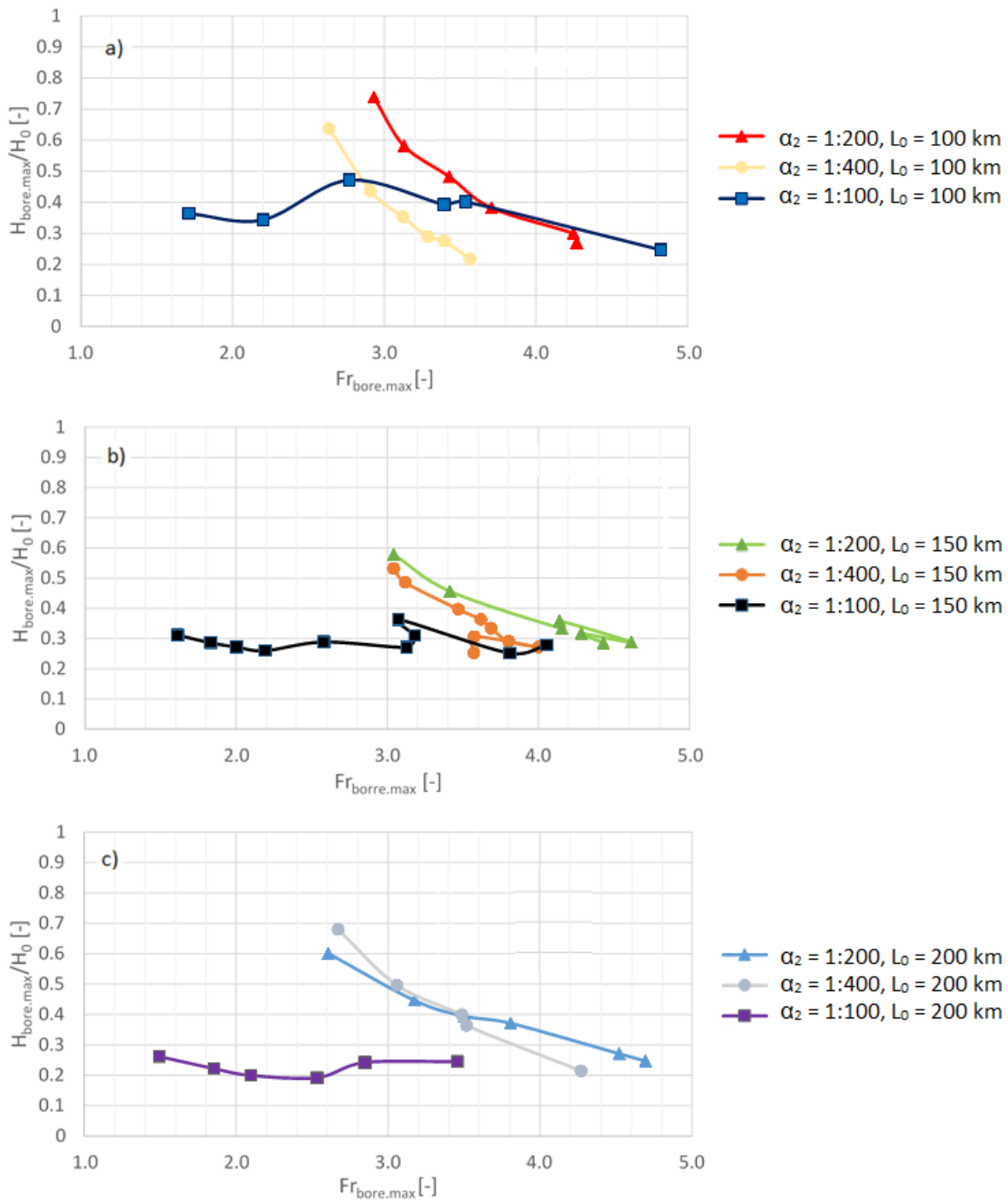
Figure 5.6: Froude number for simulations with equal slope and different wave length plotted against the bore height ratio. with a) $L_0 = 100km$ b) $L_0 = 150km$ and c) $L_0 = 200km$

5.3 Hydrodynamic force with existing force theories

In section 2.5 are several theories mentioned that calculate the forces on a coastal structure. In this section the bore characteristics to calculate the force are analysed for the SWASH simulation results. This is mainly done for the theory of FEMA [2012].

5.3.1 FEMA – [Hu^2] Maximum momentum flux

An analysis with the existing force theory of FEMA [2012] is made in this section. The theory of FEMA is given with equation [2.14]. This theory uses the maximum momentum flux to calculate the design force on a wall or structure. The maximum momentum flux is the maximum combination of (Hu^2). With the local flow depth [H] and local depth averaged velocity [u]. The effects of changes in the velocity will be much larger since the velocity is squared in the momentum flux.

The maximum momentum flux is shown at every location x for the simulations with a wave height H_0 of 4 meters and three different slopes in Figure 5.7.a. These lines are different for all the slopes. In the Figure 5.7. b, c and d is shown that the shape of these lines remain the same for higher waves and only the momentum flux becomes much higher. The 1:200 and 1:400 slope simulations also show fluctuations in the offshore part. This is due to soliton fission of the wave offshore. Closer to shore is the wave breaking and the soliton waves disappeared.

The maximum momentum flux does not occur at the bore front. The maximum (Hu^2) occurs when the bore has already passed that location and the inundation depth has increased while the velocity is still very large. The max momentum flux is very high close to the coastline. The α_2 = 1:200 simulations show the largest momentum flux that can become very high for larger waves, 500 m^3/s^2 with a H_0 of 4m and 1700m^3/s^2 for a H_0 of 8m. While the α_2 = 1:400 simulations are lower, 350 m^3/s^2 with a H_0 of 4m and 1050m^3/s^2 for a H_0 of 8m. The maximum momentum flux on the coast is at the coast line for all three slopes. Although the 1:100 slope simulations show slightly smaller momentum flux at the coastline than 100 m inland. A model like SWASH is required to calculate the maximum momentum flux.

5.3.2 Hydrostatic force

The hydrostatic force of equation [2.16] is calculated with the maximum inundation height. This inundation height at the location of the wall can be modelled with SWASH.

5.3.3 ASCE – Inundation depth and velocity based on the run-up

The force of the theory of ASCE [2016], given with equation [2.15], can be calculated without the SWASH model. To calculate the force with this theory the predominant tsunami wave period [T_{TSU}] and the offshore tsunami amplitude [H_T] are needed. The velocities and inundation depths are then based on the run-up, calculated with these factors. This theory relates the run-up to the Energy Head from which the inundation depth and the velocity can be calculated. These calculated velocities are used to calculate the Force with equation [2.15].
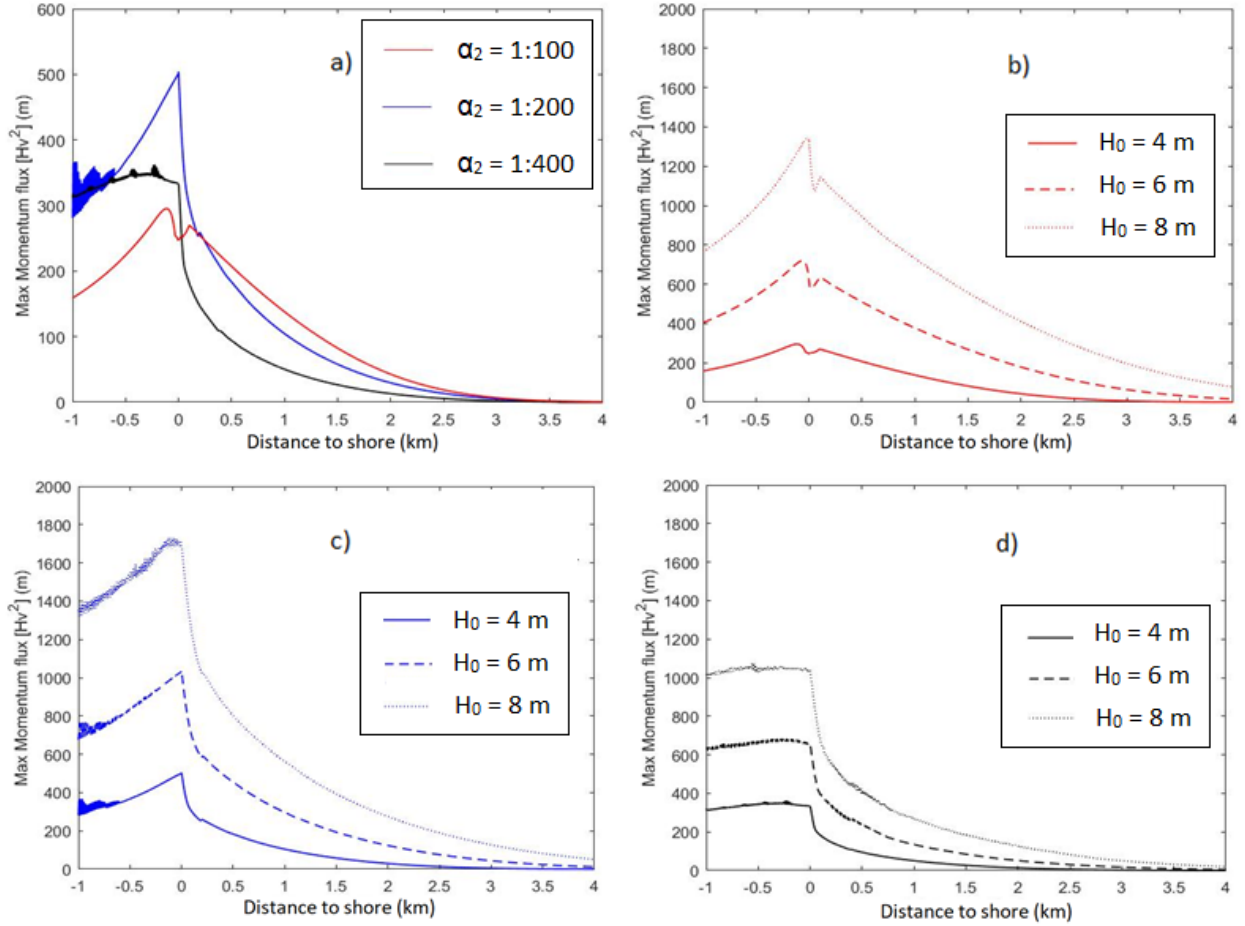
Figure 5.7: Maximum momentum flux for a) $H_0 = 4$, $L_0 = 150km$, b) $a_2 = 1:100$, $L0 = 150km$, c) $a_2 = 1:200$, $L_0 = 150km$, d) $a_2 = 1:400$, $L_0 = 150km$.

5.4 Breaker parameter ξ for Tsunami waves

Two types of breakers are found in the simulations of Figure 5.1. The plunging breaker that develops into a bore offshore and the surging breaker where the water runs up the coast. For design purposes it is important to know which type of breaker will occur. The breaking of tsunami waves can be described with a dimensionless breaker parameter or surf similarity parameter. Grilli et al. [1997] described the breaking of solitary waves with a slope parameter and this is related to the breaking parameter [ξ] in section 2.3.3. ASCE [2016] related a breaker parameter at 100m depth with the run-up in section 2.4.

The breaking type of the tsunami waves in this section will be described with the tsunami breaker parameter [$\xi_{tsunami}$]. The breaker parameter described by Iribarren and Nogales [1949] is stated in equation 5.1.

$$\xi = \frac{\tan(\alpha)}{\sqrt{\frac{H}{L}}}$$ [5.1]

To describe this parameter for the tsunami waves a clear description of the parameters is needed. The slope used for the tsunami breaker parameter [$\xi_{tsunami}$] is slope [α_2] since slope [α_1] has little influence on the wave as was found in section 4.3.2.

The wave parameters [H] and [L] should describe the wave before the wave starts breaking. This is done by taking the wave when the peak is at the location where the depth is 100m. This location is chosen because all the waves are not breaking at this depth, and is consistent with ASCE [2016]. The wave amplitude [H_ξ] at this location can be taken from the wave profile data as calculated by SWASH. The length of the wave [L_ξ] is taken as the length from the wave peak to the wave front. The tail of the wave is left out because in chapter 4 is shown that the length of the tail has no influence on the breaking of the wave. The wave length is the actual length from the point at which the water level is larger than zero until the peak of the wave at 100 m depth. The wave front is taken as the first point that is above a threshold of 0.001 m or below at threshold of -0.001m. In this case there is no leading depression and the wave front is thus the first point at which the water level becomes larger than the threshold.
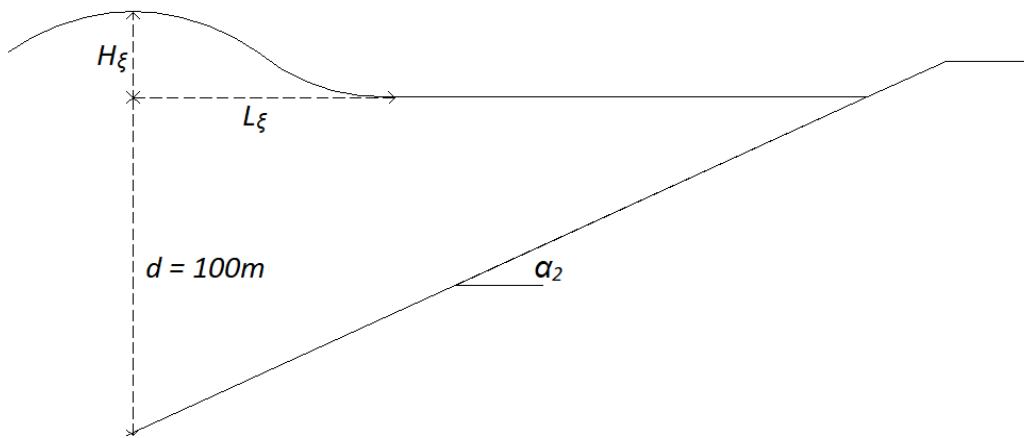
Figure 5.8: Sketch of parameters for Tsunami breaker parameter

H_ξ/L_ξ describes the steepness of the wave. The steepness of the wave is fully described by the wave front. A sketch of the parameters is shown in Figure 5.8. The tsunami breaker parameter can now be calculated with equation [5.2].

$$\xi_{tsunami} = \frac{\tan(\alpha_2)}{\sqrt{\dfrac{H_\xi}{L_\xi}}} \tag{5.2}$$

For use of the breaker parameter without SWASH, it would be easier to calculate the wave length from the wave period [T]. This can be done by taking half the total wave period to calculate the length of the wave front. From the time series in SWASH was observed that the wave period of the wave front is about half the total wave period. The wave length can then be calculated by combining this with L=cT and c=$\sqrt{gd}$ to get equation [5.3]. With d_{100} is 100 m, f is the frequency and c is the celerity. An example of a time series at 100 m depth is shown in figure 5.9.

$$L_\xi = \sqrt{g * 100} * \frac{1}{2}T \qquad\qquad [5.3]$$

This breaker parameter is calculated for all the simulations and shown in Table C.3. All the simulations are categorized in two groups. Group *A* consist of the simulations with waves that break before the coastline like the simulation of Figure 5.1.a. Group *B* consists of the simulations with waves that break after the coastline, like the simulations of Figure 5.1.b. The division between the groups is made by taking group *A* as all the simulations where the maximum local depth averaged bore front velocity [u_{bore}] is located no further than 30m inland. And taking group *B* as all the simulations further than 30m inland. The simulations are divided in groups in Table C.3.

These values for tsunami breaker parameter [$\xi_{tsunami}$] are also shown in Figure 5.10. The figure shows that waves with breaker parameter smaller than 0.35 are in group A and larger than 0.35 in group B. The black line shows that all the points to the right of the line are in group B. The breaking of the tsunami waves can then be described with the following relationship:

A (Plunging): $\xi_{tsunami} < 0.35$ [5.4]

B (Surging): $\xi_{tsunami} > 0.35$
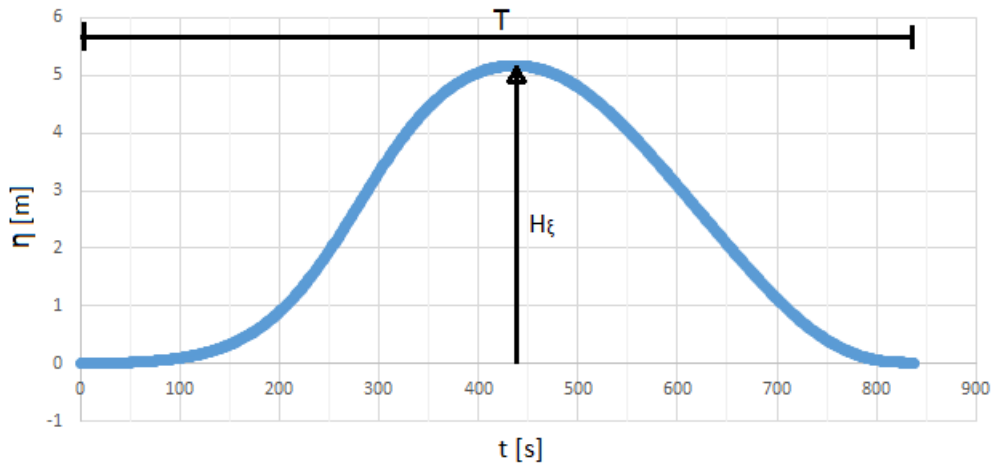
Figure 5.9: Time series of the Tsunami wave in SWASH at 100 m depth for the simulation with H_0 = 4 m, L_0 150 km and α_2 = 1:200
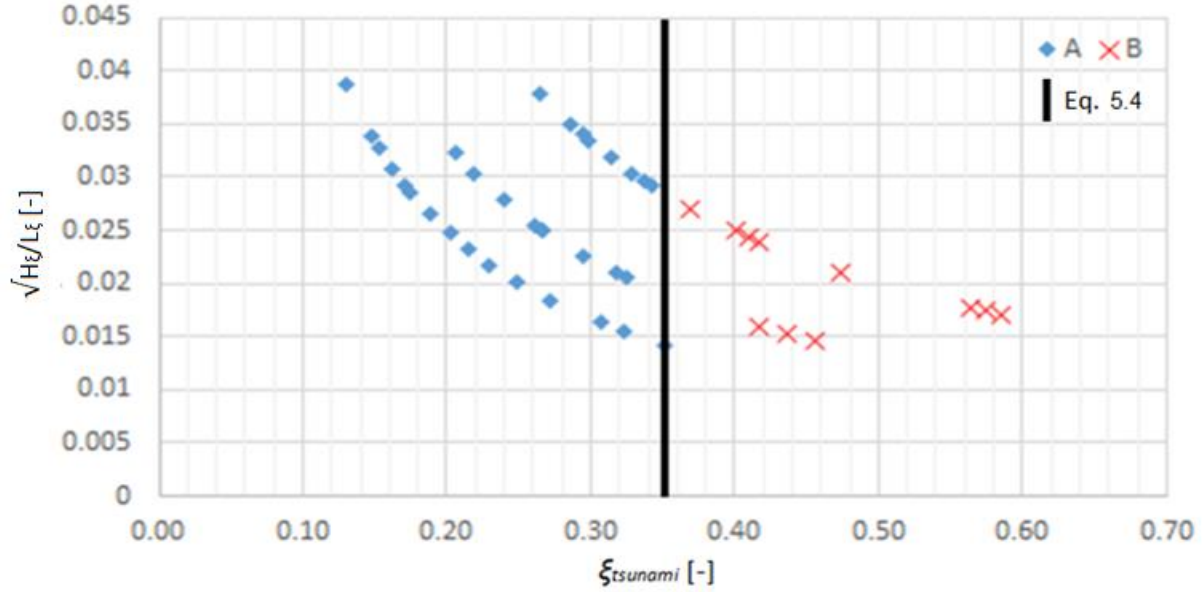
Figure 5.10: Tsunami breaker parameter, black line divides surging and plunging waves.

Breaker parameter with offshore wave parameters

The breaker parameter is defined at a location where the tsunami wave is not breaking and still subjected to shoaling. This gives the possibility to relate the breaker parameter to a more offshore location with the Green's law, equation [2.5]. The breaker parameter can be expressed by the parameters of the offshore wave. By substituting the offshore parameters in equation [2.5] the following relationship is found for the wave height at 100 m depth:

$$H_\xi = (\frac{d_{offshore}}{d_{100}})^{0.25} H_{offshore} \tag{5.5}$$

The same can be done for the wave length. The Green's law states that $\frac{L}{\sqrt{gd}} = constant$ [Camfield, 1980].

The wave length in the breaker parameter is the length from the front to the top of the wave. This is approximately half the wave length at the offshore location when the wave is not skewed and has a more symmetrical shape. At the location of the breaker parameter has the wave become skewed and the required length is not half of the wave length. This factor of a half is still used for simplicity. The following relationship for the wave length at 100 m depth is found:

$$L_\xi = \frac{\sqrt{d_{100}}}{\sqrt{d_{offshore}}} \frac{1}{2} L_{offshore} \tag{5.6}$$

Where [$d_{offshore}$], [$H_{offshore}$] and [$L_{offshore}$] are the depth, wave height and wave length at the offshore location respectively. The offshore wave height [$H_{offshore}$] can be taken as half the offshore tsunami elevation [H_0] because the tsunami elevation splits into two waves in opposite directions with half the elevation height. The offshore wave length is equal to the initial wave length [L_0]. The depth [d_{100}] is 100 m. Substituting equations [5.5] and [5.6] into equation [5.2] leaves equation [5.7].

$$\xi_{tsunami} = \frac{\tan(\alpha_2)}{\sqrt{2(\frac{d_{offshore}}{100})^{3/4} \frac{H_{offshore}}{L_{offshore}}}} \tag{5.7}$$

This equation can be used to calculate the breaker parameter with the offshore parameters of the wave.

5.4.1 Breaker parameter compared to ASCE [2016]

The breaker parameter [$\xi_{tsunami}$] is defined at the same location as the breaker parameter [ξ_{ASCE}] by ASCE [2016]. This location is at 100 m depth. The two breaker parameters are thus calculated based on the same wave. However, there are some differences in the definition of these breaker parameters. [ξ_{ASCE}] uses the whole period of the wave while [$\xi_{tsunami}$] uses the length of the wave front. The breaker parameter of ASCE [2016] is calculated for the same SWASH simulations as in section 5.4 and are shown in table D.3 and D.4. This table shows that $\xi_{ASCE} \approx 11.25* \xi_{tsunami}$. The values of the ASCE breaker parameter of the simulations are shown in figure 5.11. The division between plunging end surging is around $\xi_{ASCE} = 4$.

The new breaker parameter [$\xi_{tsunami}$] is easy to calculate and describes the wave only by the part that is important for breaking. The wave front is used and the tail is left out because this does not contribute to breaking. The breaker parameter by ASCE [2016] uses the complete wave. Also the boundary between the breaking types is clearer for the new breaker parameter. The simulation in group A are all lower than the black line and the simulations in group B are all higher than the black line in figure 5.10. In figure 5.11 is some overlap between the breaker types visible.

The breaker parameter ξ_{ASCE} is advised to be used by ASCE [2016] to find the run-up of the tsunami. This run-up can be found using figure 2.5. The run-up of the simulations, shown in table D.3 with R/H_ξ, is lower than the run-up in figure 2.5. This different could be due to roughness in the SWASH model. This could be part of further research.
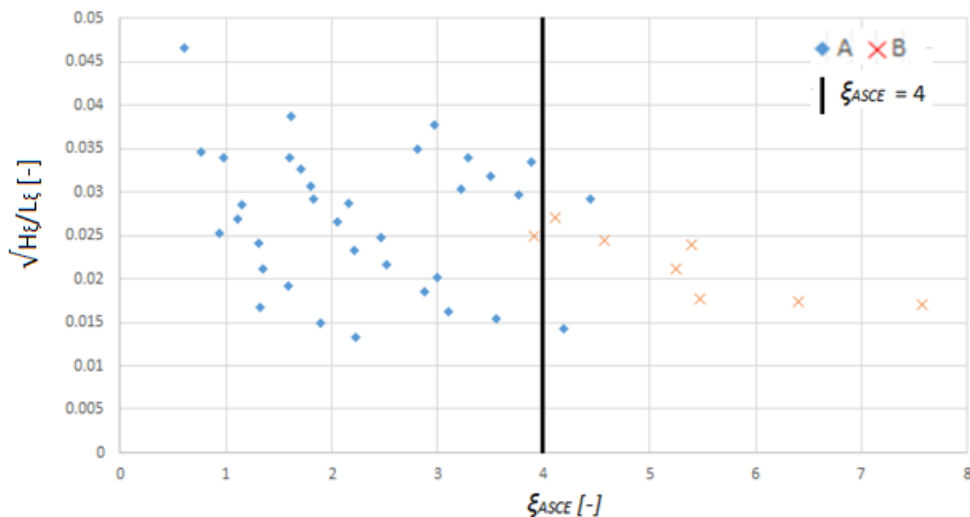
Figure 5.11: ASCE breaker parameter, black line divides surging and plunging waves.

5.4.2 Breaker parameter Yuriage, case.

The breaker parameter [$\xi_{tsunami}$] can be used for a realistic case. In section 3.2 the SWASH model is validated with the 2011 Tohoku tsunami for town Yuriage, Japan. The same case is used in this section to calculate the breaker parameter. The breaker parameter requires three parameters. These are the average slope from 100 m depth up to 0 m depth, the wave amplitude at 100 m depth and the length of the wave front

up to maximum amplitude. The average slope in this case is very mild and is equal to 1:590. This tsunami has a leading depression. The length of the wave is used for the calculation includes this depression. The length of the wave front is in this case 2610 m and the amplitude of the wave at 100 m depth is 8.1 m. The breaker parameter in this case is 0.03. Due to the mild slope is this value very low. The Froude number can also be calculated for this case. This is done at the location of the existing seawall at 100 m inland. The maximum Froude number of the incoming bore in this case is 2.8. The breaker parameter and the Froude number are shown in figure 5.11. With this low breaker parameter it is expected to have a bore at the wall and before the coast line. This bore was observed during the 2011 tsunami and the breaker parameter has predicted this correctly.

5.5   Characteristics of tsunami bore

The theory of section 5.2 and 5.4 is combined into a relationship between the Froude number of the bore and the breaker parameter in this section. The Froude number describes the characteristics of the bore.

The characteristics of the tsunami bore are now described with the Froude number of the local depth averaged velocity of the bore front at the location where this velocity is maximum. Whether the wave breaks at the coastline depends on the breaker parameter. In Figure 5.12 is the Froude number of the local bore front [$Fr_{bore.max}$] at maximum velocity plotted against the breaker parameter [$\xi_{tsunami}$]. The simulations are plotted in groups with equal slope [α_2]. Immediately can be seen that the simulations with slope 1:100 to 1:200 follow the same trend. The simulations with slope 1:400 have a breaker parameter [$\xi_{tsunami}$] that would be expected looking at the steeper slope simulations. The breaker parameter decreases for a milder slope. The Froude number of the bore is lower. This is also what was found in section 4.3.2 where the Froude number around the coastline is analysed. If the continental shelf slope [α_2] becomes milder than 1:200, the Froude number becomes lower.

For the data that follows the trend, an exponential relation is plotted over the data. This relation holds for slopes equal or steeper than 1:200. From this follows an empirical relationship between the Froude number at maximum velocity and the breaker parameter:

$$Fr_{bore.max} = 6.2 * e^{-2.56*\xi_{tsunami}}$$
[5.8]

The 1:400 slope has a lower Froude number in the simulations. The location of the maximum velocity depends on the breaker parameter. When the breaker parameter is smaller than 0.35, the maximum is at the coastline and when the breaker parameter is larger than 0.35 the maximum is inland.

Equation [5.7] and the theory from section 5.2 can be used to derive the characteristics of the bore at maximum velocity. The breaker parameter can then be used to find where this maximum occurs.
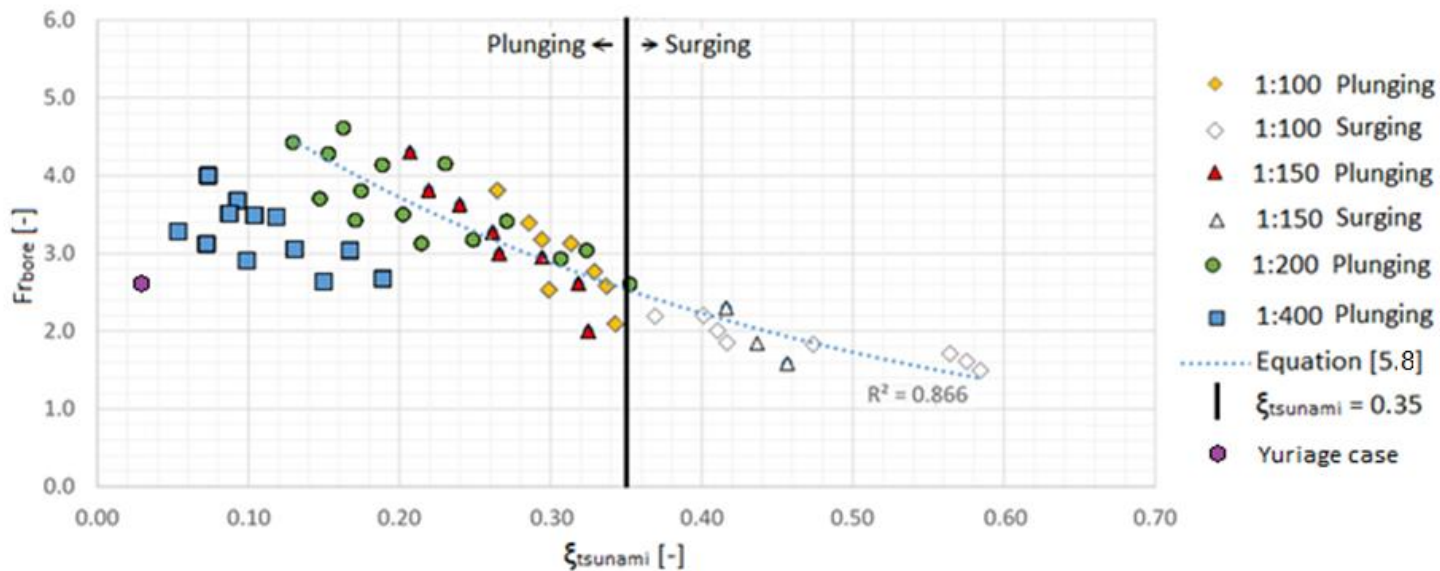
Figure 5.12: Froude number at maximum velocity vs breaker parameter. Relation between the Froude number and the breaker parameter for slopes steeper than 1:200 (dotted line). Breaker relation equation [5.4] (black line). Empty markers are surging breakers.

The breaker parameter divides the results into two groups, either a plunging or a surging breaker. It is possible that the lower Froude numbers for the simulations with an 1:400 slope show a third group. The simulations with an 1:400 slope could be spilling breakers. This would explain the lower Froude numbers. It is recommended that this is examined further in the future.

6.

Physical tests tsunami bore

6.1   Introduction

In this section the tsunami bore is tested in a lab and the bore is compared to the bore from the simulations. The aim of this analysis is to see the velocity and height of the bore in the tests and compare this with the SWASH simulations.

These tests were executed as part of another study, see Esteban et al. [2017]. The aim of the tests of Esteban et al. [2017] is to show the full process of a tsunami bore attack on a tsunami structure and to find a relationship between the energy head and the water level of the bore and the inundation behind the structure. From the energy head of the bore and the design height and type of structure, the inundation depth behind the structure can be predicted.

With this comparison between the tests and the simulations it can be shown what kind of tsunami bore is simulated with this test setup. With the SWASH simulations can be seen at which location the size, shape and velocity of the bore match these of the tests. The tests are compared to two locations in the simulation to find the location that matches best. These locations are at x = 0 and x = 500 m inland.

Because generation of a complete tsunami is not feasible is only the bore is created. This is done by performing a dam break in a flume. With this comparison can be shown if the characteristics of the bore that follows the dam break in a flume represents the characteristics of a tsunami bore as found in the simulations.

6.2   Description of test setup

The tests are performed in a 11m long flume with a width of 40 cm. A sketch with dimensions is given in Figure 6.1. On the left of the figure is a 4.5m long water basin with a variable water height. The water is kept in the basin by a 20 cm high gate. The dam break is realized by quickly opening the gate. This is done by releasing a large mass M that pulls the gate open. The water flows out of the gate with a high velocity. A 1:10 slope is used to slow the water down and to represent a sloping beach. This slope starts directly at the gate. At a height of 20cm the bottom becomes flat again. The structure is placed at 5.5 m from the gate. This location gives the possibility to do water level measurements in front of the structure on a flat bed.
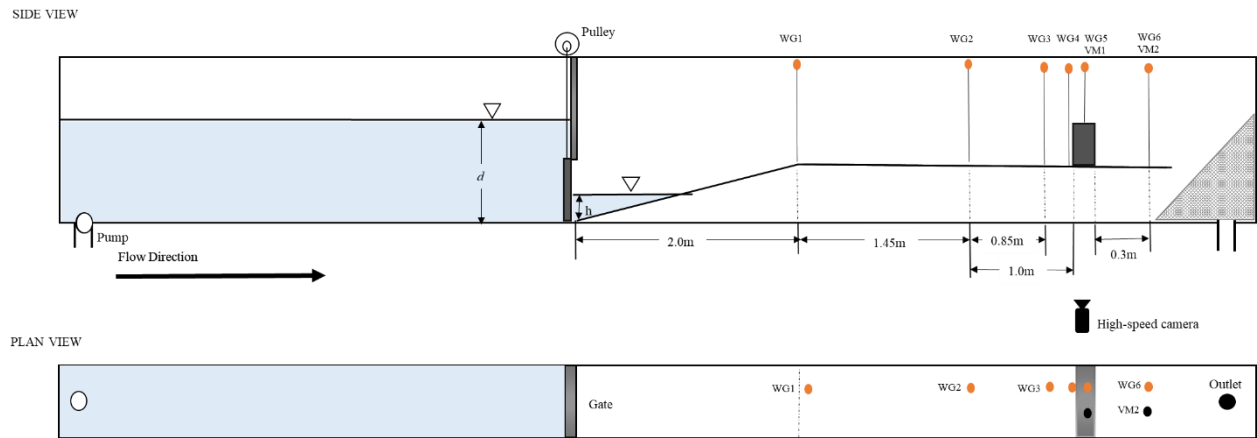
Figure 6.1: Test Setup Lab experiments at Waseda University. Not to scale. [Esteban et al., 2017]

Wave gauges and velocity meters are used to measure the water height and the velocity at several locations along the flume. The wave gauges are placed before the structure and also one gauge on top of the structure and one gauge behind the structure to measure the inundation after overtopping. The output of the velocity measure instruments was not correct due to air entrainment within the turbulent bore. Instead the bore front velocity [v_{front}] is used calculated from the wave gauges.

The bore can be changed by using different heights in the water basin or by using a layer of water in front of the gate. For this test the water height in the basin is varied between 30, 40, 50 and 60 cm. The height of the water layer in front of the gate is varied between 0, 10 and 20 cm. The height of the basin has large influence on the velocity and height of the bore, because the water flows with a bigger pressure through the gate. The water layer after the gate is used to slow the wave down to have different velocities.

These wave conditions are tested on 4 different structures as shown in Figure 6.2. These structures are:

- Vertical wall (full reflection) (a)
- Vertical wall with height of 15cm (b)
- Dyke with height of 10 cm (c)
- No structure

The bore attack in the tests on the vertical wall with a height of 15 cm is described with photos of the test in D. This is however not analysed in this thesis, see Esteban et al. [2017]. This thesis focuses on the hydrodynamics of the bore when no structure is present.
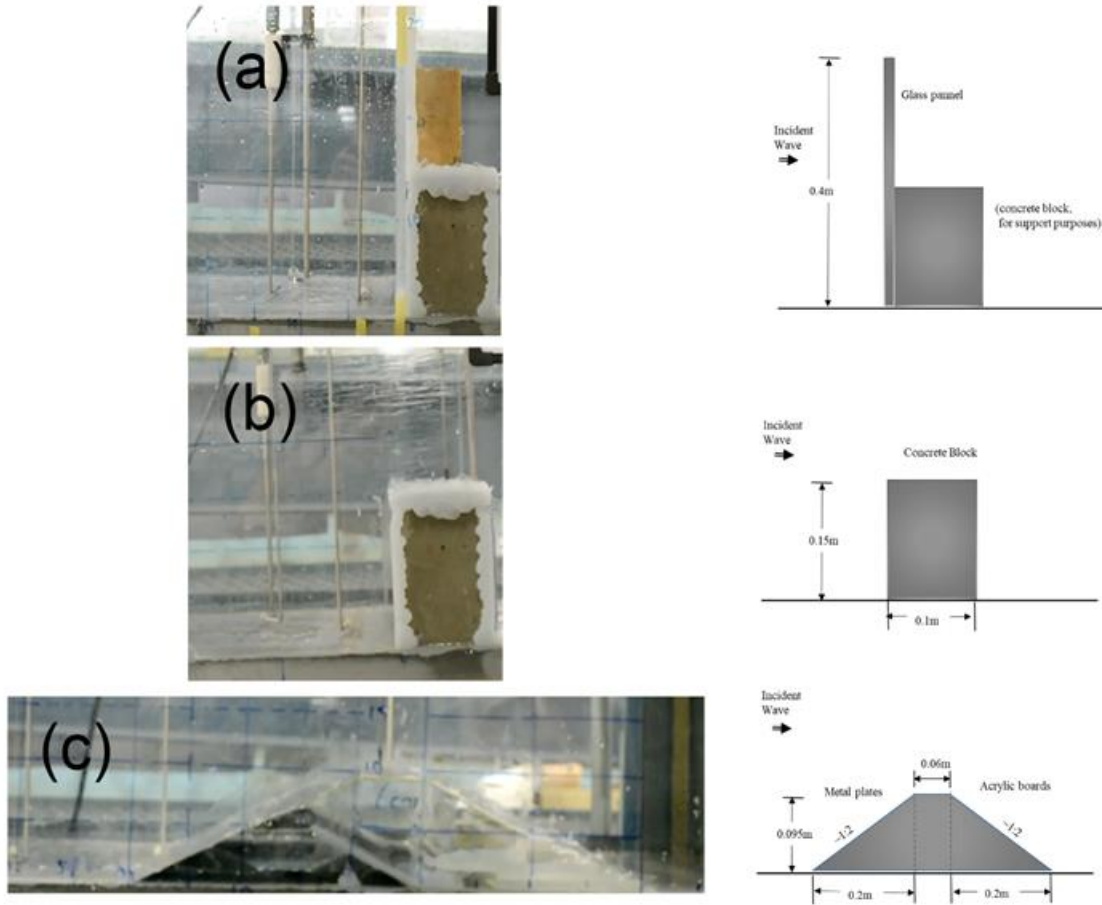
Figure 6.2: Structures used in the tests, a) Vertical wall, b) 15 cm wall, c) 10 cm dike.

6.3 Bore physical tests Compared to the Simulations

The results from the physical tests are compared to the results of the model. There are some problems with comparing the results of the simulations with the physical tests. Firstly, the output of the velocity measurements was not correct due to air entrainment within the turbulent bore. Instead, the bore front velocity [v_{front}] is used as obtained from the wave gauges. Secondly, the water surface elevation of the bore was measured with wave gauges but only the maximum inundation [H_i] of the bore could readily be obtained from the data. This gives a velocity at the front of the bore and a height at the highest water level which occurs much later. These are two values of different locations in the wave and a clear relationship between them cannot be given.

6.3.1 Scaling of the bore

The bore of the tests is scaled with 2 scaling factors in appendix D.2. The velocities [v_{front}] of the tests match the bore front velocity of the simulations [v_{front}] with a scaling of 1:50 while the heights [H_i] of the tests are too low. The inundation height of the test match the inundation height of the simulations for a scaling of 1:200. In this case the velocities far to too high. This could be due to the roughness of the bottom in the

tests. The tests are performed on a very smooth steel bottom that has very low friction. The Manning roughness coefficient should then be lower than 0.06 m$^{-1/3}$s.

6.4 Time series of Simulations and Tests

In this section is investigated if the bore front of the tests and simulations simulate the same bore and if the bore from the test looks the same as the bore in the simulations. In section 6.2 was shown that this is not the case.

The time series of the physical tests are compared to the time series of the SWASH simulations. The time series are plotted for the test with d = 40 cm and h = 10 cm, in Figure 6.3 and Figure 6.4. The time series are shown for a scale of 1:50 and 1:200. These time series are compared with time series of the bore in the simulations. This is done with the simulation at two locations, x_4 at the coastline and x_5 at 500 meters inland. The time series of the model are shown with an initial wave length of 100 and 150 km, a slope of 1:200 and an initial wave height of 6 meters. These tests have the best match for a 1:200 scale.

The time series are quite similar for the first 80 seconds. After 80 seconds the height drops in test while the model still has an increasing water level. The model also shows soliton fission at the coast line (x=0). This soliton fission is from the reflective. The bore fronts in the time series do match until the height drops in the tests. The bore at 500m inland gives the best match in the case of figure 6.3. In Figure 6.4 a zoom at the front of the bore is given. The time series match very well. The bore of the test matches the bore of the simulation quite well in this case. However, the dam-break test has a too high velocity or to low height depending on the scale.
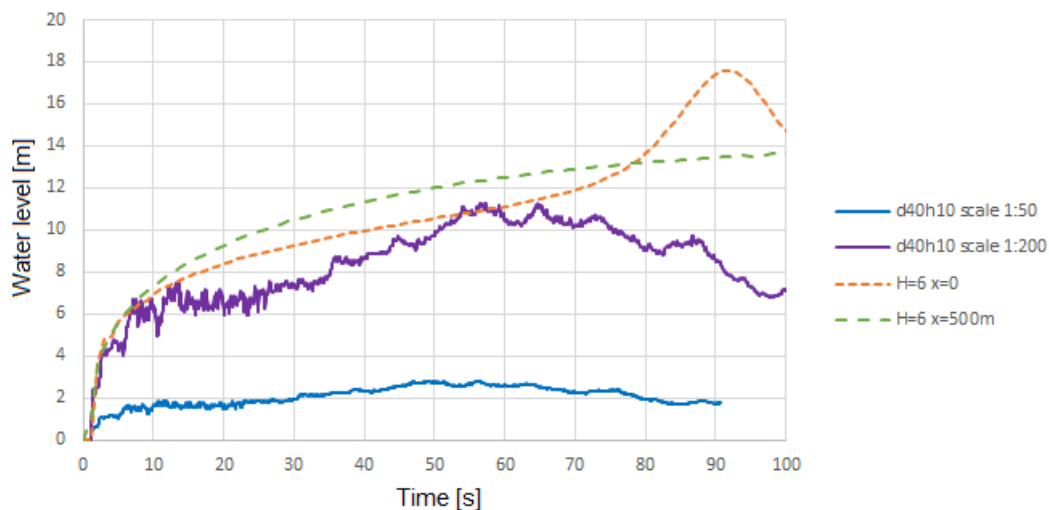
Figure 6.3: Time series of the bore. Solid line is from dam-break tests. Dashed lines are from simulations.
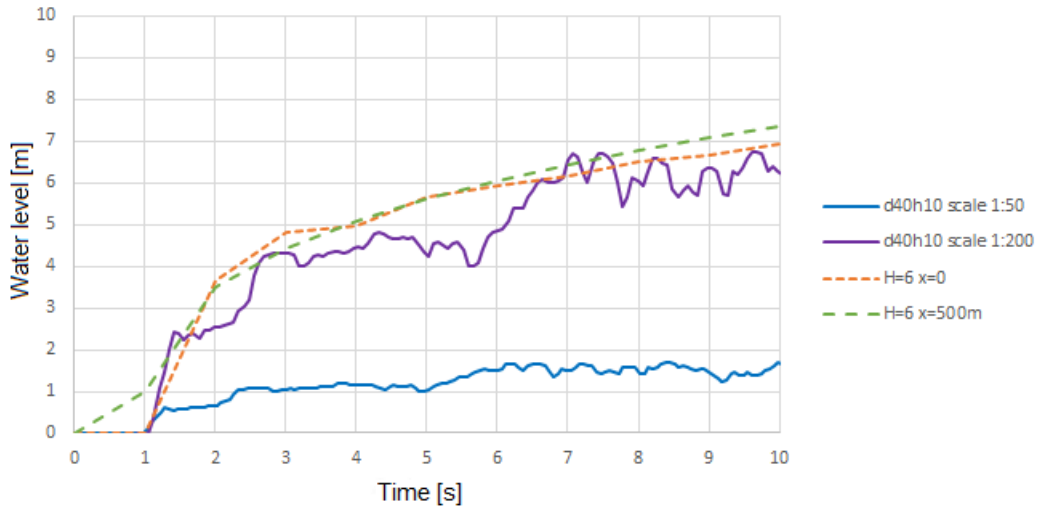
Figure 6.4: Zoom at bore front of Time series of the Bore. Solid line is from dam-break tests, Dashed lines are from simulations.

6.4.1 Dimensionless comparison of tests and simulations

A better way to look at the test and the simulations is by removing the scaling factor and comparing a dimensionless factor. This is done by using the Froude number of the bore. The inundation height obtained from the measurements is less interesting for the bore front. It is therefore better to find a bore height at the bore front H_{front}. The Froude number of the bore front can then be found with v_{front} and equation [6.1]. The time series are made dimensionless to compare the tests with the simulations.

$$Fr_{front} = \frac{v_{front}}{\sqrt{g*H_{front}}}$$ [6.1]

H_{front} is found by first multiplying time on the x-axis, see Figure 6.3, by the bore front velocity of the unscaled data. This leaves $v_{front}*t$ in Figure 6.5 a and b. Both axis have the unit meters. The bore front height H_{front} is obtained from the intersection with a line at an angle of 2.5˚ with the x-axis. With this angle the line crosses the bore relatively close to the bore front and has a clearly visible intersection with the bore. For every test and simulation the bore front height H_{front} is now obtained and is shown in Table 6.1 and Table 6.2.

The height [h_{front}] and velocity [v_{front}] at the bore front are now determined and the Froude number [Fr_{front}] of the tests and simulations at the bore front can be calculated with equation 6.1. The Froude numbers are shown in Table 6.1 and Table 6.2.
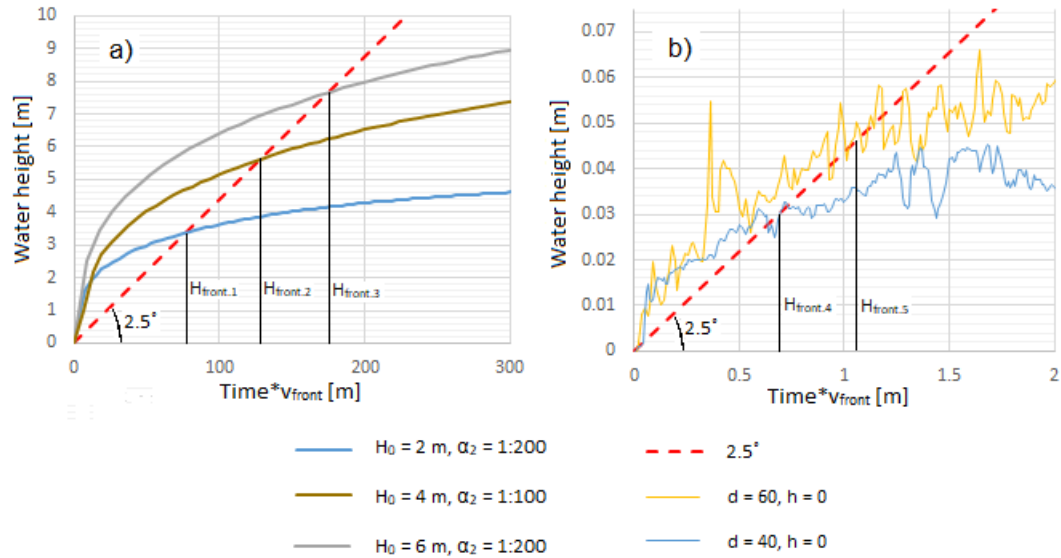
Figure 6.5: Bore obtained from time series of a) simulations at x_5 and b) tests. Red line with 2.5° angle with x-axis to find H_{front}.

The Froude numbers of the test are ranging from 1.45 to 2.69 while the Froude numbers of the simulations are ranging from 1.34 to 2.6 at the coast line x_4 and ranging from 0.65 to 1.14 at x_5. This difference between the location x_4 and x_5 is due to the difference in velocity at the two locations. This shows that the Froude numbers of the tests match the Froude numbers of the simulations at location x_4 very well. The Froude numbers do not match at location x_5. The velocity at this location has reduced to much. The Froude numbers of the test with the dam-break are correct for walls at the coastline. For a wall at a more inland location, the tsunami should be tested with a bore that has a lower velocity while the height remains same to get matching Froude numbers at location x_5.

	v_{front} [m/s]		h_{front} [m]		FR_{front} [-]	
x	x_4	x_5	x_4	x_5	x_4	x_5
H2 a1:200	8.18	3.75	2.2	3.4	1.76	0.65
H4 a1:200	14.52	6.58	3.6	5.6	2.44	0.89
H6 a1:200	18.42	8.79	5.1	7.6	2.60	1.02
H8 a1:200	19.34	10.82	6.6	9.2	2.40	1.14
H2 a1:400	9.24	3.19	1.5	2.4	2.41	0.66
H4 a1:400	12.62	5.36	2.4	4.4	2.60	0.82
H6 a1:400	15.14	6.93	3.4	5	2.62	0.99
H8 a1:400	17.09	8.18	4.0	6.8	2.73	1.00
H2 a1:100	-	3.78	-	3.4	-	0.65
H4 a1:100	-	6.22	-	5.6	-	0.84
H6 a1:100	10.99	8.39	6.9	9.1	1.34	0.89
H8 a1:100	15.53	10.41	8.2	9.6	1.73	1.07

Table 6.1: Front velocity, front height and front Froude number at x = 0m and x = 500m, for simulations with L_0 = 150 km.

d	h	v_{front} [m/s]	h_{front} [m]	Fr_{front} [-]
30	0	1.24	0.034	2.14
30	10	1.15	0.037	1.92
30	20	0.88	0.037	1.45
40	0	1.68	0.055	2.29
40	10	1.37	0.056	1.84
40	20	1.79	0.056	2.41
50	0	2.12	0.086	2.31
50	10	1.92	0.078	2.20
50	20	1.66	0.083	1.84
60	0	2.59	0.122	2.37
60	10	2.43	0.107	2.37
60	20	2.7	0.103	2.69

Table 6.2: Front velocity, front height and front Froude number of the physical tests.

7.

Discussion

One layer simulations

The SWASH model which is used for simulations has only one layer in the vertical. The SWASH simulations where supposed to be performed with multiple layer to see if there is dispersion in the wave. However, due to errors with SWASH the results from these simulations gave empty data cells. This could thus not be analysed. The velocity of the model is thus depth averaged.

No leading depression

A tsunami wave can be proceeded by a leading depression. During the simulations only one wave form is modelled and analysed. This wave had only a positive initial elevation. This is a wave consisting of two cosine waves and elevated that the wave had only positive elevation. A leading depression could increase the steepness of the wave. What this would have done to the characteristics of the bore is unclear.

Offshore roughness

The focus in this thesis is on the onshore part of the model. The roughness coefficient is thus calibrated for the onshore part of the model. For the offshore part of the model the default value of SWASH is used. The offshore (Manning's) roughness is set to be constant at 0.019 $m^{-1/3}$s. This value could be low if there are factors that give roughness, like vegetation. It is assumed that this is not the case and the roughness to be used in the SWASH simulations is equal to 0.019 $m^{-1/3}$s.

Flat onshore bottom

A flat slope is used for the onshore slope [α_3] in the simulations. This is done for two reasons. First, to let the model represent the coast at Yuriage, since this is also flat. And second, to have the same conditions as the Physical tests where the bore is also simulated on a flat slope. however, the onshore slope in not completely flat because the for the first 200 m there is a 1:200 slope that becomes flat when 1 m elevation is reached. The results would be better if the onshore slope was flat at 0 m elevation.

Wave lengths

The wave length is normally calculated with the period [T] times the celerity [$\sqrt{gd}$]. In this thesis the actual length of the wave is used and not a calculated length. The length of the point where the elevation becomes larger than zero at the front of the wave until the elevation becomes zero at the tail of the wave is used as the wave length. This is also done for the length used in the breaker parameter [L_ξ] at 100m depth. With SWASH it is possible to take the real length of the wave. The waves on slope α_2 of 1:50 have a longer length than the distance to the shore. These simulations could thus not be used. For a better result it is good to also include even steeper slopes in the analysis.

Wave skewness and offshore depth

The skewness of the wave and the offshore depth are not analysed quantitatively. These parameter are important for the steepness of the wave and for the breaker parameter. This could be included for a more complete study. However, the breaker parameter is defined in a way that takes into account skewness and steepness by taking the length of the wave front and not the complete length of the wave.

Reflection

The water level obtained from SWASH shows the total water level. This is the combination of the incoming wave and the reflective wave. Because the interest of this thesis is the incoming tsunami bore it is assumed that the wave has no reflected wave when the bore runs-up the slope and thus represents the incoming tsunami wave bore. The location of $\xi_{tsunami}$ was chosen to have no interference of the coast on the wave. The wave period in the simulations was always shorter than the time it takes for the wave to reflect from the coast. However, there can still be some be some reflection in the data obtained from SWASH.

Roughness Physical tests

The physical tests are performed in a flume with a steel plate bottom. This steel bottom could have very low friction. The Manning's friction coefficient used in the simulations is then probably higher than the tests. This could be the cause of the higher velocity in the tests. The simulations are performed with a roughness on land representing a middle density urban area. However, the offshore roughness in the model was very low. Only a Manning's roughness coefficient of 0.19 $m^{-1/3}s$ was used.

8.

Conclusion and Recommendations

The conclusions of the thesis are shown below in section 8.1. Section 8.2 shows the recommendation for further studies.

8.1   Conclusion

The dimensions of the bore that follows from a tsunami wave are investigated in this thesis. The tsunami waves were modelled with a one-dimensional numerical SWASH model. The results of this thesis are to be used for the design of coastal tsunami barriers or coastal structures. The wave was modelled from the source in offshore deep water to the coast. The most influential factors on the development of the bore are investigated.

Validation of SWASH

The SWASH model was validated by simulating the soliton breaking measured by Grilli et al. [1997]. The wave started breaking at larger depth in the SWASH model and dissipated more energy. During breaking there was not a good representation of the wave. The energy dissipation due to breaking influenced the run-up of the wave. However, most features of the wave, like the dispersion and velocity, where simulated correctly. The run-up of breaking soliton waves could not be validated because there was no relation for breaking soliton waves found in literature. The SWASH model was validated with the 2011 Tohoku tsunami at Yuriage, Japan. The friction at run-up was calibrated also with the 2011 Tohoku tsunami case of Yuriage. The Manning roughness coefficient found with this calibration was $0.06 \text{ m}^{-1/3}\text{s}$

Influential factors on the bore

SWASH simulations with different continental slope [α_1], offshore depth [d_0] and the offshore wave length [L_0] were made in order to show the influence of these factors on the characteristics of the tsunami wave around the shore line. The tsunami waves were simulated at the offshore location where the earthquake causes a water elevation. The wave moves from this offshore location to the shore.

The offshore wave length has very little influence on the water level of the wave after shoaling. The difference in water elevation at the boundary between the continental slope and continental shelf (location x_2) was only 1.3% for a 50 km difference in wave length. The difference is larger for the continental slope and the offshore depth. The differences in water elevation at location x_2 was only 1.2% for the most common slopes. The offshore depth had the largest influence on the wave during shoaling. Because of the larger difference in depth, the wave was more subjected to shoaling for a larger depth. The wave of the larger offshore depths d_0 were higher and had a shorter period and wave length and this leads

to a steeper wave. This can be calculated with Green's law. The slope of the continental shelf α_2 did not influence the shoaling at location x_2.

Characteristics for calculation of the force

The forces on the coastal structure with the FEMA [2012] theory need to be calculated with the maximum momentum flux [hu^2], equation [2.14]. The this momentum flux was maximum for different combinations of h and u at different locations on the coast. For the different slopes was the profile on the coast of the momentum flux also very different. However, the maximum was always at the coastline.

Bore parameters

Tsunami waves with different wave length [L_0], initial wave height [H_0], wave skewness, offshore depth [d_0] and the slope of the continental shelf [α_2] were simulated with SWASH. The influence of these parameters on the development of a bore at the nearshore locations was analysed.

There was not a good definition of the bore height at the bore front. A new definition of the bore front height is given in this thesis based on the SWASH simulations. The height of the bore front [h_{bore}] is defined at the location where the depth averaged velocity in the bore is maximum. This is close to the actual front of the bore (in the order 1 to 10 m). This bore height and this velocity are the characteristics of the tsunami bore and are described by the Froude number of the bore [Fr_{bore}].

The wave length, the wave skewness and the offshore depth did not influence the Froude number of the bore. They only influenced the steepness of the bore. The steepness of the bore had influence on where the wave breaks. A steeper wave breaks at a larger depth. However, the bore characteristics were not very different when it reaches the coast.

The initial elevation and the continental shelf slope were of most influence on the bore. The Froude number of the bore [Fr_{bore}] was higher due to an increase in velocity of the bore for larger wave heights [H_0]. A slope [α_2] of 1:200 had the highest Froude number while slopes of 1:100 and 1:400 had a smaller Froude number. The bore on a 1:400 slope also had a lower velocity. The bore had a maximum value for which the Froude number did not get any bigger for larger elevations. This maximum depended on the slope and the wave length.

Breaker parameter

The wave steepness of the wave determines if the tsunami wave will break or if the wave will flow on the coast without breaking. The parameters used that influence the steepness of the wave are the length of the wave front and the wave height at x_2. The slope had influence on the shoaling and therefore also on the steepness of the wave. A breaker parameter [$\xi_{tsunami}$] was used to describes the wave at 100 m depth of the coast. This parameter tells if one of two breaking types occurs when the wave arrives at the coast. There was possibly even a third breaker type in the simulations.

A tsunami that breaks and develops a bore seaward of the coast is defined as type A or plunging breaker, and when the wave is not broken and develops into a bore on land is defined as type B or surging breaker. A breaker parameter is defined based on tsunami height and wave front length at 100 m depth (equation [5.2]) and based on the simulation results. The breaking type was described with the following relationship.

Type A, bore at coastline: $\xi_{tsunami} < 0.35$ [8.1]

Type B, no bore at coastline: $\xi_{tsunami} > 0.35$

The breaking type of the bore has influence on the ideal location of the coastal structure. Breaker type A had a high velocity at the coastline. The maximum bore velocity was at the coastline when the breaker parameter is smaller than 0.35. Breaker type B had its highest velocity at an inland location. The best location for type A is thus a few 100 meters inland while the structure can best be built at the coastline for type B. An empirical relationship of the Froude number at maximum velocity with the breaker parameter is given in equation [8.2].

$$Fr_{bore} = 6.2 * e^{-2.56 * \xi tsunami}$$ [8.2]

This equation hold for slopes steeper than 1:200. For milder slopes the Froude number was lower.

The breaker parameter can analytically be found from the offshore wave characteristics. The Green's law was used to describe the breaker parameter at 100 m depth with the offshore wave characteristics at larger depth. Also the relationship between the breaker parameter [$\xi_{tsunami}$] and the breaker parameter [ξ_{ASCE}] by ASCE [2016] was investigated. This resulted in $\xi_{ASCE} \approx 11.25* \xi_{tsunami}$.

Physical tests

Physical tests with a dam-break were performed to show if the parameters of the tsunami bore found in the simulations can be reproduced with a dam-break set-up. By comparing the results of the tests and the simulations can be concluded that, depending on scaling, either the bore height is too small or the bore front velocity is too large compared to the simulations. The two bores have an equal bore front when the dimensionless time series of the waves are shown next to each other. This is also shown with the Froude number. The Froude number is equal for the simulations and tests at the coastline. However, the Froude numbers of the tests are much larger than those simulations at 500 meters inland.

8.2   Recommendation

The results of this thesis give the characteristics of the tsunami bore. However, further research is recommended.

SWASH simulations
SWASH is used for one-dimensional simulations. However, the bathymetry usually differs alongshore. The effects of refraction and diffraction can then have effect on the wave. It is thus recommended to do two-dimensional simulations. The Yuriage case can be modelled in more precision with a 2D model.

Breaker parameter
The breaker parameter criterion now states that for a breaker parameter smaller than $\xi_{tsunami} = 0.35$, the maximum velocity is not at the coastline but more inland. Further research of the data could examine at what location this maximum velocity is for a given breaker parameter.

Equation [8.4] holds for continental shelf slopes [α_2] steeper than 1:200 but deviations were apparent for $\alpha_2 = 1:400$. However, it is not investigated for which slope the Froude number starts decreasing. A more detailed study of slopes between 1:200 and 1:400 is recommended. The transition from splunging to spilling breakers can then also be investigated. The steepest slope used is 1:100. For better results it is recommended to do the tests with a 1:50 slope as well. For these simulations there should be carefully looked at the length of the wave at 100m depth, since this is longer than the distance to shore.

Physical test
The SWASH model can be used for simulation the tsunami bore in combination with a wall. The velocity of the bore can then be used to calculate the impact forces by the bore on the wall. The hydrostatic forces on the wall when the water level in front of the wall is maximum, can be calculated in combination with equation [2.14].

Another study that should be done with the model is continuing the study of Esteban et al. [2017]. The bores with different velocities and heights can be simulated with SWASH on different structures. These structures can be either vertical or sloping. The water level in front of the structure and behind the structure can then be obtained from the model and used to calculate the amount of overflow. This could give an improvement on equation [2.18]. Although it's not part of the scope of this thesis, a simulation of a bore is done in combination with a wall. The four stages of Figure D.1 of the physical tests are also visible in the simulation. With line a as the incoming bore and line d at maximum overflow, in Figure D.1. line b shows the splash when the bore hits the wall.

Bibliography

Arcas, D., & Segur, H. (2012). Seismically generated tsunamis. *Philosophical Transactions of the Royal Society A, 370*, 1505-1542. doi:10.1098/rsta.2011.0457

ASCE. (2016). Minimum Design Loads and Associated Criteria for Buildings and Other Structures. Chapter 6: Tsunami loads and effects.. *American Society of Civil Engineers*, *7-16*, 25-50.

Battjes, J. A. (1986). Energy dissipation in breaking solitary and periodic waves. *Communications on hydraulic and geotechnical engineering*, *86*(5), 466-480. uuid:79b3ffff-0c6d-4101-99fc-39facc7004db

Battjes, J.A. [1974] Surf Similarity: Civil Engineering Department Delft University of Technology, Delft, Netherlands.

Bosboom, M. J. F., & Steve, J. (2015). *Coastal dynamics 1*. Delft, Netherlands: VSSD.

Bryant, E. (2008). *Tsunami: The Underrated Hazard* (2e ed.). Chichester, UK: Springer.

Camfield, E. (1980). *Tsunami Engineering* (Report No. 6). Retrieved from
https://archive.org/details/tsunamiengineeri00camf

Charvet, I., Eames, I., & Rossetto, T. (2013). New tsunami runup relationships based on long wave experiments. *Ocean Modelling*, *69*, 79-92.

Chock, G. Y. K. (2016). ASCE 7 Tsunami Loads and Effects Design Standard For the U.S. *Journal Structural Engineering*, *142*(11), 1-12.

Dean, R. G., & Dalrymple, R. A. (1984). Water Waves Mechanics for Engineers And Scientists. London, UK*: World Scientific*.

Ei, G.A., Grimshaw, R.H.J., Tiong, W.K. [2012] Transformation of a shoaling undular bore. *Journal of Fluid Mechanics. Cambridge University Press. 709, 371-395*. doi:10.1017/jfm.2012.338

Esteban, M., Glasbergen, T., Takabatake, T., Hofland, B., Nishizaki, S., Nishida, Y., Stolle, J., Nistor, I., Bricker, J., Reniers, A., Takagi, H., T., Shibuyama T. [2017] Overtopping of coastal structures by Tsunami waves. *Geosciences 7(4), 121,* doi:10.3390/geosciences7040121

FEMA [2012] Guidelines for Design of Structures for Vertical Evacuation from Tsunamis.

González, F.I. [1999] Tsunami!, *Scientific America. 56-65.*

Grilli, S.T., Svendsen, I.A., Subtamanya, R. [1997] Breaking Criterion and Characteristics for Solitary Waves on Slopes. Journal of Waterway, Port, Coastal, and Ocean Engineering. 102 - 112.

Horsten, B.P.M. [2016] Design Study of a Flexible-Membrane. Tu Delft.

Li, Y., Pan, D.Z., Chanson, H., Pan, C.H. [2017] Tidal bore progressing on a small slope. Experimental Thermal and Fluid Science 88. 513-518. doi:10.1016/j.expthermflusci.2017.07.004

Iribarren, C.R., Nogales, C. [1949] Protection des ports. PIANC congress 1949 SII-C4 Hydraulic Engineering Reports. PIANC. uuid:7ab718ff-a74d-4141-8c3f-413044c751c4

Jager, T., Smoor, A.C., Tiehatten, B.M.H., Wester, F.E. [2015] Assessment & Mitigation Proposal in case of major tsunami impact: How to reduce the impact of a stunami in Iquique, Chile. TU Delft, Department Hydraulic Engineering.

Kaiser, G., Scheele, L., Kortenhaus, A., Løvholt, F., Romer, H., Leschka, S. [2011] The influence of land cover roughness on the results of high resolution tsunami inundation modeling. *Natural Hazards and Earth System Sciences. 11*, 2521–2540. doi:10.5194/nhess-11-2521-2011

Labeur, J.A., Battjes, R.J., [2014] Open Channel Flow: Lecture notes of CTB3350. TU Delft.

Madsen, P.A., Fuhrman, D.R., Schäfer, H.A [2008] On the solitary wave paradigm for tsunamis. Journal of Geophysical Research. Vol. 113. C12012, doi:10.1029/2008JC004932

Matsuyama, M., Ikeno, M., Sakakiyama, T., Takeda, T. [2007] A Study of Tsunami Wave Fission in an Undistorted Experimen. Pure and Applied Geophysics. 164, 617-631. doi:10.1007/s00024-006-0177-0

Munk, W. H. (1949). he Solitary Wave Theory and its Applications to Surf Problems. *Annals of the New York Academy of Sciences*, *51*, 376-424. doi:10.1111/j.1749-6632.1949.tb27281.x

Navionics. (n.d.). Retrieved from https://www.navionics.com

NOWPHAS / ナウファス [n.d.] NOWPHAS. NOWPHAS the nation wide Ocean Wave information network for ports and Harbours. Restrieved from https://nowphas.mlit.go.jp/eng/.

Okumura, N. [2016] Evaluation of a tsunami risk reduction system or Kamakura. TU Delft.

Ramsden, J. D., & Raichlen, F. (1990). Forces on vertical wall caused by incident Bores. *Journal of waterway, port, coastal, and Ocean Engineering*, *116*, 592-613.

Saito, T., Ito, Y., Inazu, D., Hino, R. [2011] Tsunami source of the 2011 Tohoku-Oki earthquake, Japan: Inversion analysis based on dispersive tsunami simulations. *Geophysicl Research Letters, 38, L00G19,* doi:10.1029/2011GL049089.

Schimmels, S., Sriram, V., Didenkulova, I. [2015] Tsunami generation in a large scale experimental facility. *Coastal engineering journal, 110.* 32-41.

Shibayama, T., Esteban, M., Nistor, I., Takagi, H., Thao, N.D., Matsumaru, R., Mikami, T., Aranguiz, R., Jayaratne, R., Ohira, K. [2013] Classification of Tsunami and Evacuation Areas. *Natural Hazards. 67*, 365-386. doi:10.1007/s11069-013-0567-4

Smit, S., Zijlema, M., Stelling, G. [2013] Depth-induced wave breaking in a non-hydrostatic, near-shore. *Coastal Engineering, 76,* 1-15

Synolakis, C.E. [1987] The runup of solitary waves. *Journal of Fluid mechanics, 185*, 523-545.

Tadepali, S., Synolakis, C.E. [1994] The run-up of N-waves on sloping beaches. *The Royal Society. 445*, 99-112. doi:10.1017/S002211208700329X

The SWASH team [2017] SWASH user manual version 4.01. Delft University of Technology.

List of Parameters

α_1	Continental slope parameter		-
α_2	Continental shelf slope parameter		-
α_3	Onshore slope parameter		-
α	Breaking factor is SWASH		-
α_{Fr}	Froude number coefficient		-
Δx_i	Horizontal distance of segment		m
$\eta_{0,1,2,3,4,5}$	Water elevation at location $x_{0,1,2,3,4,5}$		m
η_0	Initial water elevation at location $x_0 = H_0$		m
η_{max}	Max water elevation at crest of wave		m
η^+	Water elevation of wave travelling to the shore		m
$\xi_{tsunami}$	Tsunami breaker parameter at depth of 100m		-
ξ_{ASCE}	Tsunami breaker parameter at depth of 100 m by ASCE [2016]		-
ξ	Irribaren number		-
φ_i	Average ground slope between i and i-1		-
ρ_w	Density water		kg/m^3
ρ_s	Density liquid including sediment		kg/m^3
c	Wave celerity		m/s
C_d	Drag coefficient	2	-
d	Water depth		m
d_0	Initial depth		m
$d_{1,2,3,4}$	Depth at location 1, 2, 3 or 4		m
d_{100}	Depth at breaker parameter	100	m
$d_{offshore}$	Depth at offshore location before shoaling		m

$E_{g.i}$	Hydraulic Energy Head		m
F_h	Horizontal Hydrostatic Force		N/m
F_{FEMA}	Bore impact Force calculated by FEMA theory		N/m
$F_{Ramsden}$	Bore Impact Force calculated by Ramsden theory		N/m
Fr_{bore}	Froude number with H_{bore} and v_{bore}		-
$Fr_{bore.max}$	Froude number Fr_{bore} at maximum velocity in the bore [$v_{bore.max}$]		-
Fr_{front}	Froude number with H_{front} and v_{front}		-
Fr_i	Froude number at location i		-
Fr_{inun}	Froude number at maximum inundation depth		-
g	Acceleration of gravity	9.81	m/s^2
H	Wave height		m
H_ξ	Wave Height at 100m depth		m
H_0	Offshore water elevation at location x_0		m
$H_{0.grilli}$	Soliton wave Elevation – Grilli Simulations		m
$H_{0.grilli}$	Offshore depth – Grilli Simulations	1	m
H_b	Wave height at breaking - Grilli Simulations		m
h_b	Depth at breaking – Grili Simulations		m
H_{behind_wall}	Inundation depth behind a seawall		m
H_{bore}	Bore height		m
$H_{bore.max}$	Bore height at maximum velocity in the bore		m
H_i	Height incoming bore - physical tests		m
H_{inun}	Inundation depth		m
$H_{max.inun}$	Maximum inundation depth		m
H_{max}	Maximum inundation depth at location of the wall		m
$H_{offshore}$	Wave height at offshore location before shoaling		m
h_{wall}	Wall height		m
Hv^2	Momentum flux		m^3/s^2

$[Hv^2]_{max}$	Maximum momentum flux	m^3/s^2
i	Location i	-
I_{TSU}	Importance parameter	-
k	Wave number	m^{-1}
K'	Dissipation factor	-
k_s	Shoaling factor	-
L	Wave length	km
L_ξ	Wave length of wave front for wave at 100m depth	m
L_0	Initial offshore wave length at location x_0	km
$L_{offshore}$	Wave length at offshore location before shoaling	km
L_{front}	Wave length of wave front	km
L_{tail}	Wave length of wave tail	km
n	Manning roughness coefficient	$m^{-1/3}s$
R	Run-up height	m
s	Slope – Grilli Simulations	-
S_0	Slope Parameter	-
s_i	Friction slope between i and i-1	-
t	Time	s
T_{TSU}	Tsunami wave period when crest is at 100 m depth	s
u_{bore}	Maximum local depth averaged velocity in the bore front	m/s
$u_{bore.max}$	Maximum local depth averaged velocity of the bore	m/s
u_{inun}	Velocity at maximum inundation	m/s
u_i	Velocity at location I	m/s
$u_{max.inun}$	Velocity at maximum inundation	m/s
v_{front}	Velocity of the bore front	m/s
$x_{0,1,2,3,4,5}$	Location 0, 1, 2, 3, 4 and 5	m
x_b	Location of breaking – Grilli Simulations	m
x_R	Run-up distance	km

List of Figures

List of Tables

A

Soliton breaking tests

In this section the SWASH simulations are compared to the test by Grilli et al. [1997]. These simulations are performed to validate the SWASH model. The comparison between these tests is done by plotting the results of the simulations over the results of the tests. The results of the tests and the simulations are given in Table 3.1. This table shows the characteristics of the waves. In the table the breaker heights and location of the tests and the simulations are given.

slope	H_o [m]	Grilli et al. [1997]			SWASH		
		H_b [m]	h_b [m]	x_b [m]	H_b [m]	h_b [m]	x_b [m]
1:100	0.2	0.36	0.34	66	0.32	0.45	55.4
	0.4	0.63	0.60	39	0.48	0.66	33.8
	0.6	0.78	0.76	24	0.60	0.81	18.9
1:35	0.2	0.36	0.25	26	0.28	0.36	22.4
	0.4	0.59	0.43	20	0.46	0.58	14.6
	0.6	0.75	0.57	15	0.58	0.74	9
1:8	0.2	-	-	-	0.23	0.18	6.6
	0.4	0.41	0.08	7.4	0.41	0.41	4.7
	0.6	0.59	0.13	7	0.55	0.56	3.5

Table A.1: Breaker height, Breaker depth and breaker location for the test by Grilli et al. [1997] and the SWASH simulations.

In figure A.1 to A.4, the results of the simulations are plotted next to or over the results from Grilli et al. [1997].

In figure A.1 the results of the 1:100 slope simulations and tests are plotted. The wave where breaking first takes place is shown. The wave breaks at a deeper location than the tests. In figure A.3 the results of the 1:35 tests are plotted. Here, the wave where breaking first takes place are also given. For the test with H_0 = 0.2 m is the wave plotted at multiple times from the start until breaking, in figure A.2. In this figure the further development of the wave can be seen. Until the location where the simulations start breaking are the waves of the test and simulations equal. The waves are the same until the wave starts breaking at x/h_0 of 22.4. After the simulations start breaking there is loss of energy. The simulation starts to dissipate while the Grilli test is still shoaling.

In figure A.4 the test of the 1:8 slope is shown. These results are not very good. The SWASH simulations do not do well on this very steep slope.
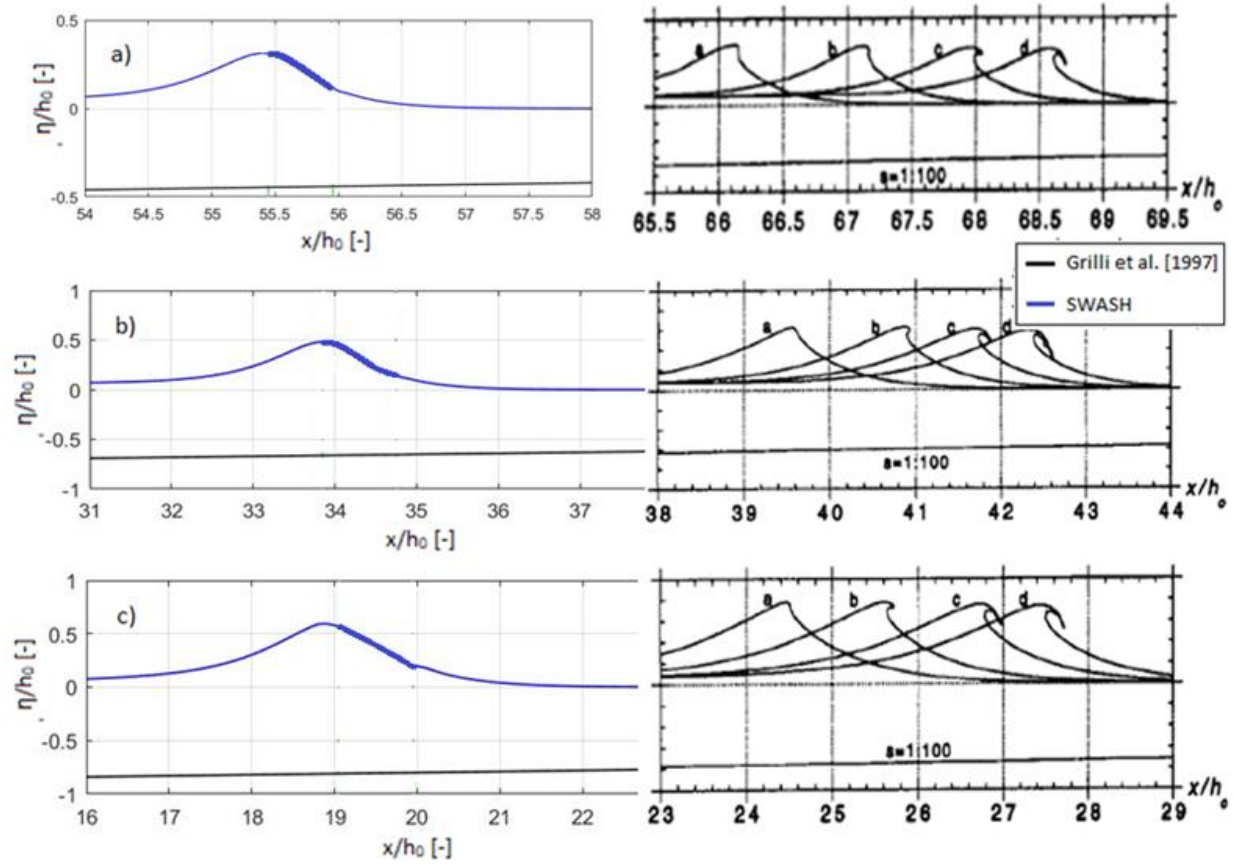
Figure A.1: Simulation of solitary wave with s = 1:100 and a) H0 = 0.2, b) H0 = 0.4and c) H0 = 0.6 .Thick line show where breaking occurs in the wave in the first breaking wave.
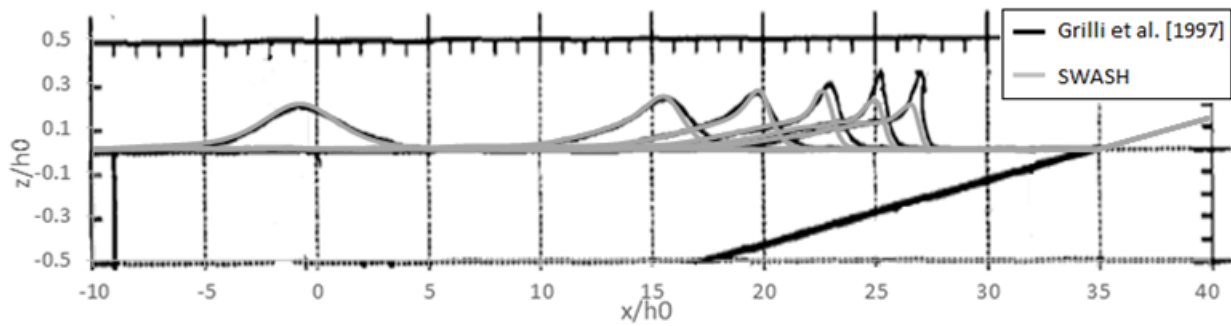
Figure A.2: Wave from SWASH simulation plotted over results from Grilli et al. [1997]. Grey: Simulations. Black: Grilli et al. [1997].
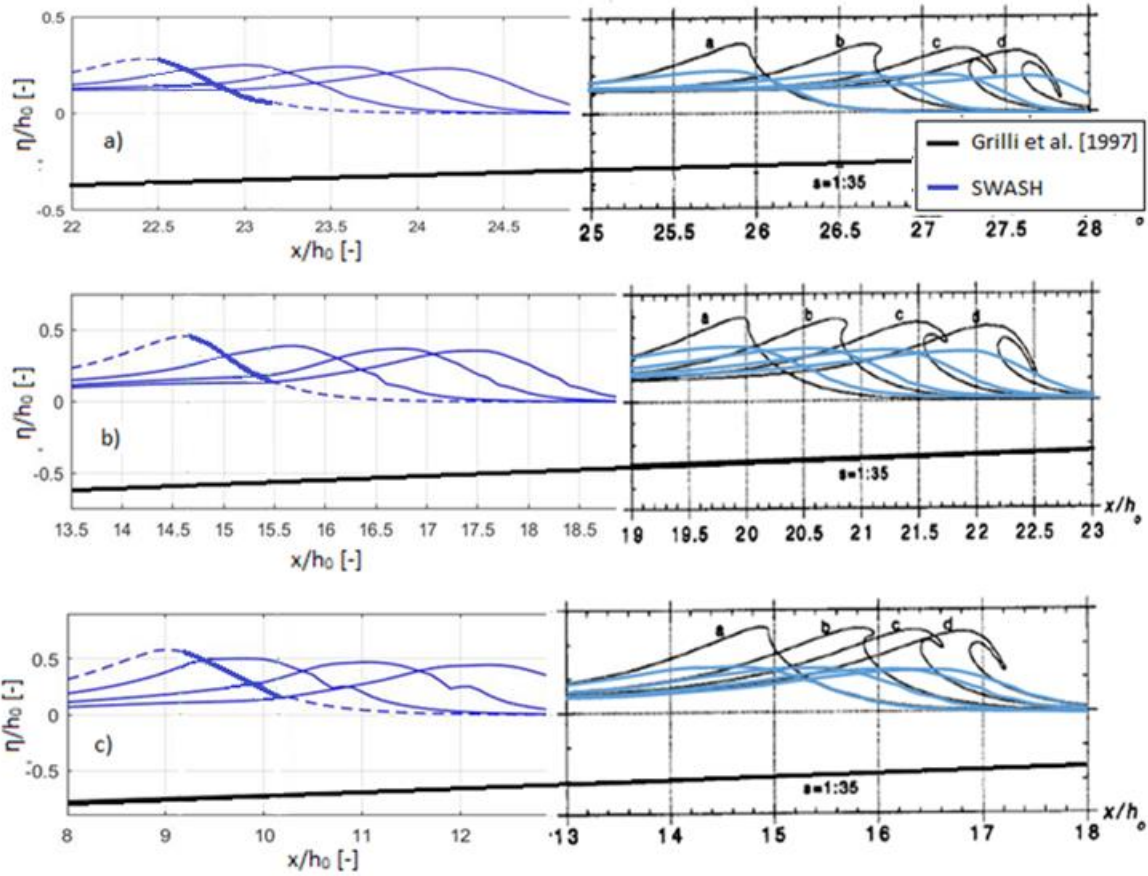
Figure A.3: Simulation of solitary wave with s = 1:35 and a) H0 = 0.2, b) H0 = 0.4and c) H0 = 0.6 . Thick line show where breaking occurs in the wave in the first breaking wave.
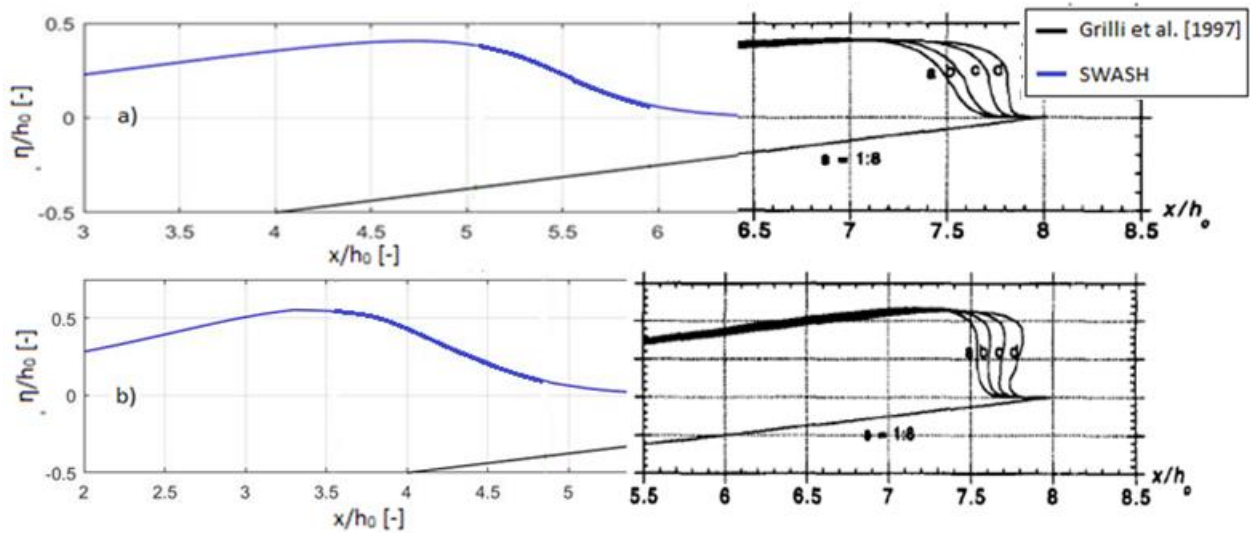
Figure A.4: Simulation of solitary wave with s = 1:8 and a) H0 = 0.2, b) H0 = 0.4and c) H0 = 0.6 . Thick line show where breaking occurs in the wave in the first breaking wave.

B

Bore Simulations

In this appendix the results from the SWASH simulations of chapter 4.2 are shown and discussed. The results are shown in figures B.1 to B.5.

In order to analyse different bores with different height and velocities, the influence of the bathymetry and wave parameters on the velocity and height of the bore should be investigated. The influence of four parameters are tested in this section. These parameters are the slope [α_2], the offshore wave elevation [H_0], the offshore wave length [L_0] and the wave skewness [L_{tail} / L_{front}].

In figure B.1 to B.5, the characteristics of tsunami bores are shown for the different tests of Table 4.1, from 200m offshore up to 1km onshore. Figure B.1 shows test 1, 2 and 6. All with a different slope [α_2] from 1:100 to 1:400. Figure B.2 shows test 1, 3, 4 and 5. All with different initial water elevation from 4m to 10m. Figure B.3 shows test 1, 7 and 8. All with different wave lengths from 100km to 200km. Figure B.4 shows test 1, 9 and 10, where wave 9 is skewed forward and wave 10 is skedded backwards. Test 1, 11 and 12 with different offshore depths [d_0] of 4, 5 and 6 km are shown in figure B.5.

The waves all show the same trend for the bore characteristics although the quantities differ. The local bore front height is very large offshore and becomes very low onshore, in the order of 2 meters, and decreases further. The velocity of the wave front speeds up close to shore and onshore it drops quickly. This shows a large peak at the shoreline for the [u_{bore}]. The front height and velocity slowly become less when the bore progresses inland. The Froude number at the front of the bore is largest where the velocity is largest. There is a peak at the coast of between 3.5 and 4.5 and becomes between 2 and 3.5 more inland.

The inundation height [$H_{max.inun}$] is large offshore and close to the shore. Also the velocity at maximum inundation [$u_{max.inun}$] is largest just onshore. The velocity at maximum inundation is significantly smaller than the velocity at the bore front. The bore height and velocity also become gradually smaller when the bore progresses. These heights and velocities can show large differences for the different wave simulations. The Froude number at maximum inundation is rather constant and only changes between 0.4 and 0.6 for this part of the coast.

Slope α_2
The effects of the different slopes on the bore are shown in Figure B.1 for simulation 1,2 and 6. In figure C.1.b the Froude number at the bore front shows a strange result. The simulation with the mean slope 1:200 has the highest Froude number and the Froude number of the 1:100 slope is a close second inland and much lower at the coastline. This is because the bore only develops on land. The 1:400 slope is lower than the 1:200 slope. This is due to the bore velocity [u_{bore}] which shows the same relation in figure C.1.f. The local bore front height [H_{bore}] is equal on land for all three simulations.

A steep slope increases the inundation height and velocity. The Froude number is thus largest for a steep slope at maximum inundation.

Offshore wave elevation H_0

Figure B.2 shows the results of simulation 1,3,4,and 5, all with different offshore water elevation. A larger water elevation leads to a higher inundation height and higher velocity. However, the Froude number is not that different.

At the wave front, the velocity has a large increase and the bore height has a small increase for a higher elevation. This leads to a larger Froude number at the bore front. The peak of the Froude number is at the shoreline for these simulations with a 1:200 slope.

Offshore wave length and skewness

Figure B.3 shows the results of simulation 1,7 and 8, with different wave lengths. It shows that the characteristics of the bore are almost the same for different wave lengths. Only the inundation height [$h_{max.inun}$] is higher for the longer wave. Also the wave skewness does not give large differences in the characteristics of the bore, Figure B.4. The only difference is the point of breaking due to the steepness of the wave front. The influences on the bore can be considered very small for the wave length and the skewness.

Offshore depth d_0

The results of tests with different offshore depth are shown in figure [C.5]. These figures show that there is no large difference in the bore characteristics between simulations with different offshore depth. The longer shoaling leads to a steeper wave at location x_2 as seen in section 4.1.2. This leads to a wave that breaks earlier. However, the bore parameters are not different for a various initial offshore depth when it reaches the coast.
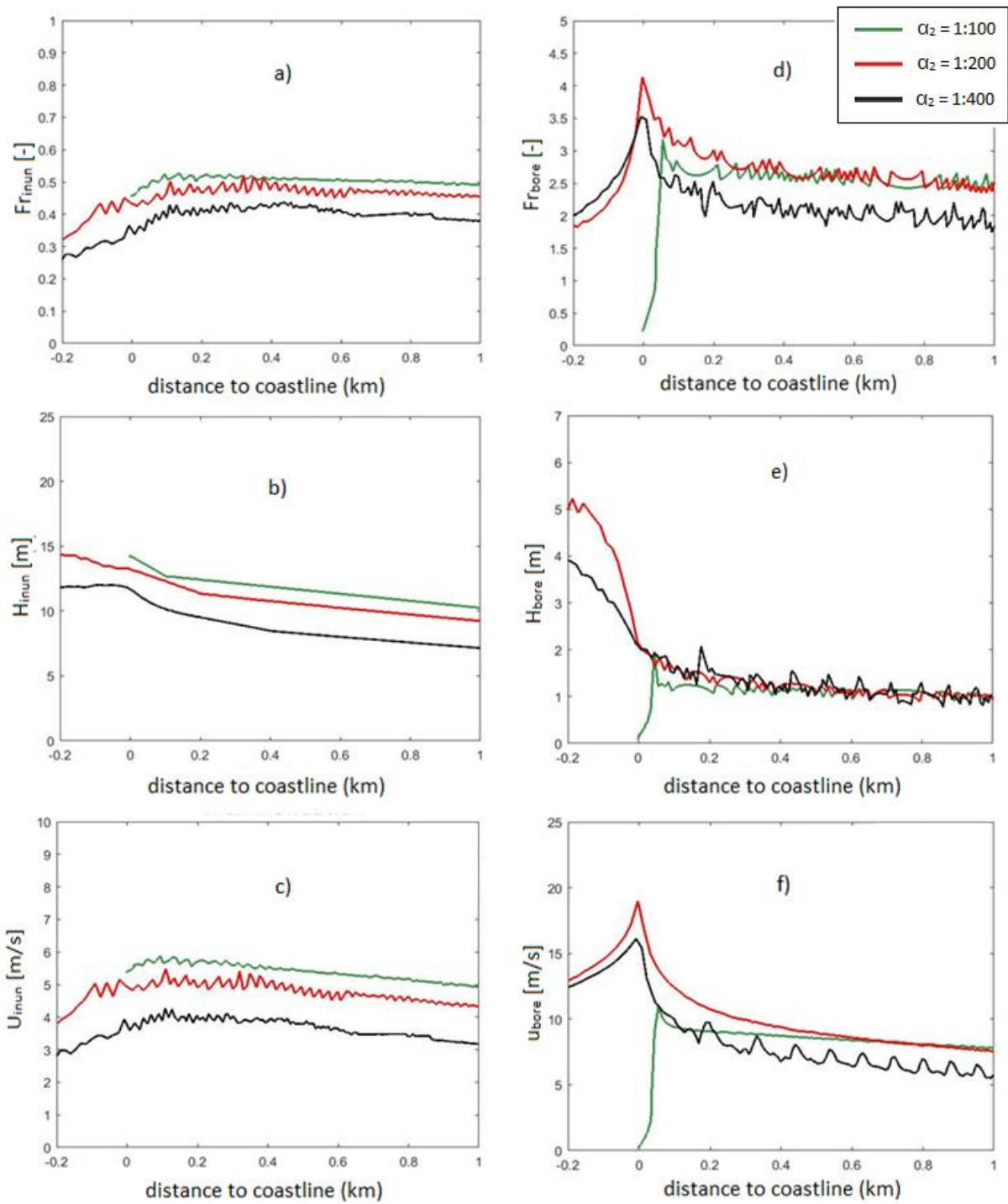
Figure B.1: a) Inundation Froude number [Fr_{inun}], b) inundation depth [H_{inun}], c) velocity [u_{inun}], d) bore Froude number [Fr_{bore}], e) bore height [H_{bore}] and f) velocity [u_{bore}] for tests with different Slope [α0].
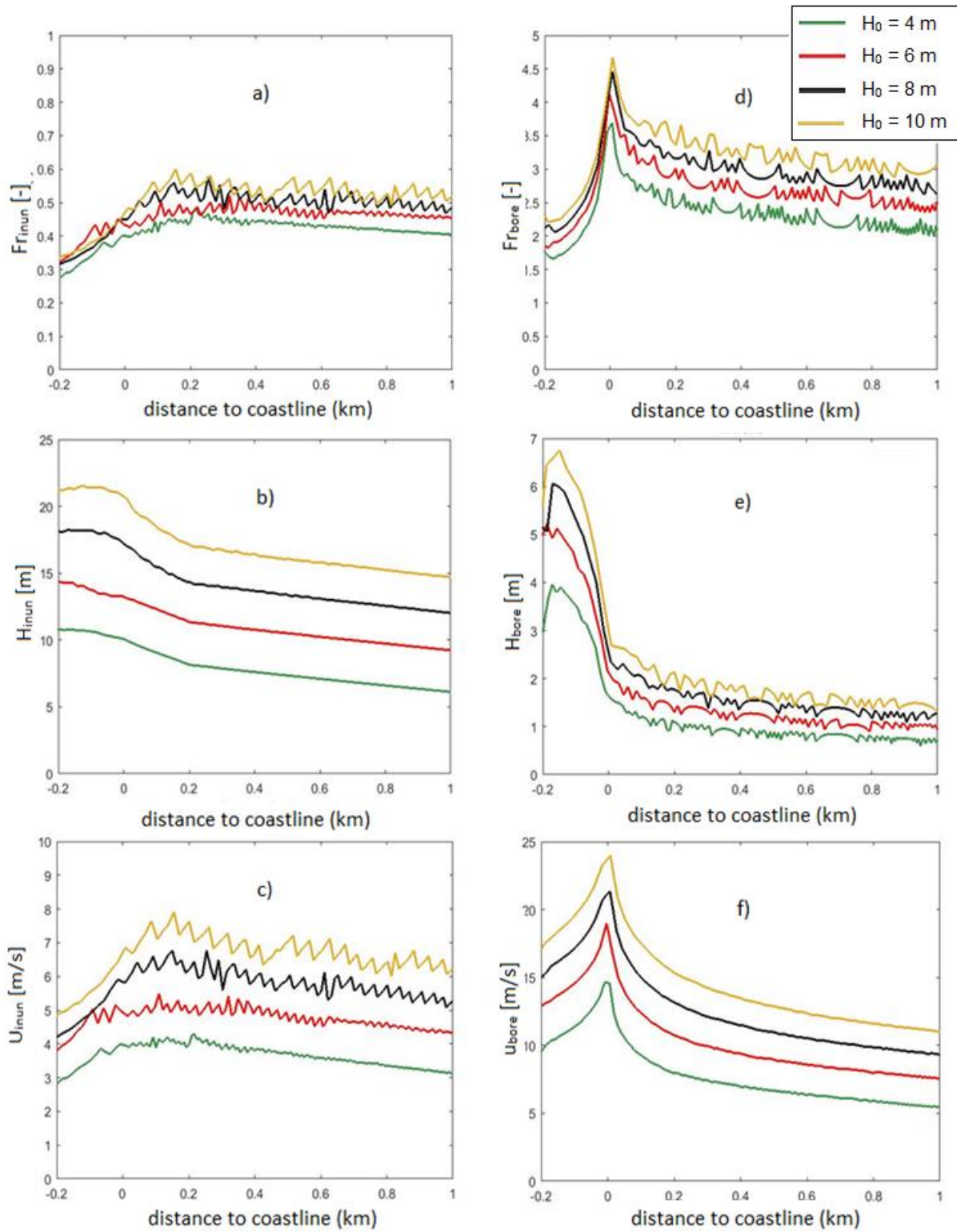
Figure B.2: a) Inundation Froude number [Fr$_{inun}$], b) inundation depth [H$_{inun}$], c) velocity [u$_{inun}$], d) bore Froude number [Fr$_{bore}$], e) bore height [H$_{bore}$] and f) velocity [u$_{bore}$] for tests with different initial wave height [h$_0$].
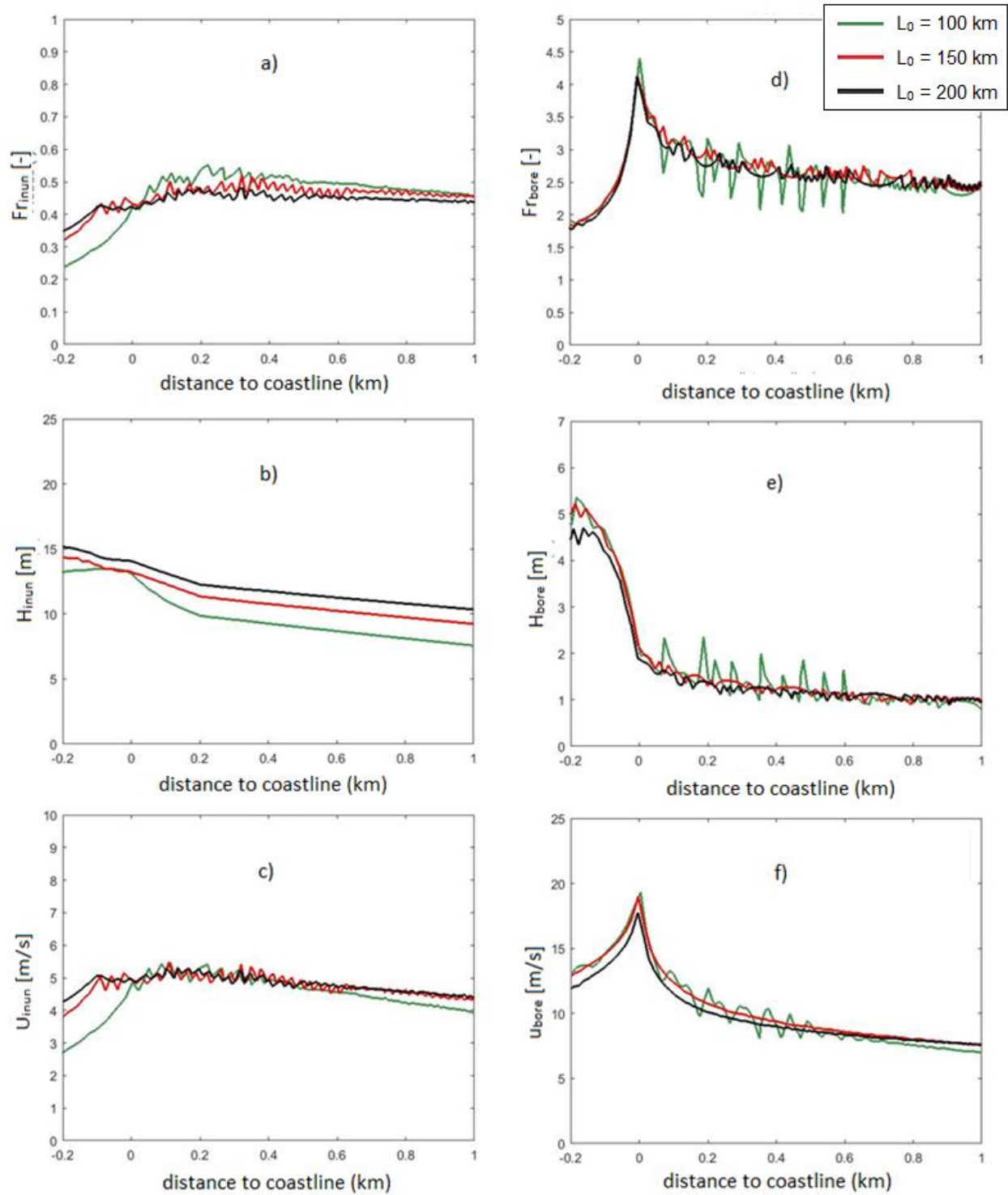
Figure B.3: a) Inundation Froude number [Fr_inun], b) inundation depth [H_inun], c) velocity [u_inun], d) bore Froude number [Fr_bore], e) bore height [H_bore] and f) velocity [u_bore] for tests with different initial Length [L0].
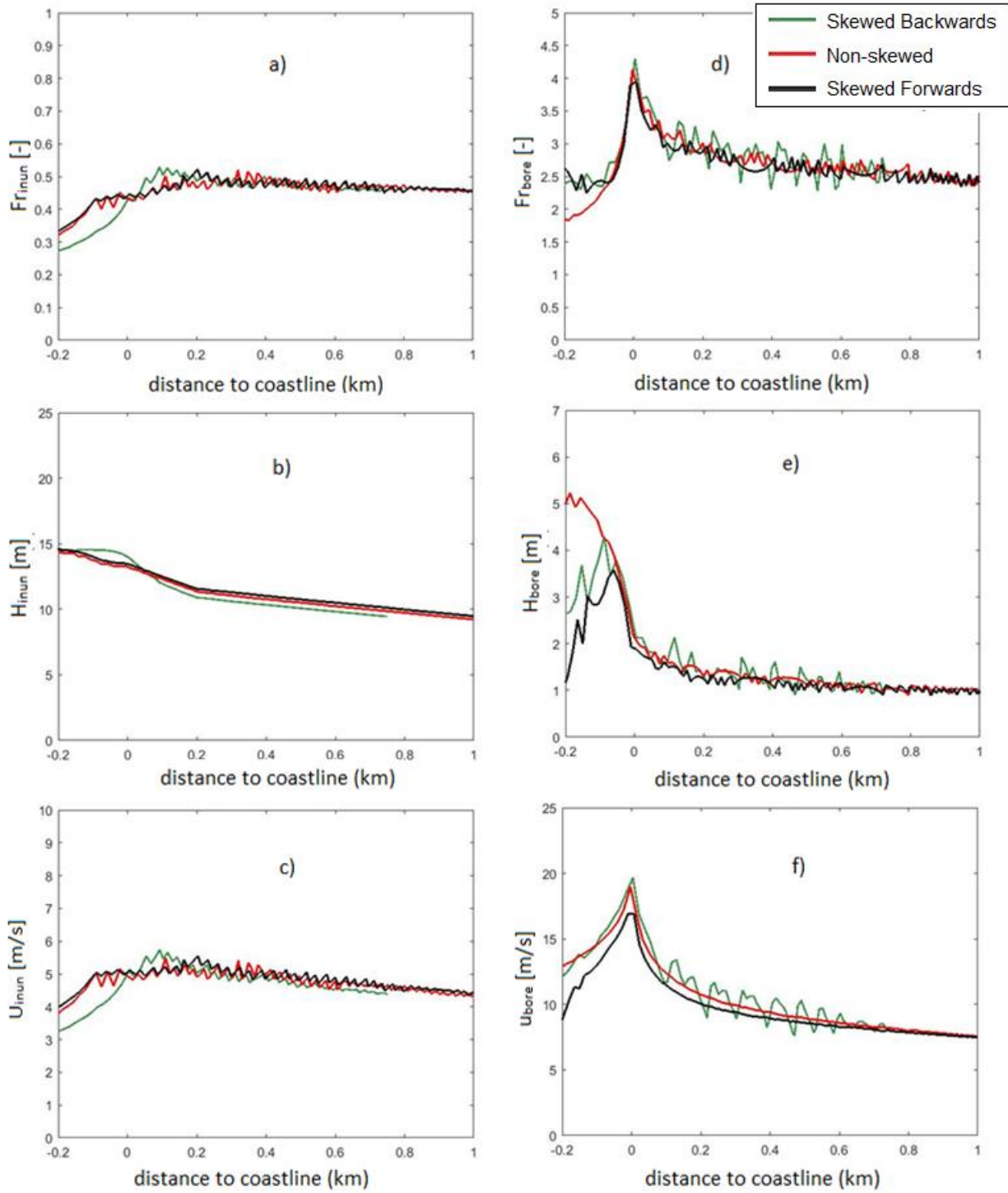
Figure B.4: a) Inundation Froude number [Fr$_{inun}$], b) inundation depth [H$_{inun}$], c) velocity [u$_{inun}$], d) bore Froude number [Fr$_{bore}$], e) bore height [H$_{bore}$] and f) velocity [u$_{bore}$] for tests with different initial wave skewness.
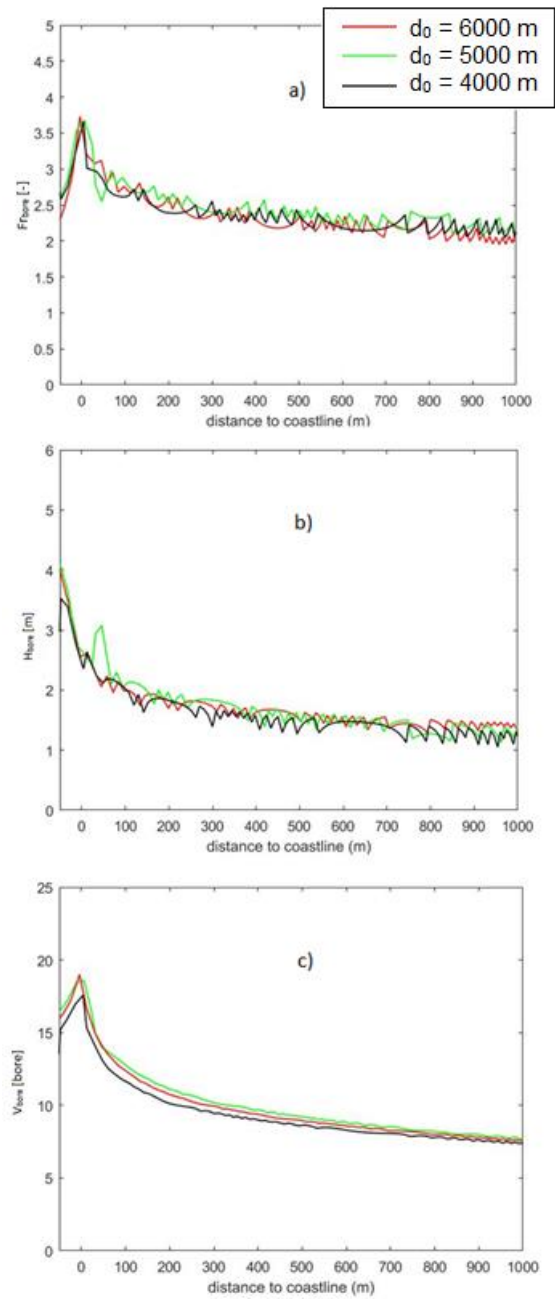
Figure B.5: a) Froude number [Fr_{bore}], b) bore height [H_{bore}] and c) velocity [u_{bore}] for tests with different initial depth [d_0].

C

Tables with results of chapter 5

In this section, the results of the simulation of chapter 5 given in four tables. Tables C.1 and C.2 show the simulations performed for this analysis and the values at the location of maximum velocity.

α_2	L_0 [km]	H_0 [m]	H_{front} [m]	H_{front}/H_0	V_{front} [m/s]	Fr_{front}	H_{inun} [m]
1:100	100	2	0.73	0.36	4.57	1.71	5.41
		4	1.37	0.34	8.08	2.20	9.86
		6	2.83	0.47	14.58	2.77	13.44
		8	3.14	0.39	18.84	3.39	16.05
		10	4.02	0.40	22.19	3.54	18.85
	150	2	0.62	0.31	3.98	1.61	5.48
		3	0.86	0.29	5.31	1.83	7.59
		4	1.09	0.27	6.54	2.00	9.67
		5	1.30	0.26	7.82	2.19	11.73
		6	1.73	0.29	10.63	2.58	13.97
		7	1.90	0.27	13.51	3.13	15.66
		8	2.48	0.31	15.67	3.18	17.32
		9	3.27	0.36	17.40	3.07	19.10
		10	2.52	0.25	18.93	3.81	20.08
		15	4.18	0.28	25.94	4.05	26.43
	200	2	0.52	0.26	3.39	1.49	5.17
		4	0.89	0.22	5.47	1.85	8.87
		6	1.20	0.20	7.18	2.10	12.65
		8	1.54	0.19	9.83	2.53	17.81
		10	2.42	0.24	13.87	2.85	21.00
1:150	100	2	1.25	0.62	8.05	2.30	6.13
		4	2.51	0.63	14.63	2.95	10.32
		6	2.76	0.46	18.86	3.63	13.57
		8	2.70	0.34	22.13	4.30	15.45
	150	2	0.99	0.50	5.75	1.84	6.36
		4	2.29	0.57	12.39	2.61	10.70
		6	2.75	0.46	17.01	3.27	14.38
		8	3.01	0.38	20.68	3.81	16.90
	200	2	0.56	0.28	3.72	1.58	5.69
		4	2.13	0.53	9.15	2.00	10.76
		6	2.33	0.39	14.32	3.00	14.49
		8	2.33	0.29	14.32	3.00	14.49

Table C.1: Simulations performed for the bore analysis in Chapter 5. Simulation input α_2, L_0 and H_0. Simulation output H_{bore}. Bore height ratio, u_{bore}, and H_{inun}. For slope α_2 of 1:200 and 1:400.

α₂	L₀ [km]	H₀ [m]	H_bore [m]	H_bore/H₀	u_bore [m/s]	FR_bore	H_inun [m]
1:200	**100**	**2**	1.48	0.738	11.15	2.93	5.98
		4	2.33	0.582	14.95	3.13	9.96
		6	2.90	0.483	18.27	3.43	12.91
		8	3.06	0.382	20.29	3.71	15.57
		10	2.99	0.299	23.01	4.24	17.86
	150	**2**	1.16	0.579	10.25	3.04	6.28
		3	1.37	0.457	12.51	3.41	8.72
		4	1.34	0.334	15.03	4.15	10.19
		6	2.15	0.358	19.00	4.14	13.24
		8	2.30	0.288	21.93	4.61	17.67
		10	3.17	0.317	23.88	4.28	20.34
		15	4.29	0.286	28.72	4.43	26.11
	200	**2**	1.20	0.602	8.89	2.61	6.41
		4	1.79	0.447	13.28	3.17	10.85
		6	2.37	0.394	16.88	3.50	14.55
		8	2.97	0.371	20.55	3.81	17.76
		10	2.71	0.271	23.31	4.52	20.02
1:400	**100**	**2**	1.28	0.638	9.31	2.63	4.30
		4	1.75	0.438	12.04	2.91	7.16
		6	2.12	0.353	14.23	3.12	9.91
		8	2.32	0.290	15.67	3.29	12.29
		10	2.76	0.276	17.67	3.39	14.26
	150	**2**	1.06	0.532	9.82	3.04	5.10
		3	1.46	0.486	11.78	3.12	7.14
		4	1.59	0.397	13.69	3.47	8.74
		5	1.82	0.363	15.27	3.62	10.29
		6	2.01	0.335	16.36	3.69	11.77
		7	2.03	0.291	16.99	3.80	13.32
		8	2.17	0.272	18.47	4.00	14.60
		10	3.06	0.306	19.58	3.57	16.23
		15	3.79	0.253	21.78	3.57	22.94
	200	**2**	1.36	0.680	9.76	2.67	5.50
		4	1.99	0.496	13.49	3.06	9.13
		6	2.40	0.399	16.89	3.48	12.59
		8	2.92	0.364	18.80	3.52	15.44

Table C.2: Simulations performed for the bore analysis in Chapter 5. Simulation input α₂, L₀ and H₀. Simulation output H_bore. Bore height ratio, u_bore, and H_inun. For slope α₂ of 1:100 and 1:150.

Table C.3 and C.4 give the breaker parameter for simulations with α_2 of 1:100, 1:150, 1:200 and 1:400. All simulations are divided into group A or B. Values to calculate Breaker parameter are also given.

α_2	L_0 [m]	H_0 [m]	H_ξ [m]	L_ξ [m]	T_{tsu} [s]	$\xi_{tsunami}$ [-]	ξ_{ASCE} [-]	R/H_ξ	group A/B
1:200	100	2	2.64	9916	806	0.31	3.10	2.01	A
		4	5.17	9512	806	0.21	2.21	1.68	A
		6	7.62	8886	806	0.17	1.82	1.46	A
		8	9.97	8636	806	0.15	1.60	1.41	A
	150	2	2.54	10657	908	0.32	3.56	2.39	A
		3	3.91	11484	908	0.27	2.87		A
		4	5.07	10749	908	0.23	2.52	2.00	A
		6	7.59	10801	908	0.19	2.06	1.79	A
		8	9.94	10527	908	0.16	1.80	1.67	A
		9	11.09	10366	908	0.15	1.70		A
		10	12.25	8202	908	0.13	1.62		A
	200	2	2.66	13196	1093	0.35	4.19	2.47	A
		4	5.22	12906	1093	0.25	2.99	2.13	A
		6	7.68	12590	1093	0.20	2.46	1.95	A
		8	10.07	12252	1093	0.17	2.15	1.84	A
1:400	100	2	2.5734	9212	681	0.15	1.33	0.00	A
		4	5.0676	7976	681	0.10	0.94	0.00	A
		6	7.8083	6528	681	0.07	0.76	0.00	A
		8	12.2342	5620	681	0.05	0.61	0.00	A
	150	2	2.5508	11432	970	0.17	1.90	0.00	A
		4	5.0081	11180	970	0.12	1.35	0.00	A
		6	7.3689	10158	970	0.09	1.12	0.00	A
		8	9.62	8306	970	0.07	0.98	0.00	A
	200	2	2.5501	14600	1140	0.19	2.23	0.00	A
		4	4.9973	13676	1140	0.13	1.59	0.00	A
		6	7.3561	12716	1140	0.10	1.31	0.00	A
		8	9.6288	11816	1140	0.09	1.15	0.00	A

Table C.3: Breaker parameter for simulations with α_2 of 1:200 and 1:400. All simulations is divided into group A or B. Values to calculate Breaker parameter are also given.

α₂	L₀ [m]	H₀ [m]	H_ξ [m]	L_ξ [m]	T_tsu [s]	ξ_tsunami [-]	ξ_ASCE [-]	R/H_ξ	group A/B
1:100	100	2	2.76	8794	728	0.56	5.47	2.03	B
		4	5.41	8714	728	0.40	3.91	1.74	B
		6	7.97	8624	728	0.33	3.22	1.59	A
		8	10.44	8522	728	0.29	2.81	1.50	A
	150	2	2.81	9314	790	0.58	5.88	2.21	B
		3	4.18	9388	790	0.47	4.83		B
		4	5.52	9308	790	0.41	4.20	1.93	B
		5	6.84	9330	790	0.37	3.77		B
		6	8.14	9240	790	0.34	3.46	1.79	A
		7	9.42	9260	790	0.31	3.22		A
		8	10.67	9230	790	0.29	3.02	1.69	A
		10	13.13	9196	790	0.26	2.72		A
	200	2	2.92	9964	1034	0.58	7.57	2.24	B
		4	5.73	9952	1034	0.42	5.40	2.00	B
		6	8.46	9936	1034	0.34	4.44	1.86	A
		8	11.10	9914	1034	0.30	3.88	1.78	A
1:150	100	2	2.68	10428		0.42	0.00		B
		4	5.25	10218		0.29	0.00		A
		6	7.73	9998		0.24	0.00		A
		8	10.11	9736		0.21	0.00		A
	150	2	2.69	11538		0.44	0.00		B
		4	5.27	12020		0.32	0.00		A
		6	7.76	11952		0.26	0.00		A
		8	10.17	10992		0.22	0.00		A
	200	2	2.74	12840		0.46	0.00		B
		4	5.37	12756		0.32	0.00		A
		6	7.92	12606		0.27	0.00		A
		8	7.92	12606		0.27	0.00		A

Table C.4: Breaker parameter for simulations with α2 of 1:100 and 1:150. All simulations is divided into group A or B. Values to calculate Breaker parameter are also given.

D

Scaling physical tests

This section contains additional information for chapter 6. The process of the bore attack is described in section D.1. The physical tests are described and compared to the SWASH simulations. The bore of the tests is compared to the simulations by scaling the physical tests by 1:50 and 1:200. The velocities and the heights of the bores are then compared to the SWASH simulations in section D.2.

D.1   Bore overtopping process tests

In Figure D.1, four snapshots of the video are show of the (d=50 and h=0) bore. The bore front travels to the structure with high velocity a. When the bore hits, the water shoots up with a splash and a roller forms on the sea side of the structure b. The height of the water in front of the structure builds up and the water overtops the structure. When the water reaches the maximum height, the water overtops the structure and the roller starts moving in negative direction c. The water level in front of the structure remains high because the long tsunami bore, due to the large water basing, keeps building up the water layer and the
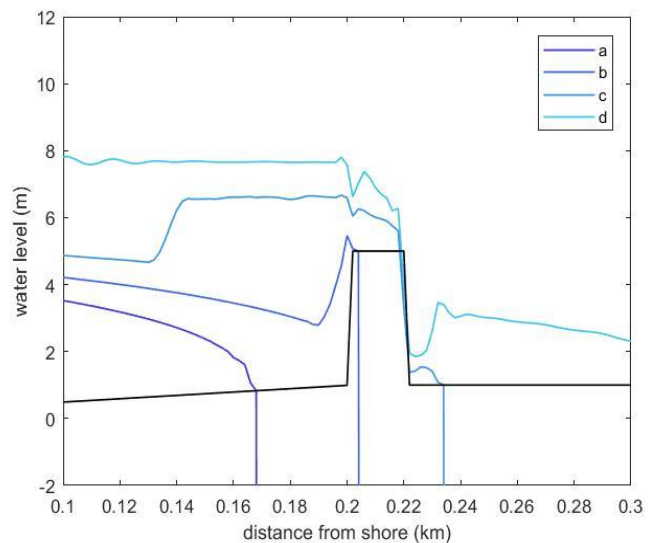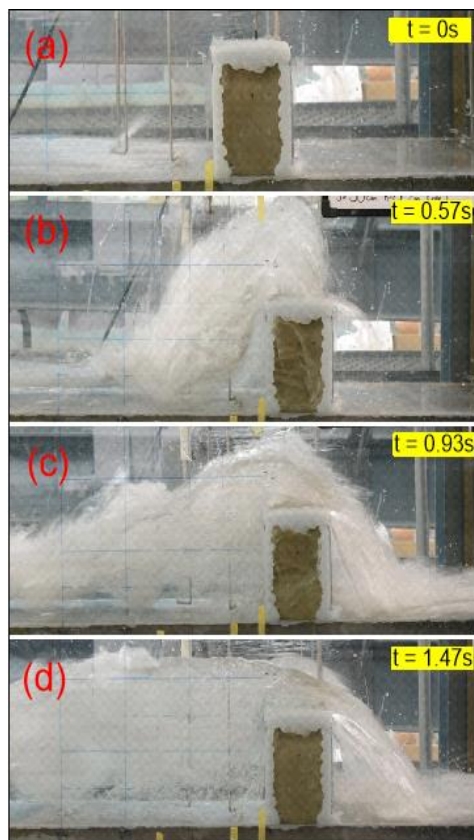
Figure D.1: a): Frames of high speed camera for the test with d= 50 an h= 0. b): Four stages of bore impact on a wall in SWASH

water continuously overflows the structure (d). When the inflow of water drops, the water level becomes lower than the structure and overflow stops.

D.2   Bore physical tests Compared to the Simulations

The results from the physical tests will be compared to the results of the model. There are some problems with comparing the results of the simulations with the physical tests. First, the output of the velocity meters was not correct air entrainment within the turbulent bore. Instead the bore front velocity [v_{front}] is used as obtained from the wave gauges. Second, the water surface elevation of the bore was measured with wave gauges but only the maximum inundation [h_{inun}] of the bore could readily be obtained from the data. This gives a velocity at the front of the bore and a height at the highest water level. These are two values of different locations in the wave and cannot give a clear relationship between them. For the maximum momentum flux as used in FEMA [2012], the velocity and height should be at the same location in time and space.

D.2.1   Bore front Velocity

For a comparison of the bore, the measured bore front velocity [v_{front}] and maximum inundation height [h_{inun}] are the parameters that will be compared with the simulations. The measured bore front velocity [v_{front}] and the maximum inundation height [h_{inun}] are given in Table D.1. Subscript (m) shows the measurements in small scale. The bore front velocity [v_{front}] and the maximum inundation height [h_{inun}] are scaled to normal scale with a 1:50 scale. This scale is chosen to match the velocities of the bore to real tsunamis. This gives velocities of 6.2 m/s up to 19.1 m/s and inundation heights of 1.7m up to 6.1m.

d	h	v_{front} (m/s)	h_{nun} (cm)	v_{front} [m/s]	h_{inun} [m]	Fr_{front}	v_{front} [m/s]	h_{inun} [m]	Fr_{front}
30	0	1.24	3.42	8.8	1.71	2.15	17.54	6.84	2.14
30	10	1.15	3.67	8.1	1.84	1.91	16.26	7.34	1.92
30	20	0.88	3.73	6.2	1.87	1.45	12.45	7.46	1.45
40	0	1.68	5.49	11.9	2.75	2.29	23.76	10.98	2.29
40	10	1.37	5.64	9.7	2.82	1.84	19.37	11.28	1.84
40	20	1.79	5.64	12.6	2.82	2.40	25.31	11.28	2.41
50	0	2.12	8.59	15	4.3	2.31	29.98	17.18	2.31
50	10	1.92	7.79	13.6	3.9	2.20	27.15	15.58	2.20
50	20	1.66	8.32	11.7	4.16	1.83	23.48	16.64	1.84
60	0	2.59	12.17	18.3	6.09	2.37	36.63	24.34	2.37
60	10	2.43	10.74	17.2	5.37	2.37	34.37	21.48	2.37
60	20	2.7	10.27	19.1	5.14	2.69	38.18	20.54	2.69
				scale: 1:50			scale: 1:200		

Table D.1: Front velocity and inundation height for tests and simulations. Froude number for simulations.

The bore front velocity [v_{front}] of the simulations with different initial wave elevation is shown in Figure D.2 a and b. The bore front has a clear acceleration when the wave starts breaking. Then the bore front reaches a rather constant velocity that is maintained until the coastline where the velocity peaks. This is visible with the 1/400 slope in Figure D.2.b, where the wave starts breaking earlier. When the bore is on land the

velocity energy reduces gradually to zero. The rate of reduction at every is location the same for all the bores (with equal wave length). In Figure D.2.c can this be seen for different slopes and heights. For different wave lengths this reduction is different, Figure D.2.d. With a longer wave there is more water that is transported onto shore and the energy reduces slower. These longer waves also have lesser steepness, since the wave is a part of a cosine function with equal front and back steepness.

The maximum bore front velocity ranges from 7.5 to 20 m/s for the 1:200 slope and from 9 to 18 m/s for the 1:400 slope with an initial wave height ranging from 2 to 10 m. This is the same range as in the physical tests. The velocity from the dam-break tests do represent good value for the velocity of a tsunami bore at a 1:50 scale.
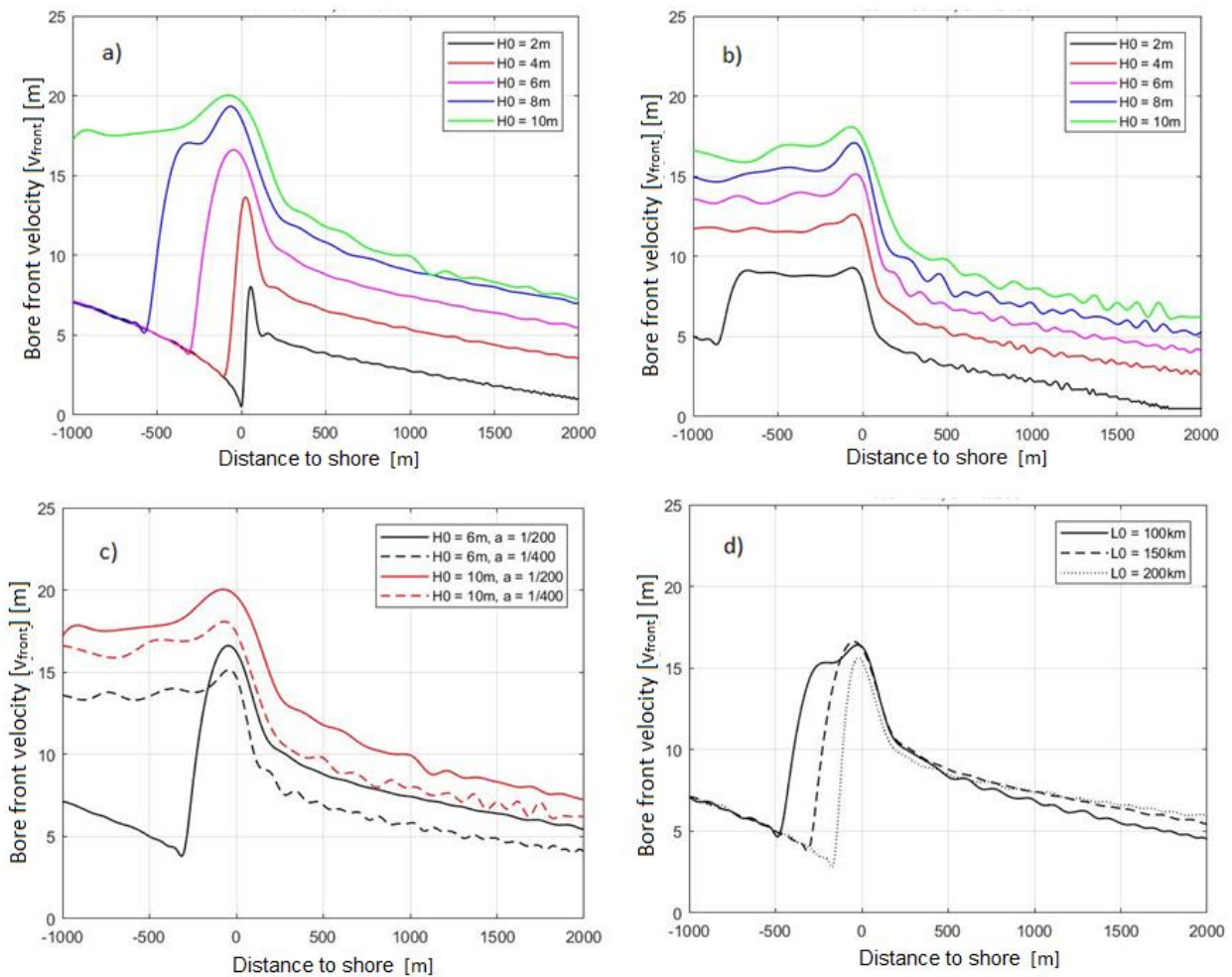
Figure D.2: Bore front velocity for different initial heights a) with slope 1:200 an L_0 = 150km. b) with slope 1:400 an L_0 = 150km. c) with slope 1:400 an L_0 = 150km. d) bore front velocity for different initial wave lengths with height H_0 = 4m and slope is 1:200.

D.2.2 Inundation height

Comparing the height of the bore from physical tests with the bore from the simulations gives some issues. The height that can be obtained from the data of the physical tests is the maximum height that is reached at the measuring location. This is the inundation height of the wave and not the height of the bore front. This parameter is useful if the overtopping is investigated and less useful for the force of the incoming bore on a wall. However, this value can still be compared to the inundation height of the simulations. Although, the relationship of the two height is doubtful since the bore in the model is followed by a 150km long wave while the water basin in the lab is not long enough to represent such a long wave. The inundation heights in Table D.1 ranges from 1.7 up to 6.1m height. To compare this with the simulations the same range of wave heights as with the velocity in the previous section is used.

Figure D.3.a shows the inundation height of the simulations with α_2 = 1:200 and L_0 = 150km. The inundation height at the coastline (x_4 = 0m) has a range of 7 to 20 m. Also further inland (at x_5 = 500m) the inundation height is much larger than in the physical tests. This is considerably larger than the inundation height of the physical tests at this scale. This difference in height can be due to the difference in wave length. This can also be seen in Figure D.3.b, where the inundation height is equal at the coastline for waves with different length but decreases much faster for shorter waves as it progresses inland. This can be explained by the amount of water that flows onto the shore with tsunamis with different wave lengths. The longer waves have the same shoaling and therefore the same height at the coastline but the longer waves have a longer period of water that flows inland. This could indicate that the bore in the physical test is much shorter and is somewhat inland where the inundation height is reduced. Unfortunately, the length of the wave of the physical tests is incomparable due to the different wave generation.

If a scale of 1:200 is used for the tests then the inundation height of the dam-break tests matches the simulations better. With a height ranging from 6.8 to 24.3m compares good to Figure D.3.a. With 38 m/s the velocity in this case is much to large compare to the simulations.
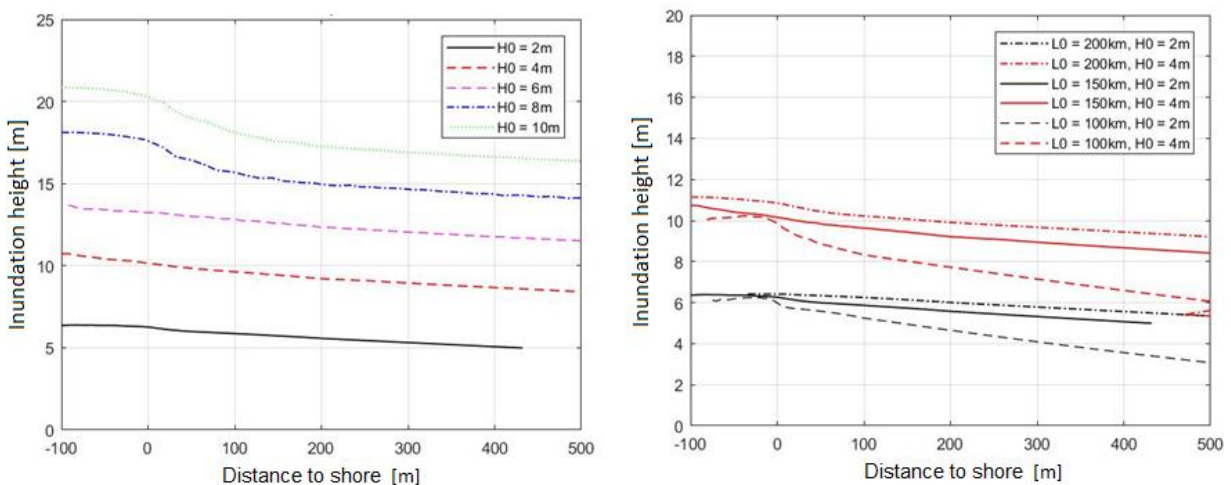
Figure D.3: a) Inundation height for different initial wave heights with slope 1:200 and L_0 = 150km. b) inundation height for simulations with different wave lengths with H_0 = 4m (red) and H_0 = 2m (black)

E

SWASH input file

The SWASH input file that was used for the simulations is shown here. The commands can be found in the SWASH user manual. The SWASH impute file used for the simulations in this thesis:

MODE DYNamic ONEDimensional

CGRID 0. 0. 0. 20000. 0. 20000 0

INPgrid BOTTOM 0. 0. 0. 20000 0 1. 0.

INPgrid WLEVel 0. 0. 0. 20000 0 1. 0.

INPgrid FRICTION 0. 0. 0. 20000 0 1. 0.

READinp   BOTTOM 1. 'bottomfile.bot' 1 0 FREE

READinp   WLEVel 1. 'waterlevel.wlev' 1 0 FREE

READinp   FRICTION 1. 'Frictionfile.fr' 1 0 FREE

$ -----conditions

INITial ZERO

BOU SIDE W CCW BTYPE WEAK CON SERIES 'timeseriesboundary.bnd' 4

$BOU SIDE W CCW BTYPE RADIATION

BOU SIDE E CCW BTYPE RADIATION

FRICtion MANNing

BREAK

NONHYDrostatic

$ -----output

TIMEI METH IMPL

GROUP 'data' 1 15000 1 1

TABLE 'data' HEAD 'd4H4.tbl' BRKP WATL VEL OUTPUT 000000.000 1 SEC

COMPute 000000.000 0.001 sec 010000.000

STOP